The bacterial division protein MinDE has an independent function in flagellation

Pinkilata Pradhan[1,2,‡], Ashoka Chary Taviti[1,†], and Tushar Kant Beuria[1,*]

From the [1]Infectious Disease Biology, Institute of Life Sciences, Bhubaneswar, Odisha, India; [2]Regional Centre for Biotechnology, Faridabad, Haryana, India

---

Targeting the Achilles Heel of FtsZ: The Interdomain Cleft

Pinkilata Pradhan[1,2], William Margolin[3]* and Tushar Kant Beuria[1]*

[1]Institute of Life Sciences, Nalco Square, Bhubaneswar, India, [2]Regional Centre for Biotechnology, Faridabad, India, [3]Department of Microbiology and Molecular Genetics, McGovern Medical School, Houston, TX, United States

Widespread antimicrobial resistance among bacterial pathogens is a serious threat to public health. Thus, identification of new targets and development of new antibacterial agents are urgently needed. Although cell division is a major driver of bacterial colonization and pathogenesis, its targeting with antibacterial compounds is still in its infancy. FtsZ, a bacterial cytoskeletal homolog of eukaryotic tubulin, plays a highly conserved and foundational role in cell division and has been the primary focus of research on small molecule cell division inhibitors. FtsZ contains two drug-binding pockets: the GTP binding site situated at the interface between polymeric subunits, and the inter-domain cleft (IDC), located between the N-terminal and C-terminal segments of the core globular domain of FtsZ. The majority of anti-FtsZ molecules bind to the IDC. Compounds that bind instead to the GTP binding site are much less useful as potential antimicrobial therapeutics because they are often cytotoxic to mammalian cells, due to the high sequence similarity between the GTP binding sites of FtsZ and tubulin. Fortunately, the IDC has much less sequence and structural similarity with tubulin,

---

MazEF-rifampicin interaction suggests a mechanism for rifampicin induced inhibition of persisters

Cyrus Alexander[1,2], Ankeeta Guru[1,3], Pinkilata Pradhan[1,3], Sunanda Mallick[1,2], Nimai Charan Mahanandia[4], Bharat Bhusan Subudhi[5] and Tushar Kant Beuria[1]*

The bacterial division protein MinDE has an independent function in flagellation

Pinkilata Pradhan[1,2,‡], Ashoka Chary Taviti[1,‡] , and Tushar Kant Beuria[1,*]

From the [1]Infectious Disease Biology, Institute of Life Sciences, Bhubaneswar, Odisha, India; [2]Regional Centre for Biotechnology, Faridabad, Haryana, India

Before preparing for division, bacteria stop their motility. During the exponential growth phase in *Escherichia coli*, when the rate of bacterial division is highest, the expression of flagellar genes is repressed and bacterial adhesion is enhanced. Hence, it is evident that cell division and motility in bacteria are linked; however, the specific molecular mechanism by which these two processes are linked is not known. While observing *E. coli*, we found that compared to the WT, the *E. coli* (Δ*min*) cells show higher motility and flagellation. We demonstrated that the higher motility was due to the absence of the Min system and can be restored to normal in the presence of Min proteins, where Min system negatively regulates flagella formation. The Min system in *E. coli* is widely studied for its role in the inhibition of polar Z-ring formation through its pole-to-pole oscillation. However, its role in bacterial motility is not explored. MinD homologs, FlhG and FleN, are known to control flagellar expression through their interaction with FlrA and FleQ, respectively. AtoC, a part of the two-component system AtoSC complex, is homologous to FlrA/FleQ, and the complex is involved in *E. coli* flagellation *via* its interaction with the *fliA* promoter. We have shown that MinD interacts directly with the AtoS of AtoSC complex and controls the *fliA* expression. Our findings suggest that the Min system acts as a link between cell division and motility in *E. coli*.

During bacterial division, a division ring (Z-ring) is formed at the midcell by the divisome complex. FtsZ, a bacterial cytoskeletal protein, assembles in a GTP-dependent manner to form protofilaments, which form the skeleton of the Z-ring (1). The inhibition of FtsZ functions by small molecules leading to inhibition of Z-ring formation and results in cell filamentation (2–5). Bacteria that divide by binary fission, such as *Escherichia coli*, typically designate their cell division sites at the midpoint. This ensures that cell division should be symmetric, and the resulting daughter cells are approximately uniform in both size and shape (6). The placement of the Z-ring at the midcell in *E. coli* is guided by the Min system through its polar oscillation (7, 8). The Min system in *E. coli* comprises of three proteins named MinC, MinD, and MinE. MinC is an inhibitor of FtsZ assembly; MinD is an ATPase and contains a membrane-targeting sequence that binds to the inner membrane. MinE stimulates MinD ATPase activity, leading to the release of MinD from the membrane. The polar oscillation of the Min system results from the intricate interplay between ATP-dependent membrane association, subsequent MinD oligomerization, and MinE-induced local release of MinD from the membrane upon ATP hydrolysis. MinC essentially acts as a "passive rider" on these oscillations. The membrane-bound MinD forms a complex with MinC and inhibits the Z-ring formation at the poles, thereby facilitating the placement of Z-ring at the midcell. Furthermore, this process is enhanced by the interaction of MinD with FtsZ (9). Apart from regulating cytokinesis in *E. coli*, the Min system is also associated with other cellular processes in bacteria, such as chromosome segregation, virulence, and motility (10–12).

Motility in bacteria is a complex phenomenon mediated by flagella. Flagellation in *E. coli* is regulated by class I, class II, and class III flagellar genes. FlhDC is a class I gene and a master regulator that regulates the expression of the class II flagellar genes. FliA is a flagella-specific sigma factor that positively regulates the expression of all the class III flagellar genes and thus controls flagellation (13). The expression of *fliA* can be regulated at several levels. The presence of an insertion element at upstream of the *flhDC* promoter can increase the *flhDC* expression, which in turn induces *fliA* gene expression and the motility of the bacteria (14). Similarly, the phosphorylated AtoC, a part of the AtoSC two-component system (TCS), interacts with and positively regulates *fliA* promoter expression. The deletion of AtoSC from *E. coli* genome leads to a nonmotile phenotype (15). Further, FliA protein can positively autoregulate itself and FlgM, upon interaction with FliA, can negatively regulate *fliA* expression (13).

The distribution of flagella on the surface of bacteria shows a particular pattern and maintains a specific position and number. One such pattern regulatory protein, FlhG, is involved during flagellation in *Campylobacter jejuni* (*C. jejuni*). Similarly, in *Pseudomonas aeruginosa* deletion of FleN, an ortholog of FlhG, results in hyperflagellation (16). FlhG/FleN regulate flagellation through their interactions with regulatory proteins FlrA/FleQ, respectively (17–19). However, FlhG/FleN and FlrA/FleQ are absent in *E. coli*. FlhG/FleN are ATPases and homologous to MinD. FlhG is structurally and

---

functionally similar to MinD (20). Like MinD, FlhG forms a homodimer in the presence of ATP, tethers to the membrane with the help of conserved membrane-targeting sequence, and forms foci at both the poles. Recent reports have shown that the deletion of FlhG in *C. jejuni* results in polar minicells formation, mirroring the effects of MinD deletion in *E. coli*, suggesting that FlhG is functionally similar to MinD (21). Interestingly, the Min system is present in *Pseudomonas* and is not reported for its involvement in flagellation or motility (22). Similarly, FleN deletion in *Pseudomonas* leads to higher flagellation but does not form minicells (16). Whereas, studies indicated that the Min system in some bacteria like *Helicobacter pylori* is involved in bacterial motility (18). The role of the Min system in controlling motility in *E. coli* is not known. In the present study, we investigated the effects of the Min system on motility and flagellation in *E. coli*. We also explored if the homologs of FlrA/FleQ are present in *E. coli* and whether these homologs interact with MinD. Our findings showed that the MinDE complex plays a role during *E. coli* flagellation through its interaction with AtoS of the AtoSC complex and thus by controlling *fliA* expression. In this study, we report for the first time the involvement of MinDE during flagellation in *E. coli*.

Results

E. coli (Δ min) cells showed hypermotility

During our observation of *E. coli* (Δ min) cells under microscope, we found that compared to *E. coli* WT (MG1655) cells, *E. coli* (Δ min) cells showed random and faster movement (Fig. 1A). To check whether this motility is due to the absence of the Min system, we examined the motility of *E. coli* (WT), *E. coli* (Δmin), and *E. coli* (Δmin) complemented with *minCDE* cells using live-cell imaging microscope. We observed that the WT cells showed little movement under this condition, whereas, *E. coli* (Δmin) cells showed considerably high motility (Movies S1 and S2). When *E. coli* (Δmin) cells were complemented with plasmid containing *minCDE*, the WT phenotype of the cells was regained (Movie S3). To further confirm the motility of the above strains we performed soft agar motility assay, which showed similar results, that is, *E. coli* (WT) showed least motility, *E. coli* (Δmin) showed high motility, and *E. coli* (Δmin) complemented with *minCDE* showed reduced motility (Fig. 1, B and C). Our above observations indicated that the Min system might be involved in *E. coli* motility.

Min system regulates flagellation in E. coli

Increased flagellation or flagellar activity could cause hypermotility in bacteria (23). So, the observed hypermotility in *E. coli* (Δmin) cells could be due to an increase in the flagellation or flagellar activity. To visualize the flagellation, we stained *E. coli* using Alexa Fluor 488, which binds to the amine-rich protein flagellin, and was observed under a fluorescent microscope. Our results showed that *E. coli* (Δmin) cells were hyperflagellated that are characterized by dense flagella located all over the cells (Fig. 2A). However, we did not

observe any flagella in WT cells (Fig. 2A). Furthermore, the transmission electron microscopy analysis also confirmed that *E. coli* (Δmin) cells contain intact multiple flagella, whereas WT cells are majorly lacking flagella (Fig. 2B). Our result was also supported by the previous reports that the lab strain MG1655 (CGSC 6300) shows no or minimal motility in laboratory conditions and thus the flagella could not be visualized in these cells (24).

To identify the components of the Min system that are responsible for the flagellar regulation, we performed motility assay, Alexa Fluor 488 staining and transmission electron microscopy (TEM) analysis of *E. coli* (Δmin) cells and *E. coli* (Δmin) cells complemented with different Min components (25). Consistent with the previous results, our analysis revealed hypermotility, dense flagellation, and longer flagella in *E. coli* (Δmin) cells when compared to WT *E. coli* (MG1655) (Fig. 2). However, when *E. coli* (Δmin) cells were complemented with plasmids expressing MinCDE or MinDE proteins, the cells exhibited lower motility than *E. coli* (Δmin) cells (Fig. 1, B and C). Further, we observed flagellation using fluorescence microscopy and TEM imaging. No reduction in the flagellation was observed when *E. coli* (Δmin) was complemented with *minC*, or *minD*, or *minE* individually. However, *minDE* or *minCDE* complementation leads to a significant decrease in flagellation (Figs. 2 and S1). It is known that neither MinD nor MinE alone can restore the requirement of the Min system in cell division, and a similar trend was observed in flagellar regulation (26, 27). Further, the number of bacteria containing flagella was determined and plotted (Fig. 2C). It was found that ∼90% of the *E. coli* (Δmin) cells possess flagella, which decreased significantly (by >50%) when the cells were complemented with *minCDE*.

Min system negatively regulates the expression of flagellar genes

E. coli motility relies on flagella rotation, and *E. coli* (Δmin) cells show hyperflagellation and increased motility. To understand how the hyperflagellated morphology is happening in *E. coli* (Δmin) cells, we checked the expression of flagellar genes and their regulators in the absence of Min system. A flagellum is consisting of several structural proteins, which are governed by its regulators (Fig. 3A). The flagellar expression is majorly controlled by the transcription factor FlhDC, a master regulator of flagellar expression (28, 29). FlhDC regulates the expression of the *fliA* gene, which encodes FliA, sigma factor 28 that acts as a regulator for several flagellar genes such as *fliC* (codes for Flagellin), *motA*, and *motB* (30). In order to understand how min proteins might be regulating the expression of flagellar genes and their regulators, we performed quantitative reverse transcription-PCR (qRT-PCR) for flagellar regulators *flhDC*, *fliA*; structural genes *fliC*, *flgE*, *fliE*; motor genes *motA*, *motB*, and transcription factor *Rcsb*. Our result showed that compared to the WT *E. coli* the expression of *fliA*, *motA*, *motB*, and *fliC* were significantly upregulated in the *E. coli* (Δmin) cells (Fig. 3B). Whereas, the expression of *flhDC*, the transcription factor
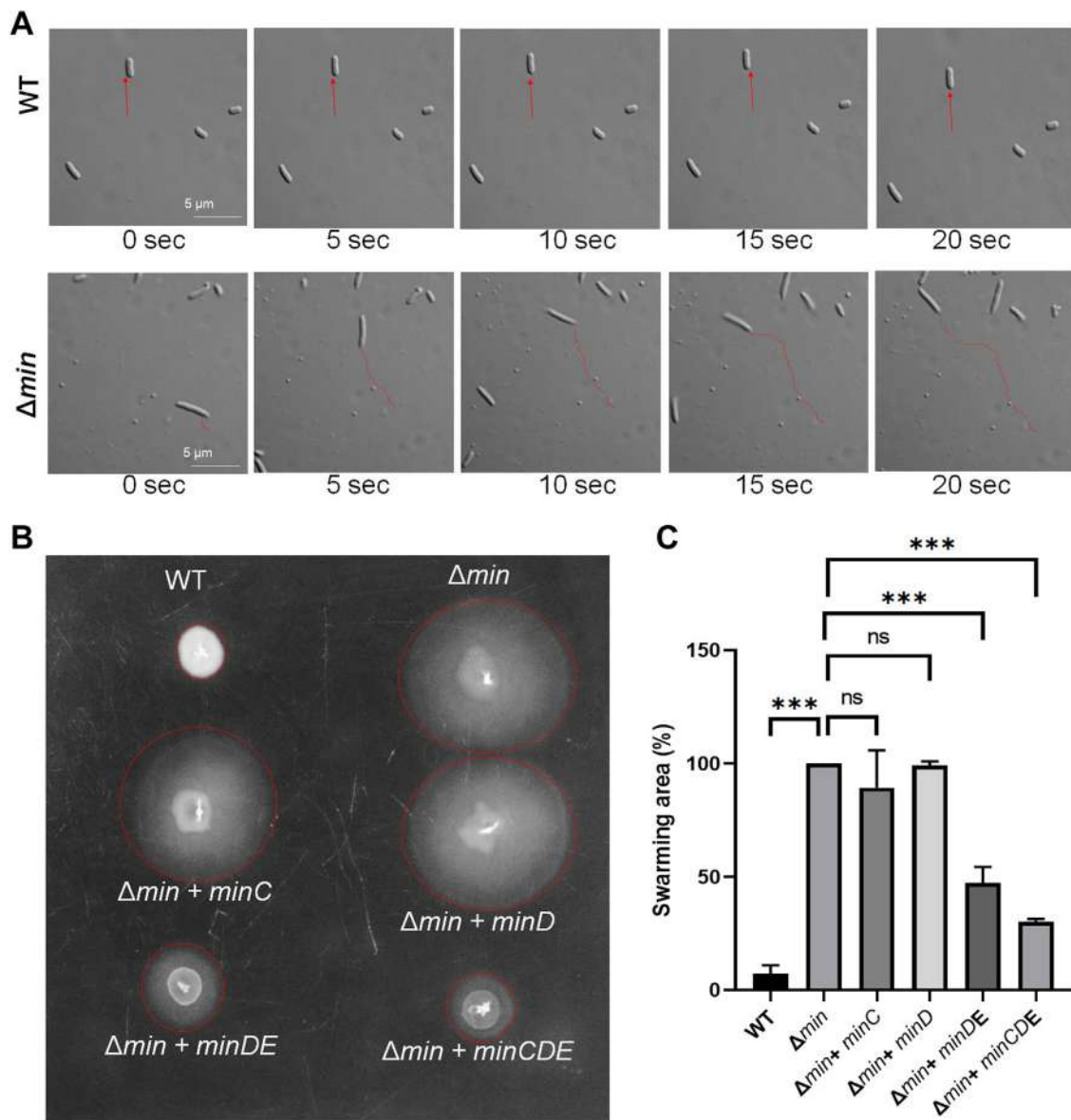
Figure 1. Min system regulates motility in *Escherichia coli*. *E. coli* MG1655 (WT) WT and *E. coli* JS964 (Δ *min*) were grown in motility media. Few drops were added on to agar over a glass slide and observed under microscope (Olympus BX51). *A*, shows bacterial movement, snapshots of different time points. The *red lines* indicate the path followed by the bacterial during its movement (the scale bar represents 5 μm). *B*, the control strain *E. coli* MG1655 (WT) and *E. coli* (Δ *min*) carrying plasmids (pTrc99a) containing various Min components were grown overnight and 3 μl culture from each strain were spotted on 0.3% soft-agar plates containing ampicillin (100 μg/ml) and 0.1 mM IPTG. The plates were incubated at 37 °C for 12 to 18 h and bacterial motility was observed. *C*, the swarming area percentage in each strain in the form of bar graph. Error bars shows the ± SEM determined and *p* values (<0.05) were determined using an unpaired parametric *t* test (n = 3).

and the global regulator, did not change much in the absence of Min system. To verify this observation, we performed Western blot analysis using anti-flagellin antibody. We examined flagellin (FliC) production in *E. coli* (WT), *E. coli* (Δ*min*), and *E. coli* (Δ*min*) cells complemented with different min components. The *minC*, *minD*, and *minE* complementation did not affect the flagellin production, whereas it decreased considerably when complemented with *minDE* or *minCDE* (Figs. 3, *C* and *D* and S1). A high level of flagellin protein production was found in *E. coli* (Δ*min*) compared to the *E. coli* (WT) cells (Fig. 3, *C* and *D*). Our qRT-PCR findings align with and support this result.

The role of Min system in controlling fliA promoter activity

In *E. coli*, FlhDC binds to the promoter region of *fliA* and regulates its expression (14). Thus, the change in either *flhDC* or *fliA* expression can affect the flagellation. In order to understand how the Min system is affecting the *flhDC* or *fliA* expression, we examined the strength of *flhDC* and *fliA* promoter activity in WT and *E. coli* (Δ*min*) cells using an enhanced green fluorescent protein (eGFP) reporter assay (Fig. 4, *A* and *B*). A promoter-less pET22b-eGFP vector was constructed by removing its T7 promoter (Fig. S2) and then the native *E. coli fliA* promoter or the *flhDC* promoter was cloned into it. The promoter activity was studied by
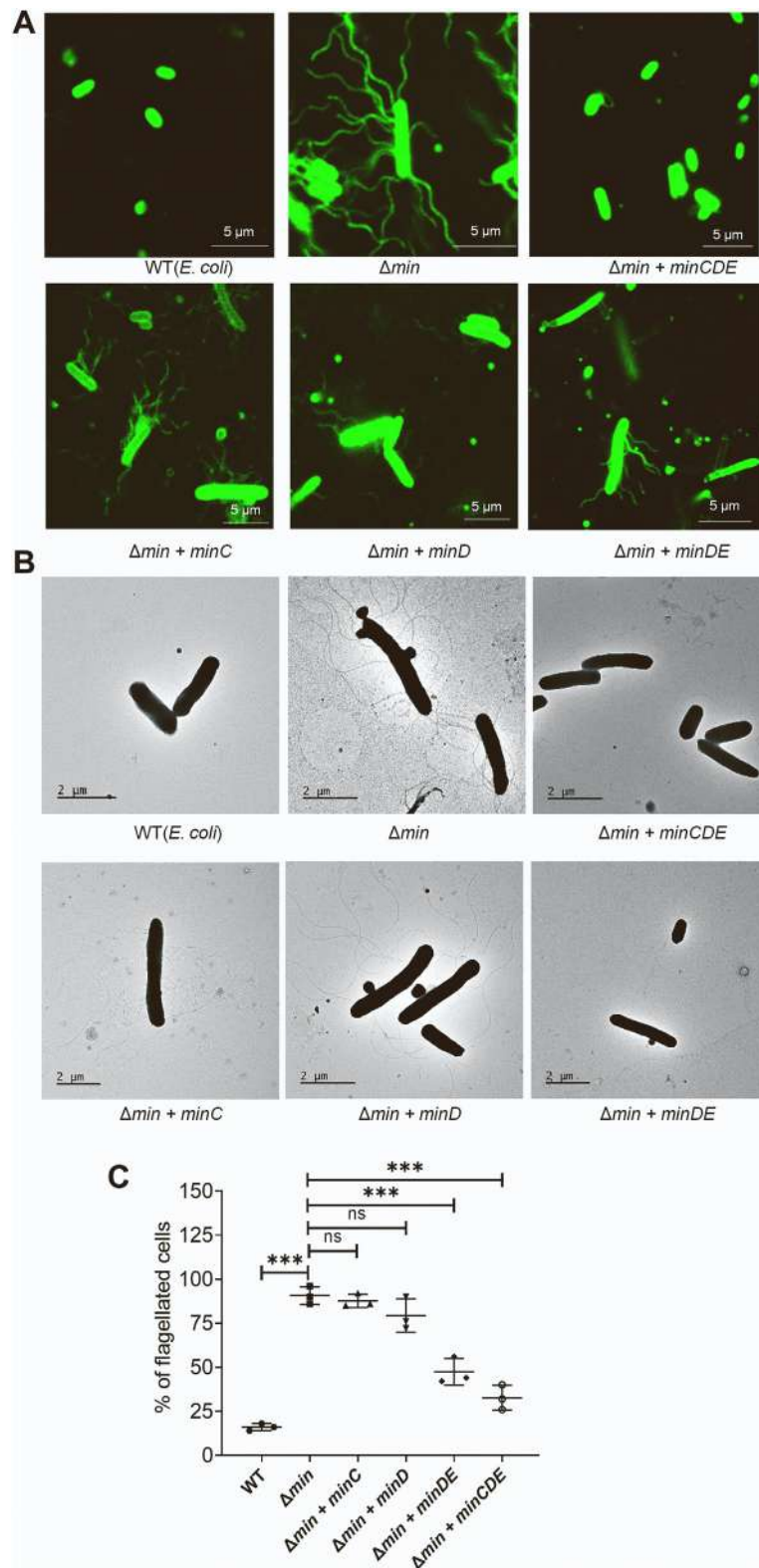
Figure 2. Phenotype of the Δ min cells. The *Escherichia coli* MG1655 (WT), *E. coli* (Δ *min*), and *E. coli* (Δ *min*) with various min components complemented cells were grown and bacterial morphology was observed using different techniques. *A*, *E. coli* flagella stained with Alexa Fluro-488 and observed using fluorescence microscope (the scale bar represents 5 μm). *B*, transmission electron micrographs showing the presence of flagella in different bacterial strains (the scale bar represents 2 μm). *C*, the %age of flagellated cells in each observed strain represent as scatter plot. Error bars shows the ± SEM values of three replicates (n = 50) determined using an unpaired parametric *t* test.
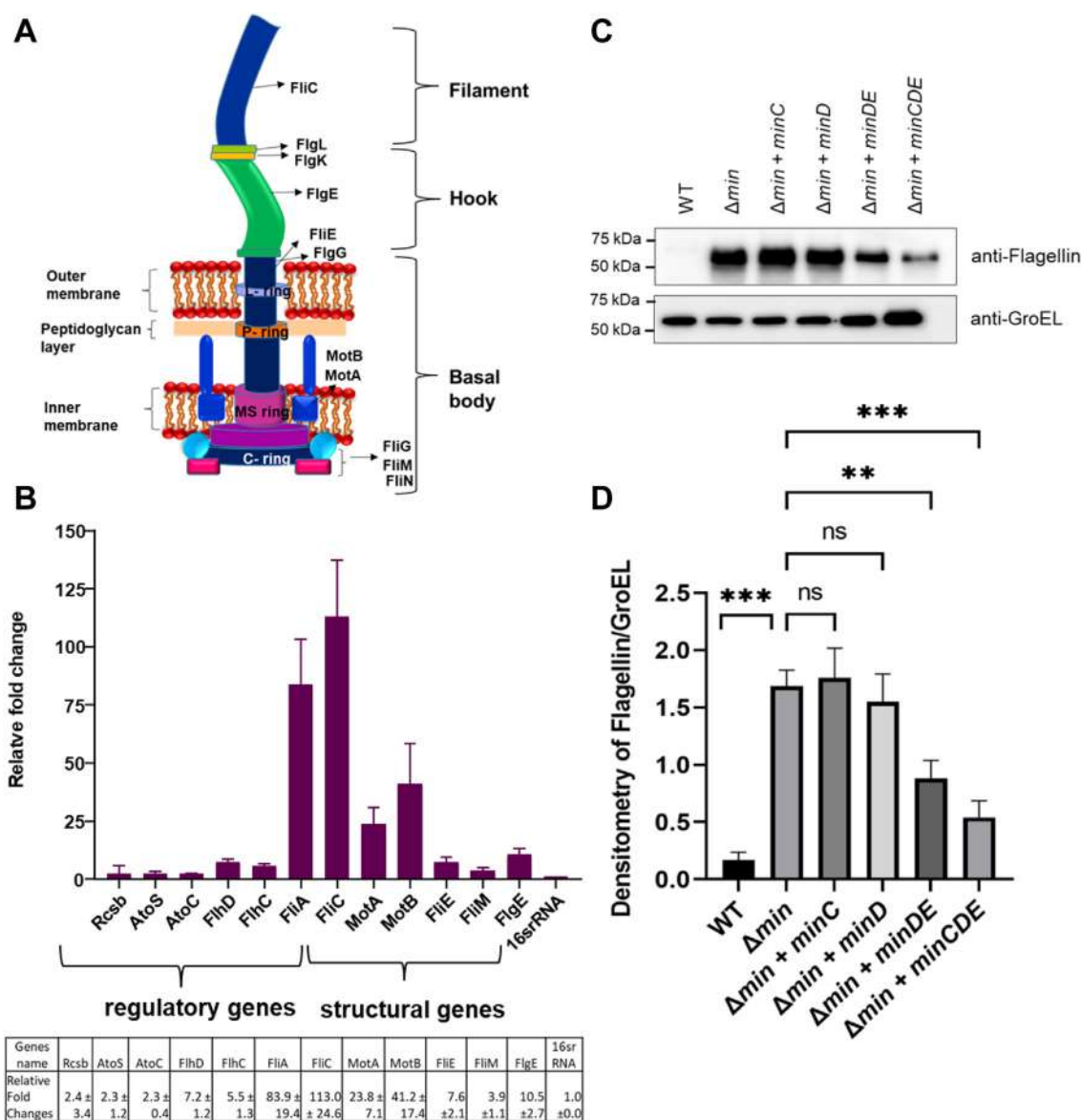
Figure 3. Flagellar gene expression in *Escherichia coli* (Δmin) cells. *A, cartoon representation* showing the flagella machinery and proteins involved in it. *B*, the RT-PCR analysis of flagellar gene expression in *E. coli* (Δ *min*) cells compared to *E. coli* (WT). Both the types of cells were grown in LB broth, total RNA was isolated, complimentary DNA was synthesized and RT-PCR was performed. The expression of flagellar genes in *E. coli* (Δ *min*) cells was plotted against WT. *C*, the Western blot of flagellin expression in *E. coli* (WT), *E. coli* (Δ *min*), and *E. coli* (Δ *min*) cells complemented with different min components using anti-flagellin antibody was performed. *D*, the relative intensity of flagellin with respect to GroEL was determined and plotted. The error bars show the ± SEM values and *p* values using an unpaired parametric *t* test. Each experiment was repeated three times.

measuring the expression of GFP by Western blot using an anti-GFP antibody (Fig. 4*C*). We observed that in *E. coli* (Δ *min*) cells, the *fliA* promoter got activated significantly, whereas, no activity was observed for the *flhDC* promoter. The results suggested that the Min system does not affect the *flhDC* expression, whereas, it negatively affects the *filA* expression. We further found that the complementation of *E. coli* (Δ *min*) cells with *minDE* or *minCDE* lead to reduced eGFP expression, whereas, complementation with any of the single Min components did not affect eGFP expression (Fig. 4, *D* and *E*). The eGFP intensity was also measured using a fluorimeter and we found that compared to the *E. coli* (Δ *min*) cells, the induction of *minDE* reduced the eGFP expression (Fig. 4*F*). Our results showed that the *fliA*

promoter activity was low in *E. coli* (WT) cells and high in *E. coli* (Δ *min*) cells. Moreover, the *fliA* promoter activity was reduced when *E. coli* (Δ *min*) cells were complemented with *minDE* indicated the role of MinDE in controlling *fliA* expression.

MinD does not interact with FlhDC, a class I transcription factor of flagellar regulation

FlhDC, a class-I flagellar protein, controls the expression and regulation of the class-II flagellar protein FliA, which in turn controls the expression of class-III genes (*fliC, motAB, cheAW, flgKL,* and *flgMN*) (31). Our results showed an upregulation of the *fliA* gene and other flagellar genes in *E. coli* (Δmin) cells (Fig. 3*B*) and this can be rescued with MinDE
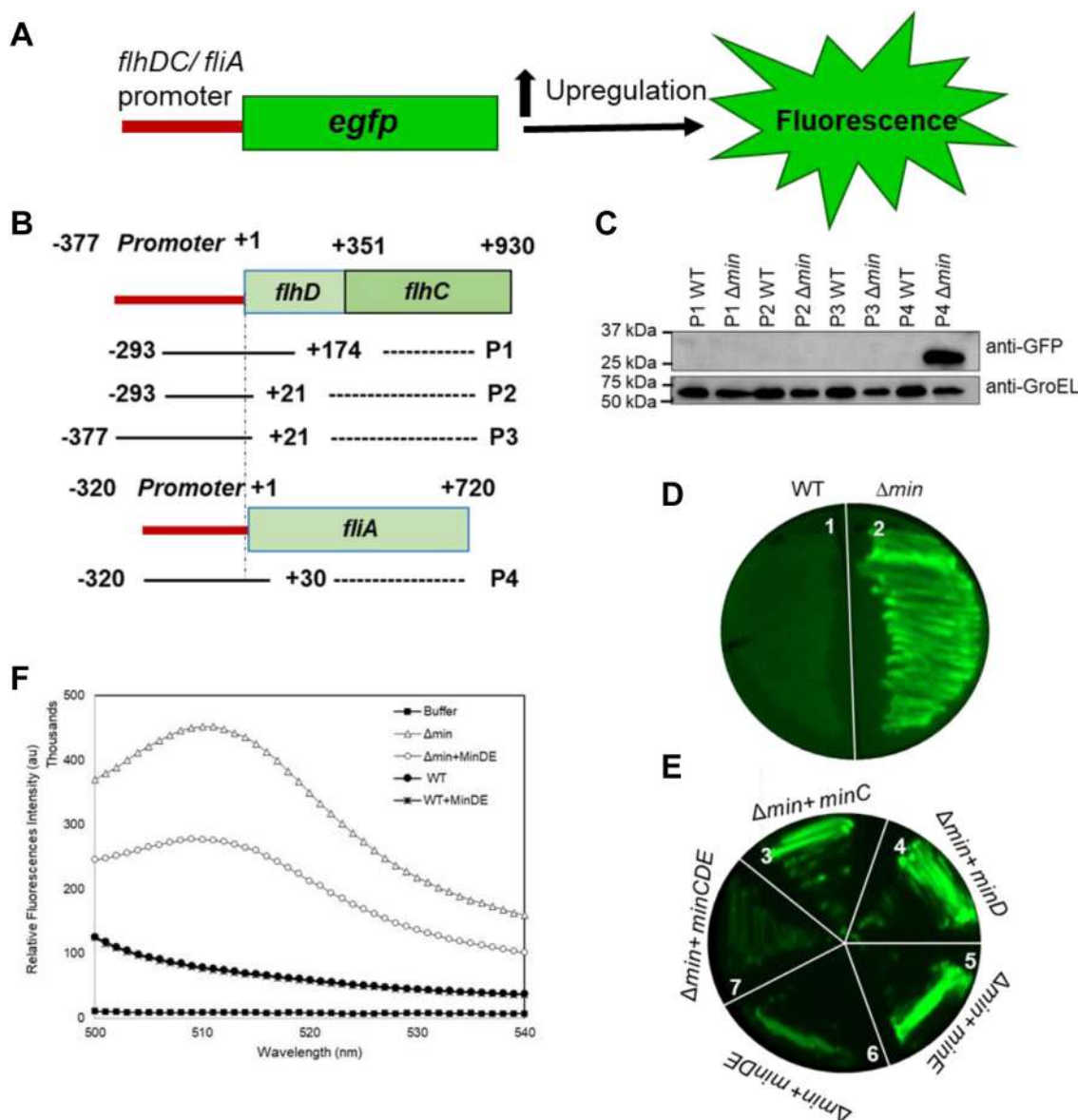
Figure 4. eGFP reporter assay. Native promoters of *flhDC* and *fliA* were cloned with eGFP reporter to check the expression of *flhDC* and *fliA* gene. eGFP expression was checked with anti GFP antibody, while keeping anti-GroEL as loading control. *A*, the *pictorial representation* of eGFP reporter assay was shown. *B*, the *schematic representation* of different truncated *flhDC* and *fliA* promoters constructed for the promoter assay. *C*, the expression of eGFP in the presence of different promoter constructs in *E. coli* (Δ *min*) cells and *E. coli* (WT) cells (P1 = *flhDC* 467 bp, P2 = *flhDC* 314 bp, P3 = *flhDC* 398 bp, P4 = *fliA* 350 bp). *D*, shows the *fliA* promoter activity in WT and in Δ*min* system (1): pCDFDuet-1-*fliAp*-eGFP-WT, (2): pCDFDuet-1- *fliAp*-eGFP (Δ *min*). *E*, shows *fliA* promoter with eGFP reporter was cloned into pCDFDuet-1 vector and the expression of *fliA* promoter was studied with various complementation of min proteins (3): pCDFDuet-1-*fliAp*-eGFP/ Δ *min* +*minC*, (4): pCDFDuet-1- *fliAp*-eGFP/ Δ *min* +*minD*, (5): pCDFDuet-1- *fliAp*-eGFP/ Δ *min* +*minE*, (6): pCDFDuet-1-*fliAp*-eGFP/ Δ *min* +*minDE* (7): pCDFDuet-1-*fliAp*-eGFP/ Δ *min* +*minCDE*. *F*, shows the eGFP fluorescent intensity in *E. coli* (WT), *E. coli* (Δ *min*), and *E. coli* (Δ *min*) cells complemented with *minDE*. eGFP, enhanced green fluorescent protein.

complementation. Thus, there is a possibility that MinDE represses the expression of the *fliA* promoter through binding to the FlhDC complex or to the promoter region of *fliA*. Our bioinformatics analysis showed that MinDE lacks DNA-binding domain, suggesting that MinDE does not bind to the promoter region of *fliA*; however, it may bind to the FlhDC complex, a class I transcriptional factor that controls *fliA* expression. In order to check this, we performed yeast two-hybrid assay. The yeast two-hybrid assay showed that MinC, MinD, or MinE did not interact with FlhDC or with other flagellar proteins (FliA or FliC) (Figs. 6*A* and S3). Our findings suggested that the regulation of flagellar expression by MinDE

is not through its interaction with flagellar master regulators and maybe through some other mechanism.

MinD homologs are flagella regulatory proteins

As MinDE did not directly interact with FlhDC, it encouraged us to identify the partners of MinDE that are involved in flagellar regulation. To understand the roles of MinDE homologs in other bacteria, we performed a BLAST search. Interestingly, our result showed that MinD homologs such as FlhG/FleN are flagella regulatory proteins (16, 32, 33). Multiple sequence alignments of MinD homologs showed highly conserved regions between these proteins (Fig. 5*A*).
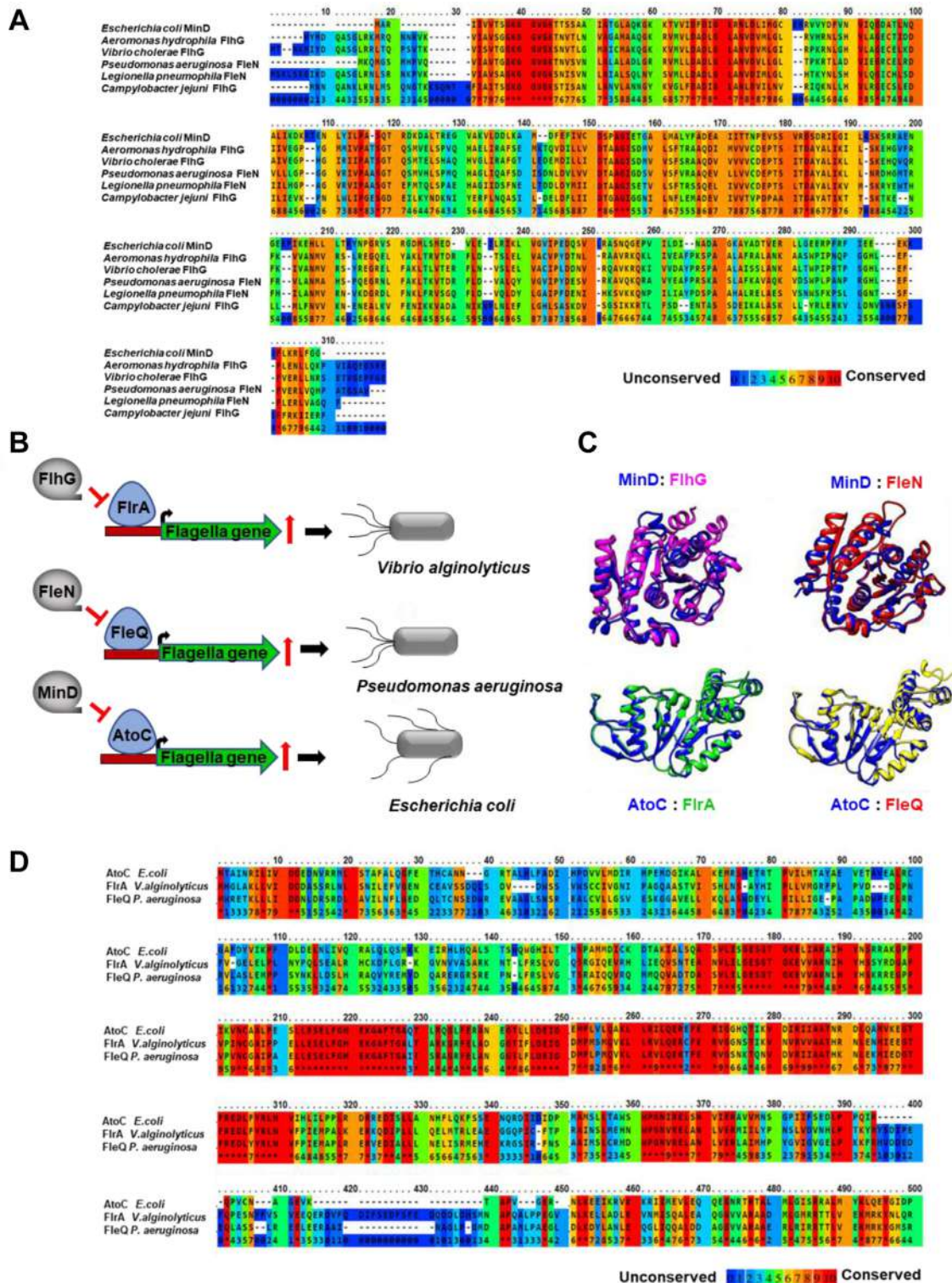
Figure 5. *Escherichia coli* MinD homologs in bacteria and MinD binding partners for flagella synthesis. Multiple sequence alignment of MinD homologs from different bacteria was performed using Praline multiple sequence alignment program and is shown in *A*. *B*, *schematic diagram* for MinD homologs and their regulatory partners involved in flagellation in different bacteria. *C*, shows the structural alignment of MinD (PDB: 3Q9L), FlhG (PDB: 4RZ2), and FleN (PDB: 5J1J) was performed using Chimera (MinD-*blue colour ribbon*, FlhG-*pink colour ribbon*, and FleN-*red colour ribbon*). This panel also shows the structural alignment of "FleQ (139aa–394aa) with "AtoC" (139aa–378aa) and "FlrA" (143aa–374aa) with "AtoC" (139aa–378aa). FleQ, FlrA, and AtoC structure was downloaded from Alpha fold database and the structure was analyzed by PROCHEK. The structural alignment of FleQ (*Pseudomonas aeruginosa*), FlrA (*Vibrio alginolyticus*), and AtoC (*Escherichia coli*) performed using Chimera (AtoC-*blue*/FlrA-*green*/FleQ-*yellow*). *D*, shows the multiple sequence alignment of FleQ, FlrA, and AtoC.

Role of Min system in flagellation

FlhG is a MinD-like ATPase that binds to the cell membrane and controls the flagella number in *Vibrio alginolyticus* (20). Similarly, FleN, another homolog of MinD, controls the flagella number in *P. aeruginosa* (16). We further performed structural alignment between MinD and FlhG/FleN. The results showed that the structure of MinD is quite similar to that of FlhG (RMSD = 1.05 Å) and FleN (RMSD = 1.09 Å) (Fig. 5*C*). Interestingly, both FlhG and FleN are absent in *E. coli*. As in *E. coli*, MinD is a part of the Min system; these observations indicated a possible involvement of the Min system during the flagellation in *E. coli*.

MinD interacts with AtoSC, a homolog of FlrA/FleQ

Like MinD, its homologs FlhG/FleN also do not contain any DNA-binding domains, whereas they negatively regulate flagellar gene expression by interacting with sigma-54–dependent regulators FlrA/FleQ, respectively (Fig. 5*B*). FlrA and FleQ interact with the promoter region of the *fliA* gene and induce its expression, which then positively regulates the expression of flagellar genes (34–36). We hypothesized that MinD might work in a similar manner by interacting with a regulatory protein that is similar to FlrA/FleQ (Fig. 5*B*). To identify their homolog in *E. coli*, we performed a BLAST search of FlrA/FleQ against the *E. coli* K12 genome. Interestingly, we found that the *E. coli* protein AtoC showed more than 40% similarities with these proteins, and upon multiple sequence alignments, we found that these proteins share several conserved regions (Fig. 5*D*). Further, the structural alignment showed that AtoC possesses similar folds as both the proteins, with RMSD 0.5-0.8 Å (Fig. 5*C*). We hypothesized that MinD may directly interact with AtoC and in turn, regulates the flagellar gene expression in *E. coli*.

To validate our hypothesis, we performed yeast two-hybrid assay, which showed no direct interaction between MinD and AtoC (Fig. 6*B*). AtoC is generally present as AtoSC complex, where AtoS is the sensor histidine kinase that regulates AtoC functions (37). A study by Theodorou *et al.* showed that AtoSC is a TCS that positively regulates motility and flagellar gene expression in *E. coli* (15). Thus, we were curious to know if MinD interacts with the AtoSC complex and in turn controls motility. Interestingly, our yeast two-hybrid result showed that MinD, in fact, directly interacts with AtoS rather than AtoC (Fig. 6*B*). To further validate the MinD and AtoS interaction, we performed pull-down assay. For this, we cloned and purified GST-MinD and His-tagged cytoplasmic parts of AtoS (232–608aa, cyto-AtoS). GST-MinD (5 µM) was incubated with His-cyto-AtoS (5 µM) and pulled down using cobalt resin. MinD that bound with cyto-AtoS was eluted using imidazole, and Western blotting was performed using anti-GST and anti-His antibodies. The pull-down assay showed that MinD directly interacts with cyto-AtoS (Fig. 6*C*). Additionally, we examined the interaction of AtoSC with flagella regulator FlhDC using a yeast two-hybrid assay, which did not show any interaction (Fig. 6*D*). Our result was consistent with the previous findings that AtoC is probably interacting with the promoter region of *fliA* and *flhDC* operons (15).

AtoSC regulates *fliA* expression through its interaction with *fliA* promoter, whereas MinD regulates flagellation through its interaction with AtoS of AtoSC

It has previously been established that the AtoSC complex positively regulates the motility in *E. coli* (15). As MinD directly interacts with AtoS, we wanted to determine the impact of the MinD–AtoS interaction on bacterial motility. We performed an eGFP reporter assay to study the effect of MinD and AtoSC on *fliA* promoter activity (Fig. 6*E*). We transferred cyto-AtoSC and MinD into pET-P4-eGFP/C41 cells and found that *fliA* promoter activity was high in the presence of AtoSC, whereas the promoter activity went down when MinD was expressed (Fig. 6*F*). The results suggested that MinD interacts with AtoS to control the flagellation in *E. coli*.

MinDE complex regulates AtoSC phosphorylation

Theodorou *et al.* have shown that phosphorylation of AtoC is necessary for regulating motility. So, next we wanted to measure the phosphorylation status of AtoSC in the presence of MinDE, but we failed to measure it directly (data not shown). Upon stimuli, AtoS undergoes autophosphorylation and transfers its phosphate group to AtoC (37). The phosphorylated AtoC then binds to the *atoDAEB* promoter and positively regulates its expression (Fig. 7*A*). It was also shown that the ATP-binding–deficient and phosphorylation-deficient mutants of AtoS were unable to activate *atoDAEB* promoter activity. In order to understand the effect of MinD on regulating AtoS phosphorylation, we constructed a reporter assay where the *atoDAEB* promoter was cloned with a GFP reporter and the promoter activity was studied in the presence of AtoSC and MinDE. A positive regulation of AtoS phosphorylation will lead to higher AtoC phosphorylation and activation of the *atoDAEB* promoter, leading to higher GFP expression. Our results showed that in the presence of AtoSC, the promoter activity of the *atoDAEB* is enhanced; however, the expression of MinDE in these cells reduced the *atoDAEB* promoter activity, indicating the involvement of MinDE in negatively regulating AtoS phosphorylation (Fig. 7*B*). It is reported that phosphorylation of AtoC leads to higher flagellation and motility in *E. coli*. As MinDE also negatively regulates flagellation (Fig. 2), the results indicate that inhibition of flagellation in *E. coli* may be attributed to MinDE-mediated inhibition of phosphorylation of the AtoSC complex.

Discussion

Simultaneous examination of bacterial division and motility is extremely challenging; thus the relationship between cell division and cell motility is poorly understood. A recent study showed that *Myxococcus xanthus* stops its motility during its division and resumes only after completion of the division (38). Similarly, during the exponential growth of *E. coli*, the flagellar gene expression is repressed and bacterial adhesion is enhanced (39). Likewise, in *Caulobacter crescentus*, before undergoing division, the bacterium modifies its flagella into a stalk-like structure that helps it to attach to the surface and stop its motility (40). Thus, it is evident that there is a direct
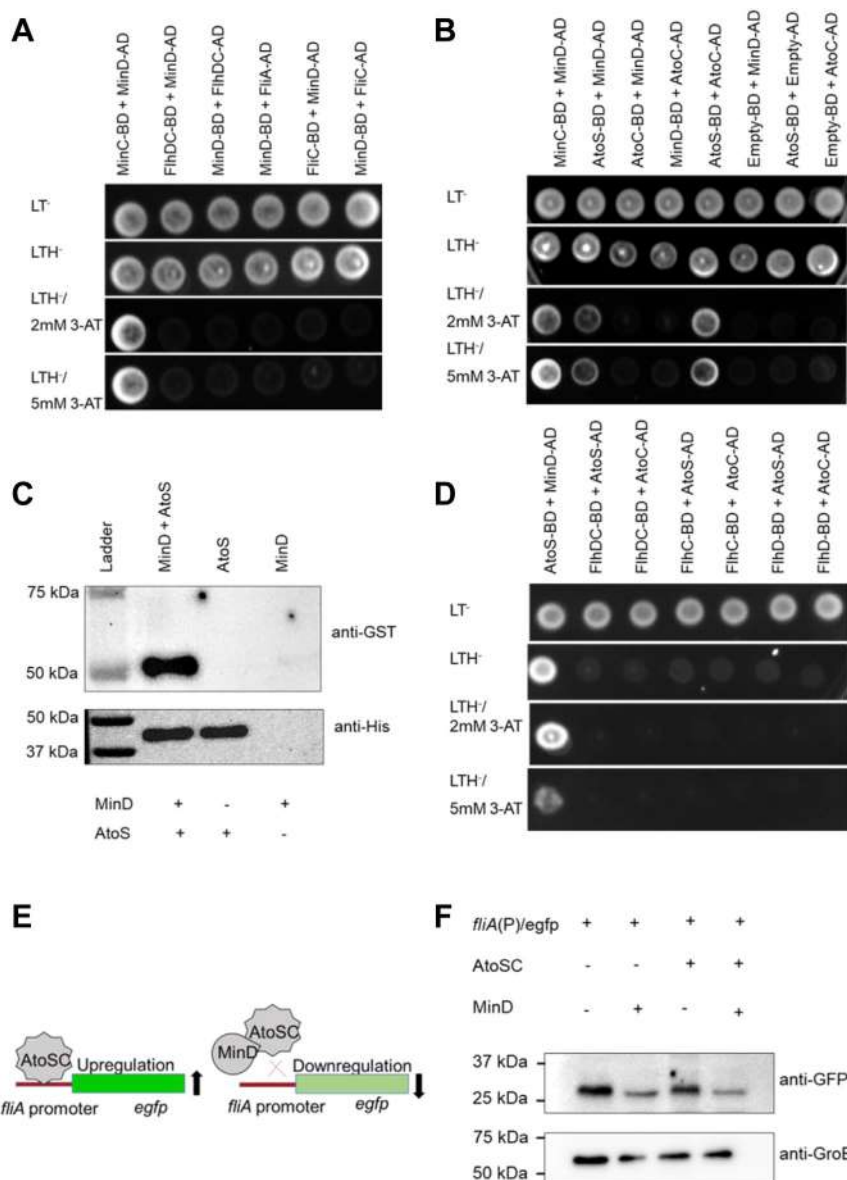
Figure 6. Interaction of MinD with AtoSC, FlhDC, and role in *fliA* expression. Interaction between different proteins was assessed through HIS3 reporter assay using yeast two-hybrid system. Various combinations of proteins were cotransformed into HFY7c yeast strain, and 10 μl of each cotransformed cells were spotted on synthetic defined (SD) medium as described in methods section. The cells were grown at 30 °C for 3 to 4 days. Positive interaction was indicated by the presence of colonies in -Leu-Trp-His plates with 3-AT. *A*, shows the interaction of MinD with FlhDC, FliA, and FliC flagellar proteins. *B*, shows the interaction of MinD with AtoC and AtoS on yeast two-hybrid assay. Further, to show the interaction between MinD and AtoS in *in vitro* system, a pull-down assay was performed using His-AtoS and GST-MinD purified proteins. His-AtoS was pulled using Cobalt NTA resin and a Western blot was performed using anti-His or anti-GST antibodies. The Western blot is shown in *C*. The interaction of AtoSC with FlhDC through yeast two-hybrid system is shown on *D*. *E*, shows the schematic representation of eGFP reporter assay. *F*, to check the role of MinD and AtoSC in regulating expression of *fliA* promoter, eGFP expression was monitored with an anti-GFP antibody. The plasmid containing MinD and cyto-AtoSC was transferred into pET-P4-eGFP/C41strain the expression of eGFP was monitored using Western blot. 3-AT, 3-amino-1,2,4-triazole; eGFP, enhanced green fluorescent protein.

link between cell division and motility in bacteria; however, the specific molecular mechanism by which these two processes are linked is not yet clear. While observing the *E. coli* under live-cell microscopy, we found that compared to the *E. coli* (WT), the *E. coli* (Δ *min*) bacteria show higher motility (Fig. 1). We further confirmed using the soft agar motility assay that the hypermotility was due to the absence of Min proteins and can be rescued by overexpressing Min proteins (Fig. 1). Specifically, MinDE and MinCDE complementation was able to rescue the motility phenotype considerably, whereas individual min proteins could not. Subsequently, we noted that the

increased motility was attributed to hyperflagellation in the *E. coli* (Δ *min*) cells (Fig. 2). The Min system in *E. coli* is widely studied for its role in inhibiting polar Z-ring formation and guiding proper cell division. However, its role in *E. coli* motility was never explored. In this study, we focused on understanding the role of the Min system in bacterial motility.

The motility of various bacteria differs from each other and is dependent on the environment. Although the basic design of the bacterial locomotory organ, the flagellum, is similar in all species, there are differences in the number and arrangement of the flagella. In addition, the mechanisms of flagellar
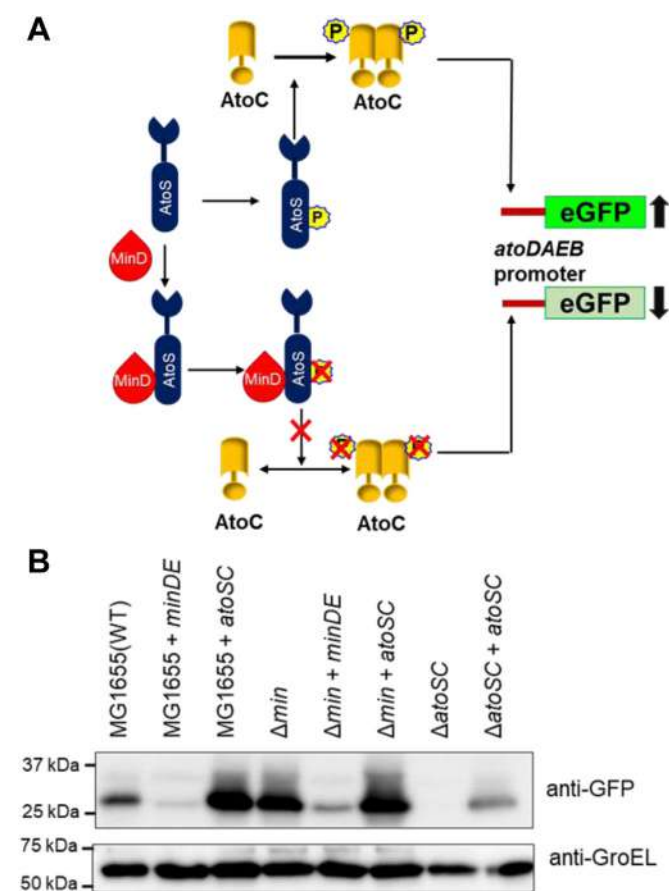
Figure 7. Effect of MinDE on AtoSC function. *A*, a *pictorial representation* of the pathway of AtoSC mediated *atoDAEB* gene expression was shown. *B*, shows the effect of MinDE and AtoSC on *atoDAEB* promoter activity. The pACYCDuet-1- *tac* -minDE, and pACYCDuet-1- *tac-atoSC* plasmids along with pET22b-*atoDAEBp*-eGFP vector transferred into the *E. coli* (WT), *E. coli* (Δ *min*), and *E. coli* (Δ *atoSC*) cells and the *atoDAEB* promoter activity was studied using anti-GFP antibody while GroEL was used as loading control. eGFP, enhanced green fluorescent protein.

biosynthesis and flagellar regulatory machinery differ between species. Flagellation in different bacteria is controlled by >60 genes that are majorly divided into class I, class II, and class III flagellar genes. The class I flagellar genes act as the master regulator, which directly regulates the promoter activity of class II flagellar genes and controls the expression of class III flagellar genes. FlhDC, FleQ, and FlrA are the most common class I master regulators found in different flagellated bacteria (41–43). The class-II operon encodes for the genes responsible for basal body formation (*i.e.*, FliM, FliE, etc), the flagellar export system (*i.e.*, FlhA, FlhB), and other regulatory proteins (*i.e.*, FliA and FlgM). FliA, a sigma 28 factor, is a transcriptional activator of class III flagellar genes, whereas FlgM, an anti-sigma factor, is a transcriptional repressor for class-III operon (44). Similarly, FlhF, FlhG, FleN are essential for defining flagella numbers and the correct placement of flagella in various organisms. For example, in *Vibrio, Bacillus*, and other related species, FlhF and FlhG work in coordination to control flagellar location and number. The deletion of FlhF leads to the mis-localization of flagella, and the FlhG deletion caused hyperflagellated phenotype (32, 45). Likewise, in *P. aeruginosa*, deletion of FleN, an ortholog of FlhG, resulted in

hyperflagellation and reduced motility (16). Interestingly, the absence of FlhG in *C. jejuni* (*C. jejuni*), apart from inducing flagellation, also resulted in polar minicell formation, a phenotype found during the deletion of the Min system in *E. coli.* The Min system is absent in *C. jejuni* and FlhG or FleN are absent in *E. coli*. Our experiment showed that the deletion of the Min system in *E. coli* generates both motile cells and polar mini cells (Fig. 1*A*). Incidentally, FlhG, FleN, and MinD, belong to the ParA ATPase family and share a high degree of structural and functional similarities. Although the role of FlhG and FleN are well studied in flagellation and motility, the role of the Min system during flagellation in bacteria is not yet known.

The increased motility of *E. coli* (Δ *min*) cells made us curious to examine the bacterial morphology and their flagellation pattern. The fluorescence microscopy and TEM imaging showed that the *E. coli* (Δ *min*) cells contain long, dense, and peritrichous flagella (Fig. 2). This result is consistent with the previous findings that the deletion of MinD homologs, that is, FlhG and FleN, etc., leads to multiflagellated phenotypes (16, 45). We wanted to know why such multiflagellated phenotype was found in the absence of the Min system. This phenotype in the *E. coli* (Δ *min*) cells could be due to the higher expression of flagella regulatory genes or the flagellar structural genes. From qRT-PCR analysis, we found that the expression of the flagella regulatory gene *fliA* and the class-III structural genes like *fliC*, *motA*, and *motB* were increased by several folds in the *E. coli* (Δ *min*) cells (Fig. 3*B*). This result was also supported by the Western blotting analysis, which showed flagellin, a core structural flagellar protein, was highly expressed in these cells (Fig. 3, *C* and *D*). In order to identify if and how the Min system controls the flagellar expression, we need to first understand the flagellar biosynthesis pathway; a concise description is given in Figure 8*C*. Briefly, the master regulator FlhDC (class I flagellar gene) positively controls the expression of the flagellar regulator FliA (class II flagellar gene), which in turn controls the expression of other flagellar proteins (class III flagellar genes). The qRT-PCR data showed that there was an upregulation of most of the flagellar regulators and structural genes (Fig. 3*B*). In addition, Western blot analysis showed that *E. coli* (Δ *min*) cells produce more flagellin than WT cells and that the complementation of the MinDE/MinCDE proteins in *E. coli* (Δ *min*) cells decreased the synthesis of flagellin (Fig. 3, *C* and *D*). This suggested that either MinDE directly interacts with the master regulator FlhDC and controls the expression of downstream genes or controls the expression of flagellar regulator *fliA* expression through binding to its promoter region. Our experiment showed that there is no direct interaction of MinDE with FlhDC (Figs. 6*A* and S3). In order to identify if MinD/E can interact with *fliA* promoter, we performed *in silico* evaluations. The *in silico* analysis showed that like its homologs FleN and FlhG, the DNA binding domain is absent in MinD, suggesting that it may not interact with the *fliA* promoter. Previous studies showed that several MinD homologs (*i.e.*, FlhG/FleN, etc.) negatively control flagellation in different bacteria by interacting with different regulatory proteins (46). For example, FlhG or FleN deletion leads to hyperflagellation
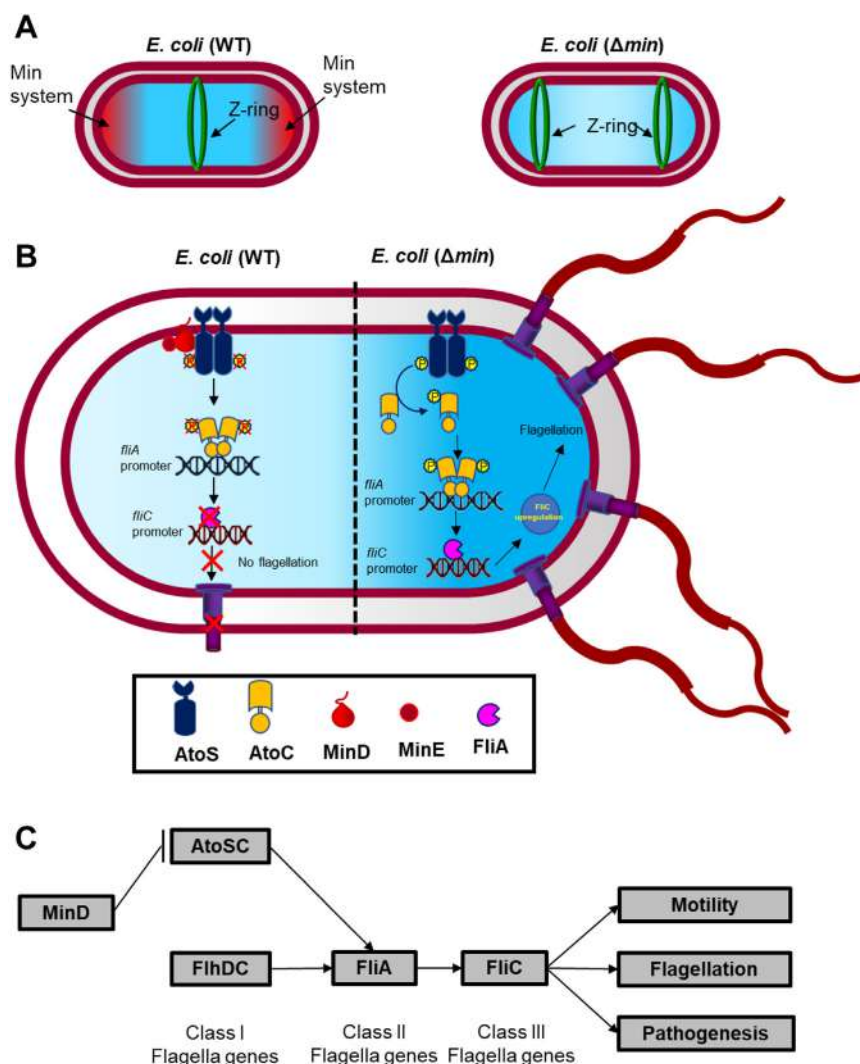
Figure 8. Mechanism of MinDE mediated flagellation in *Escherichia coli*. Min deletion *E. coli* shows hyper flagellated morphology. The position of the Z-ring (divisome ring) in *E. coli* (WT), and *E. coli* (Δ *min*) cells is schematically depicted in *A*, which highlights the functions of the Min system in *E. coli* during cell division. *B* and *C*, are showing the suggested mechanism by which MinDE may control the flagellation. Briefly, AtoC of AtoSC complex binds to the *fliA* promoter and controls the *fliA* expression, which in turn controls expression of flagellar genes. MinDE complex interacts with AtoS and hinders binding of AtoC to the *fliA* promoter and thus inhibits flagellation. In the absence of MinDE, AtoSC is free to induce *fliA* expression and thus hyper flagellation occurs.

morphology similar to *E. coli* (Δ *min*) cells (45). Further, similar to MinD, its homologs FlhG/FleN also lack a DNA binding motif; however, they act as antiactivators for flagellation. Previous studies have reported that FlhG/FleN work with sigma factor 54 activators FlrA/FleQ that directly bind to the promoter region of class-II flagellar gene *fliA* and thus regulate flagellar gene expression (19, 45). So, there is a possibility that MinD has another partner that binds to the promoter region of *fliA* and controls the flagellation in *E. coli*. When FlrA/FleQ sequences were BLAST against the whole *E. coli* K-12 genome, a highly similar protein AtoC was identified. Similar to FlrA and FleQ, AtoC also belongs to the sigma-54–dependent member and is present as a complex AtoSC. This AtoSC complex belongs to the TCS, where AtoS acts as the sensor kinase and AtoC acts as the response regulator. Interestingly, AtoC homologs FlrA and FleQ lack the phosphorylation domain and the genes encoding a sensor kinase upstream of these genes and do not belong to the TCS (47, 48). A study by

Theodorou et al. has shown that the AtoSC complex controls *E. coli* motility by regulating transcription of both class-I (*flhDC*) and class-II (*fliA*) flagella operons, and AtoSC more effectively enhances the *fliAZY* operons rather than *flhDC* operon (15). The genome-wide promoter analysis of AtoC revealed that the *fliA* promoter contains an AtoC binding site (49). This suggested that to control the flagellation, MinD probably interacts with AtoC. However, our results showed that MinD does not interact with AtoC; instead, it interacted with its complex partner AtoS (Fig. 6*B*). Both MinC and MinE do not interact with either AtoS or AtoC (Fig. S3). AtoS, a sensor histidine kinase, is mostly found in eubacteria that form TCS with AtoC, where AtoC is the response regulator that controls certain gene expressions. In its ATP-bound form AtoS undergoes autophosphorylation and transfers the phosphate group to AtoC, which facilitates dimerization of AtoC. The AtoC dimer binds to the promoter region of target genes and controls their expression (50, 51). As ATP binding and

phosphorylation of AtoS is important for controlling the function of AtoC, we speculated that MinD controls AtoSC functions through its binding to the AtoS protein.

Now the question arises; can MinD control flagellar gene expression through AtoSC and how MinD is doing it? Previous studies have shown that MinD homologs FlhG/FleN interact with FlrA/FleQ and repress the expression of flagellar genes (17, 19). In order to identify a similar mechanism, the *fliA* promoter activity was studied in the presence of AtoSC alone or with both AtoSC and MinD (Fig. 6F). For this study, native *fliA* promoter was cloned with an eGFP reporter in a promoter-less eGFP vector, where a higher promoter activity will result in higher eGFP expression and will show higher fluorescence. We observed that *fliA* promoter activity was decreased when MinD was expressed in *E. coli* C41 (pET-P4-eGFP/C41) cells, and it increased upon expression of the cyto–AtoSC complex, which further decreased when both cyto-AtoSC and MinD were overexpressed (Fig. 6F). These observations confirmed that MinD interacts with the AtoSC complex and negatively regulates *fliA* expression and thus the flagellar expression. As a control, *flhDC* native promoter was used, which did not show any eGFP fluorescence in *E. coli* (Δmin) cells, which indicated that MinD neither interacted with FlhDC nor binds to its promoter. This further confirms our hypothesis that FlhDC does not play any role in the MinD-controlled flagellation in *E. coli*.

The AtoSC two-component signal transduction system in *E. coli* plays a crucial role in regulating the expression of genes within the *atoDAEB* operon, which is essential for short-chain fatty acid catabolism. Following the induction by acetoacetate, the AtoS sensor kinase initiates autophosphorylation, leading to the subsequent phosphorylation and activation of the response regulator AtoC. The phosphorylated AtoC binds to the *ato-DAEB* promoter and positively regulates its expression. The phosphorylation-deficient mutant of AtoS was unable to activate AtoC. Hence, the functionality of the complex requires phosphorylation of both the proteins. The results of yeast two-hybrid and pull-down assays suggested that MinD interacts with AtoS. Further, the AtoSC complex positively regulates *fliA* promoter expression, and MinDE negatively regulates *fliA* promoter activity. The phosphorylation of AtoC is necessary for controlling *E. coli* motility. So, in order to identify the regulation of MinDE in AtoSC phosphorylation and functions, we studied the *atoDAEB* promoter activity in the presence of MinDE. We hypothesized that if MinDE inhibited AtoS phosphorylation, then the *atoDAEB* promoter activity would be downregulated (Fig. 7A). While studying the *atoDAEB* promoter activity in *E. coli* WT and (Δmin) cells, we found that MinDE decreased the promoter activity, whereas AtoSC enhanced the *atoDAEB* promoter activity (Fig. 7B). These findings indicated that MinDE may inhibit AtoSC phosphorylation.

The Min oscillation is important for the midcell placement of the Z-ring (Fig. 8A). Based on our findings, we hypothesize that the AtoSC complex interacts with the *fliA* promoter and positively regulates its expression, which in turn controls the expression of downstream flagellar proteins and flagellar expression. Our findings suggest that in WT *E. coli*, MinD interacts with the AtoS protein of the AtoSC complex and

inhibits AtoC's interaction with the *fliA* promoter through inhibiting AtoS phosphorylation. Due to the lack of this interaction, there is a reduction in *fliA* expression that leads to lower flagellar expression. In the absence of MinD, the AtoSC complex is free to bind to *fliA* promoter and induces *fliA* expression, leading to higher flagellar expression (Fig. 8B). Our study suggests that along with the cell division, the Min system is also involved in *E. coli* motility.

Experimental procedures
Materials

Hepes, Tris, KCl, NaCl, sodium phosphate, synthetic defined medium -Leu-Trp-His (SD medium), 3-amino-1,2,4-triazole (3-AT), and IPTG were purchased from MP Bio-medicals, and LB broth and LB agar were obtained from HiMedia. Anti-flagellin and anti-GroEL antibodies were purchased from Abcam. The remaining chemicals used were of molecular biology grade and were obtained from Sigma-Aldrich.

Strains and plasmids

E coli Δmin (JS964) was a gift from Dr Lutkenhaus lab, and WT lab strain MG1655 (CGSC6300) was used in all experiments (7). The Δ*atoSC* strain was a kind gift from Hirofumi Aiba (Nagoya University) (52). Cloning of *minD*, *atoS*, cyto-*atoS*, and *atoC* in respective plasmid vectors was constructed by amplifying the specific ORF from *E. coli* K-12 genomic DNA. The cloning was confirmed by restriction digestion and DNA sequencing. All the strains and plasmids used in this study are summarized in Tables S1 and S2.

Protein overexpression and purification

His-MinD and GST-MinD were purified using previously described methods (9). The purified protein was dialyzed against buffer A (50 mM Hepes buffer pH 7.4, 150 mM KCl, 10% glycerol) and stored at –80 °C until further use. *E. coli* BL21 [DE3] cells carrying ORF of the cytoplasmic fraction of AtoS (cyto-AtoS)/BL21 [DE3] cells were grown at 37 °C in Luria–Bertani medium containing 50 μg/ml kanamycin. At A_{600} ~0.5, 1 mM IPTG was added to the cells to induce recombinant protein production (50). Cells were harvested using centrifugation after 4 h postinduction, resuspended in ice-cold lysis buffer [50 mM Hepes pH 7.4, 300 mM KCl, and 1% (v/v) Triton X-100] containing lysozyme (60 μg/ml), protease inhibitor cocktail, and cells were broken using Stansted pressure cell homogenizer. The cell lysate was centrifuged at 10,000*g* for 30 min at 4 °C, and the supernatant was treated with DNase I (6 units/ml) for 10 to 15 min at 4 °C. The lysate was further centrifuged at 10,000*g* for 30 min at 4 °C, and the supernatant was subjected to affinity chromatography using Ni^{2+}–NTA agarose column (37). The column was washed with ten column volumes of washing buffer (50 mM Hepes pH 7.4, 300 mM KCl, and 20 mM imidazole). His-tagged proteins were then eluted with 50 mM Hepes (pH 7.4) buffer containing 300 mM KCl and 300 mM imidazole.

Motility assay

E. coli WT (MG1655), *E. coli* (Δ*min*), and *E. coli* (Δ*min*) complemented with different Min components were grown in M-media (LB broth + 0.5% NaCl). From this, 3 μl of culture was spotted on plates containing 0.3% agar in M-media and grown at 37 °C. The motility was observed visually after 12 to 18 h. For live-cell motility imaging, WT *E. coli* (MG1655), *E. coli* (Δ*min*), and Δ*min* cells complemented with *minCDE* were inoculated into the LB broth and grown overnight at 37 °C. From this, 1% of the culture was inoculated and grown in a flat, wide-bottom flask at 37 °C until A_{600} reached ∼0.5, where it was added with 1 mM IPTG and grown for 2 h at 60 rpm. From this, 2 μl of culture was placed on the glass slide, and the motility of the cells was observed under the live-cell imaging microscope (Zeiss, cell discoverer) with a 50× water immersion lens.

Flagella staining and imaging

Flagella were stained with Alexa-488 fluorescent dye as described previously with slight modification (53). Briefly, *E. coli* WT (MG1655), *E. coli* (Δ*min*), and different Min complementation strains were inoculated into the LB broth and grown at 37 °C overnight. From this, 1% of the culture subinoculated into the M-media and allowed to grow at 37 °C for 5 to 6 h at 60 rpm in a flat, wide-bottom flask. Culture (0.5 ml) was pelleted at 1000*g* and resuspended in 1 ml of 0.01 M potassium phosphate buffer, pH 7.4, containing 67 mM NaCl, 0.4 mM EDTA, and 0.002% Tween 20. To 500 μl of the bacterial suspension, 10 μl of Alexa-488 (5 mg/ml) and 50 μM of sodium bicarbonate were added and incubated for 2 h at room temperature. The suspension was washed twice with the above buffer at 500*g* for 5 min. Two microliters sample was taken on a glass slide and observed under a confocal microscope (Leica STED-SP8 microscope). For electron microscopy analysis of flagella, *E. coli* (WT), *E. coli* (Δ*min*), and *E. coli* (Δ*min*) containing min components were grown in M-media, and bacteria were fixed with 2.5% glutaraldehyde for 10 min. Negative staining was performed using the previously described protocol (3). A drop of bacteria culture was applied to a formvar-carbon coated copper grid, negatively stained with 2% uranyl acetate, air dried, and were visualized using a transmission electron microscope (JEOL-TEM JEM-2100 Plus).

RT-PCR analysis of flagellar genes

E. coli cells from the motility area of WT and Δ*min* was swabbed into the motility media and grown at 37 °C. From the exponentially growing cell, total RNA was isolated using a bacterial RNA isolation kit (Qiagen), and complimentary DNA was prepared from 0.2 μg of total RNA using PrimerScript RTase reverse transcriptase (Takara). The resulting DNA was quantified and subjected to qRT-PCR using SYBER Green Master mix (Applied Biosystems). The relative expression of target genes was calculated using the $2^{-\Delta\Delta CT}$ method by taking 16srRNA as a reference gene (54, 55).

Immunoblotting

An equal number of bacteria cells *E coli* (WT), *E. coli* (Δ*min*), and *E. coli* (Δ*min*) complemented with different Min components were loaded onto the SDS-PAGE. After electrophoresis separation, the samples were transferred onto a poly(vinylidene fluoride) membrane using a Mini *Trans* Blot apparatus (Bio-Rad) at 90 V for 2 h in Towbin transfer buffer. Blots were blocked using 5% skim milk prepared in Tris-buffered saline with Tween 20 for 1 h. To detect the flagellar filament protein flagellin, the membrane was immune-stained with the rabbit anti-flagellin polyclonal antibody with a dilution of 1:10,000 (Abcam-ab93713), and after washing with Tris-buffered saline with Tween 20, the blot was incubated with anti-rabbit antibody labeled with horseradish peroxidase (anti-rabbit-HRP-A6154) (1:10,000). The anti-GroEL monoclonal antibody was taken as loading control (Abcam-ab82592), and anti-mouse antibody (1;10,000 dilution) was used as the secondary antibody. The expression of flagellin was quantified densitometrically using ImageJ software (https://imagej.net/ij/).

Yeast two-hybrid assay

Yeast two-hybrid analysis was performed using the protocol mentioned earlier, where the yeast strain HFY7c containing plasmids pGAD424 (Clontech) with the GAL4 activating domain (GAL4-AD) and PGBT9 (Clontech) with the GAL4 DNA-binding domain (GAL4-BD) were used (56). For the yeast two-hybrid analysis, HIS3 was used as a nutritional reporter system. Briefly, yeast strain HFY7c was grown at 30 °C in YPD broth until midlog phase (A_{600} = 0.5–0.8). Once it reached the midlog phase, competent cells were prepared, and various combinations of GAL4-AD and GAL4-BD containing MinC, MinD, AtoC, AtoS FlhD, FlhC, FliA, and FliC were cotransformed into the competent cells. The positive transformants were screened on synthetic defined medium (SD medium) without leucine and tryptophan. To verify interaction, cotransformants were spotted on -Leu-Trp-His selection media plates without and with various concentrations of 3-AT and grown at 30 °C for 3 to 4 days. Yeast transformants exhibiting growth on plates lacking histidine and the presence of 3-AT suggest a positive protein–protein interaction. Each interaction was investigated in biological triplicate experiments.

GST-MinD/His-cyto-AtoS pull-down assay

GST-MinD (5 μM) was incubated with His-cyto-AtoS (5 μM) in buffer-B (50 mM Hepes pH 7.4, 150 mM KCl) at room temperature for 30 min. HisPure cobalt resin was added to the reaction mixture and incubated for 1 h at 4 °C. His-cyto-AtoS (5 μM) or GST-MinD (5 μM) alone were used as controls. The whole reaction mixture was transferred to a spin column, washed three times with buffer B containing 20 mM imidazole and eluted with buffer containing 50 mM Hepes pH 7.4, 150 mM KCl, and 300 mM imidazole. The GST-tagged MinD fraction eluted along with His-cyto-AtoS was verified on a 12% SDS-PAGE and also subjected to Western blot analysis. Anti-GST (Invitrogen: 136700), anti-His primary antibodies (Sigma),

and anti-mouse-horseradish peroxidase–conjugated secondary antibodies (Sigma) were used for the detection of MinD and cyto-AtoS. All antibodies were used at a 1:10,000 dilution.

Promoter activity assay

To study the native promoter activity of *flhDC* and *fliA* through the eGFP reporter assay, we first cloned the *egfp* gene in the pET22b vector and removed the T7 promoter by digestion with BglII and NdeI restriction enzymes. Next, we identified the promoter regions of *flhDC* and *fliA* from the *E. coli* K-12 genome, and different truncated parts of the promoter were PCR amplified using specific primers. These promoter regions were cloned into the upstream eGFP of the promoter-less pET22b-eGFP vector at BglII and NdeI sites. The clone was confirmed by restriction digestion and sequencing. To study the promoter activity, we transferred the plasmids containing various truncated *flhDC* promoter (pET-P1-eGFP, pET-P2-eGFP, pET-P3-eGFP) and pET-P4-eGFP plasmid (containing *fliA* promoter) into *E. coli* (WT) and *E. coli* (Δ*min*) cells. Further, to verify the roles of MinD and AtoSC on *fliA* promoter activity, we transferred pACYCDuet-1-*minD* and pCDFDuet-1-cyto-*atoSC* to the pET-P4-eGFP/ C41strain. The strains containing respected plasmid were grown at 37 °C and at A_{600} ~0.5 induced with 1 mM IPTG for 3 h. An equal number of cells were loaded on an SDS-PAGE, and Western blot was performed using an anti-GFP mAb (Invitrogen: 332600). Anti-GroEL antibody (Abcam: ab82592) was used as a loading control. Anti-mouse antibody was used as secondary antibody to stain the blot. All the antibodies used in this experiment were 1:10,000 dilutions.

Reporter assay for fliA promoter activity

For this assay, *fliA* native promoter from *E. coli* was cloned in pCDFDuet-1- eGFP plasmid and both the T7 promoter was removed. This plasmid was transferred into *E. coli* (WT), *E. coli* (Δ *min*), and *E. coli* (Δ *min*) with Min complementation strains, streaked on a LB agar plate containing respective antibiotics, 0.1 mM IPTG and grown at 37 °C for 12 to 16 h. Images were taken on the Bio-Rad Chemidoc imaging system. To measure the eGFP intensity, cells were grown until A_{600} ~ 0.5 at 37 °C and induced with 1 mM IPTG for 3 h. Next, the cells were washed with 0.85% NaCl, and an equal number of cells were taken for fluorimeter to measure the eGFP fluorescence intensity.

atoDAEB promoter activity

In alignment with the above-describe procedures, the *ato-DAEB* promoter was cloned into the eGFP-pET22b vector following the elimination of the T7 promoter. Subsequently, the resulting patoD1-eGFP-pET22b vector was introduced into *E. coli* (WT) and into *E. coli* (Δ *min*), along with MinDE and AtoSC. The cells were grown at 37 ºC in the presence of 10 mM acetoacetate and respective antibiotics. At $A{600}$ ~0.5, the cells were induced with 1 mM IPTG for 2 h. Equal numbers of cells were loaded onto an SDS-PAGE, and a Western blot was performed utilizing a mouse anti-GFP mAb

(Invitrogen: 332600). Anti-GroEL mAb (Abcam: ab90522) was used as a loading control

Data availability

All data are contained within the manuscript.

Author contributions—P. P., A. C. T., and T. K. B. conceptualization; P. P., A. C. T., and T. K. B. methodology; P. P. and A. C. T. investigation; P. P., A. C. T., and T. K. B. formal analysis; P. P. writing-original draft; A. C. T. and T. K. B. writing-review and editing; T. K. B. supervision; T. K. B. funding acquisition.

Conflict of interest—The authors declare that they have no conflicts of interest with the contents of this article.

Abbreviations—The abbreviations used are: 3-AT, 3-amino-1,2,4-triazole; eGFP, enhanced green fluorescent protein; qRT-PCR, quantitative reverse transcription-PCR; TCS, two-component system; TEM, transmission electron microscopy.

References

1. Beuria, T. K., Krishnakumar, S. S., Sahar, S., Singh, N., Gupta, K., Meshram, M., *et al.* (2003) Glutamate-induced assembly of bacterial cell division protein FtsZ. *J. Biol. Chem.* **278**, 3735–3741
2. Pradhan, P., Margolin, W., and Beuria, T. K. (2021) Targeting the achilles heel of FtsZ: the Interdomain Cleft. *Front. Microbiol.* **12**, 732796
3. Panda, P., Taviti, A. C., Satpati, S., Kar, M. M., Dixit, A., and Beuria, T. K. (2015) Doxorubicin inhibits E. coli division by interacting at a novel site in FtsZ. *Biochem. J.* **471**, 335–346
4. Beuria, T. K., Singh, P., Surolia, A., and Panda, D. (2009) Promoting assembly and bundling of FtsZ as a strategy to inhibit bacterial cell division: a new approach for developing novel antibacterial drugs. *Biochem. J.* **423**, 61–69
5. Beuria, T. K., Santra, M. K., and Panda, D. (2005) Sanguinarine blocks cytokinesis in bacteria by inhibiting FtsZ assembly and bundling. *Biochemistry* **44**, 16584–16593
6. Rowlett, V. W., and Margolin, W. (2013) The bacterial Min system. *Curr. Biol.* **23**, R553–R556
7. Hu, Z., and Lutkenhaus, J. (1999) Topological regulation of cell division in Escherichia coli involves rapid pole to pole oscillation of the division inhibitor MinC under the control of MinD and MinE. *Mol. Microbiol.* **34**, 82–90
8. Raskin, D. M., and de Boer, P. A. (1999) Rapid pole-to-pole oscillation of a protein required for directing division to the middle of Escherichia coli. *Proc. Natl. Acad. Sci. U. S. A.* **96**, 4971–4976
9. Taviti, A. C., and Beuria, T. K. (2017) MinD directly interacting with FtsZ at the H10 helix suggests a model for robust activation of MinC to destabilize FtsZ polymers. *Biochem. J.* **474**, 3189–3205
10. Taviti, A. C., and Beuria, T. K. (2019) Bacterial Min proteins beyond the cell division. *Crit. Rev. Microbiol.* **45**, 22–32

ASBMB

11. Di Ventura, B., Knecht, B., Andreas, H., Godinez, W. J., Fritsche, M., Rohr, K., *et al.* (2013) Chromosome segregation by the Escherichia coli Min system. *Mol. Syst. Biol.* **9**, 686

12. Parti, R. P., Biswas, D., Wang, M., Liao, M., and Dillon, J. A. (2011) A minD mutant of enterohemorrhagic E. coli O157:H7 has reduced adherence to human epithelial cells. *Microb. Pathog.* **51**, 378–383

13. Kutsukake, K., and Iino, T. (1994) Role of the FliA-FlgM regulatory system on the transcriptional control of the flagellar regulon and flagellar formation in Salmonella typhimurium. *J. Bacteriol.* **176**, 3598–3605

14. Barker, C. S., Pruss, B. M., and Matsumura, P. (2004) Increased motility of Escherichia coli by insertion sequence element integration into the regulatory region of the flhD operon. *J. Bacteriol.* **186**, 7529–7537

15. Theodorou, M. C., Theodorou, E. C., and Kyriakidis, D. A. (2012) Involvement of AtoSC two-component system in Escherichia coli flagellar regulon. *Amino Acids* **43**, 833–844

16. Dasgupta, N., Arora, S. K., and Ramphal, R. (2000) fleN, a gene that regulates flagellar number in Pseudomonas aeruginosa. *J. Bacteriol.* **182**, 357–364

17. Blagotinsek, V., Schwan, M., Steinchen, W., Mrusek, D., Hook, J. C., Rossmann, F., *et al.* (2020) An ATP-dependent partner switch links flagellar C-ring assembly with gene expression. *Proc. Natl. Acad. Sci. U. S. A.* **117**, 20826–20835

18. Chiou, P. Y., Luo, C. H., Chang, K. C., and Lin, N. T. (2013) Maintenance of the cell morphology by MinC in Helicobacter pylori. *PLoS One* **8**, e71208

19. Dasgupta, N., and Ramphal, R. (2001) Interaction of the antiactivator FleN with the transcriptional activator FleQ regulates flagellar number in Pseudomonas aeruginosa. *J. Bacteriol.* **183**, 6636–6644

20. Schuhmacher, J. S., Rossmann, F., Dempwolff, F., Knauer, C., Altegoer, F., Steinchen, W., *et al*. (2015) MinD-like ATPase FlhG effects location and number of bacterial flagella during C-ring assembly. *Proc. Natl. Acad. Sci. U. S. A.* **112**, 3092–3097

21. Balaban, M., and Hendrixson, D. R. (2011) Polar flagellar biosynthesis and a regulator of flagellar number influence spatial parameters of cell division in Campylobacter jejuni. *PLoS Pathog.* **7**, e1002420

22. Huang, H., Wang, P., Bian, L., Osawa, M., Erickson, H. P., and Chen, Y. (2018) The cell division protein MinD from Pseudomonas aeruginosa dominates the assembly of the MinC-MinD copolymers. *J. Biol. Chem.* **293**, 7786–7795

23. Partridge, J. D., and Harshey, R. M. (2013) More than motility: salmonella flagella contribute to overriding friction and facilitating colony hydration during swarming. *J. Bacteriol.* **195**, 919–929

24. Archer, C. T., Kim, J. F., Jeong, H., Park, J. H., Vickers, C. E., Lee, S. Y., *et al.* (2011) The genome sequence of E. coli W (ATCC 9637): comparative genome analysis and an improved genome-scale reconstruction of E. coli. *BMC Genomics* **12**, 9

25. Amann, E., Ochs, B., and Abel, K. J. (1988) Tightly regulated tac promoter vectors useful for the expression of unfused and fused proteins in Escherichia coli. *Gene* **69**, 301–315

26. Sherratt, D. J. (2016) Oscillation helps to get division right. *Proc. Natl. Acad. Sci. U. S. A.* **113**, 2803–2805

27. Park, K. T., Wu, W., Battaile, K. P., Lovell, S., Holyoak, T., and Lutkenhaus, J. (2011) The Min oscillator uses MinD-dependent conformational changes in MinE to spatially regulate cytokinesis. *Cell* **146**, 396–407

28. Wei, B. L., Brun-Zinkernagel, A. M., Simecka, J. W., Pruss, B. M., Babitzke, P., and Romeo, T. (2001) Positive regulation of motility and flhDC expression by the RNA-binding protein CsrA of Escherichia coli. *Mol. Microbiol.* **40**, 245–256

29. Liu, X., and Matsumura, P. (1994) The FlhD/FlhC complex, a transcriptional activator of the Escherichia coli flagellar class II operons. *J. Bacteriol.* **176**, 7345–7351

30. Ohnishi, K., Kutsukake, K., Suzuki, H., and Iino, T. (1990) Gene fliA encodes an alternative sigma factor specific for flagellar operons in Salmonella typhimurium. *Mol. Gen. Genet.* **221**, 139–147

31. Kutsukake, K., Ohya, Y., and Iino, T. (1990) Transcriptional analysis of the flagellar regulon of Salmonella typhimurium. *J. Bacteriol.* **172**, 741–747

32. Correa, N. E., Peng, F., and Klose, K. E. (2005) Roles of the regulatory proteins FlhF and FlhG in the Vibrio cholerae flagellar transcription hierarchy. *J. Bacteriol.* **187**, 6324–6332

33. Ono, H., Takashima, A., Hirata, H., Homma, M., and Kojima, S. (2015) The MinD homolog FlhG regulates the synthesis of the single polar flagellum of Vibrio alginolyticus. *Mol. Microbiol.* **98**, 130–141

34. Nogales, J., Vargas, P., Farias, G. A., Olmedilla, A., Sanjuan, J., and Gallegos, M. T. (2015) FleQ coordinates flagellum-dependent and -independent motilities in Pseudomonas syringae pv. tomato DC3000. *Appl. Environ. Microbiol.* **81**, 7533–7545

35. Schulz, T., Rydzewski, K., Schunder, E., Holland, G., Bannert, N., and Heuner, K. (2012) FliA expression analysis and influence of the regulatory proteins RpoN, FleQ and FliA on virulence and *in vivo* fitness in Legionella pneumophila. *Arch. Microbiol.* **194**, 977–989

36. Klose, K. E., and Mekalanos, J. J. (1998) Distinct roles of an alternative sigma factor during both free-swimming and colonizing phases of the Vibrio cholerae pathogenic cycle. *Mol. Microbiol.* **28**, 501–520

37. Grigoroudis, A. I., Panagiotidis, C. A., Lioliou, E. E., Vlassi, M., and Kyriakidis, D. A. (2007) Molecular modeling and functional analysis of the AtoS-AtoC two-component signal transduction system of Escherichia coli. *Biochim. Biophys. Acta* **1770**, 1248–1258

38. Harvey, C. W., Madukoma, C. S., Mahserejian, S., Alber, M. S., and Shrout, J. D. (2014) Cell division resets polarity and motility for the bacterium Myxococcus xanthus. *J. Bacteriol.* **196**, 3853–3861

39. Dudin, O., Geiselmann, J., Ogasawara, H., Ishihama, A., and Lacour, S. (2014) Repression of flagellar genes in exponential phase by CsgD and CpxR, two crucial modulators of Escherichia coli biofilm formation. *J. Bacteriol.* **196**, 707–715

40. Degnen, S. T., and Newton, A. (1972) Chromosome replication during development in Caulobacter crescentus. *J. Mol. Biol.* **64**, 671–680

41. Dufour, A., Furness, R. B., and Hughes, C. (1998) Novel genes that upregulate the Proteus mirabilis flhDC master operon controlling flagellar biogenesis and swarming. *Mol. Microbiol.* **29**, 741–751

42. Prouty, M. G., Correa, N. E., and Klose, K. E. (2001) The novel sigma54- and sigma28-dependent flagellar gene transcription hierarchy of Vibrio cholerae. *Mol. Microbiol.* **39**, 1595–1609

43. Arora, S. K., Ritchings, B. W., Almira, E. C., Lory, S., and Ramphal, R. (1997) A transcriptional activator, FleQ, regulates mucin adhesion and flagellar gene expression in Pseudomonas aeruginosa in a cascade manner. *J. Bacteriol.* **179**, 5574–5581

44. Soutourina, O. A., and Bertin, P. N. (2003) Regulation cascade of flagellar expression in Gram-negative bacteria. *FEMS Microbiol. Rev.* **27**, 505–523

45. Kusumoto, A., Shinohara, A., Terashima, H., Kojima, S., Yakushi, T., and Homma, M. (2008) Collaboration of FlhF and FlhG to regulate polar-flagella number and localization in Vibrio alginolyticus. *Microbiology (Reading)* **154**, 1390–1399

46. Kazmierczak, B. I., and Hendrixson, D. R. (2013) Spatial and numerical regulation of flagellar biosynthesis in polarly flagellated bacteria. *Mol. Microbiol.* **88**, 655–663

47. Millikan, D. S., and Ruby, E. G. (2003) FlrA, a sigma54-dependent transcriptional activator in Vibrio fischeri, is required for motility and symbiotic light-organ colonization. *J. Bacteriol.* **185**, 3547–3557

48. Jyot, J., Dasgupta, N., and Ramphal, R. (2002) FleQ, the major flagellar gene regulator in Pseudomonas aeruginosa, binds to enhancer sites located either upstream or atypically downstream of the RpoN binding site. *J. Bacteriol.* **184**, 5251–5260

49. Pilalis, E., Chatziioannou, A. A., Grigoroudis, A. I., Panagiotidis, C. A., Kolisis, F. N., and Kyriakidis, D. A. (2011) Escherichia coli genome-wide promoter analysis: identification of additional AtoC binding target elements. *BMC Genomics* **12**, 238

50. Filippou, P. S., Kasemian, L. D., Panagiotidis, C. A., and Kyriakidis, D. A. (2008) Functional characterization of the histidine kinase of the E. coli two-component signal transduction system AtoS-AtoC. *Biochim. Biophys. Acta* **1780**, 1023–1031

51. Lioliou, E. E., Mimitou, E. P., Grigoroudis, A. I., Panagiotidis, C. H., Panagiotidis, C. A., and Kyriakidis, D. A. (2005) Phosphorylation activity of the response regulator of the two-component signal

transduction system AtoS-AtoC in E. coli. *Biochim. Biophys. Acta* **1725**, 257–268

52. Oshima, T., Aiba, H., Masuda, Y., Kanaya, S., Sugiura, M., Wanner, B. L., *et al*. (2002) Transcriptome analysis of all two-component regulatory system mutants of Escherichia coli K-12. *Mol. Microbiol.* **46**, 281–291

53. Turner, L., Ryu, W. S., and Berg, H. C. (2000) Real-time imaging of fluorescent flagellar filaments. *J. Bacteriol.* **182**, 2793–2801

54. Ren, F., Lei, T., Song, Z., Yu, T., Li, Q., Huang, J., *et al*. (2018) Could FlhF be a key element that controls Campylobacter jejuni flagella biosynthesis in the initial assembly stage? *Microbiol. Res.* **207**, 240–248

55. Alexander, C., Guru, A., Pradhan, P., Mallick, S., Mahanandia, N. C., Subudhi, B. B., *et al*. (2020) MazEF-rifampicin interaction suggests a mechanism for rifampicin induced inhibition of persisters. *BMC Mol. Cell Biol.* **21**, 73

56. Mallick, S., Kumar, A., Dodia, H., Alexander, C., Vasudevan, D., and Beuria, T. K. (2021) Biochemical characterization of an E. coli cell division factor FtsE shows ATPase cycles similar to the NBDs of ABC-transporters. *Biosci. Rep.* **41**, BSR20203034

Targeting the Achilles Heel of FtsZ: The Interdomain Cleft

Pinkilata Pradhan[1,2], William Margolin[3]* and Tushar Kant Beuria[1]*

[1] Institute of Life Sciences, Nalco Square, Bhubaneswar, India, [2] Regional Centre for Biotechnology, Faridabad, India,
[3] Department of Microbiology and Molecular Genetics, McGovern Medical School, Houston, TX, United States

Widespread antimicrobial resistance among bacterial pathogens is a serious threat to public health. Thus, identification of new targets and development of new antibacterial agents are urgently needed. Although cell division is a major driver of bacterial colonization and pathogenesis, its targeting with antibacterial compounds is still in its infancy. FtsZ, a bacterial cytoskeletal homolog of eukaryotic tubulin, plays a highly conserved and foundational role in cell division and has been the primary focus of research on small molecule cell division inhibitors. FtsZ contains two drug-binding pockets: the GTP binding site situated at the interface between polymeric subunits, and the inter-domain cleft (IDC), located between the N-terminal and C-terminal segments of the core globular domain of FtsZ. The majority of anti-FtsZ molecules bind to the IDC. Compounds that bind instead to the GTP binding site are much less useful as potential antimicrobial therapeutics because they are often cytotoxic to mammalian cells, due to the high sequence similarity between the GTP binding sites of FtsZ and tubulin. Fortunately, the IDC has much less sequence and structural similarity with tubulin, making it a better potential target for drugs that are less toxic to humans. Over the last decade, a large number of natural and synthetic IDC inhibitors have been identified. Here we outline the molecular structure of IDC in detail and discuss how it has become a crucial target for broad spectrum and species-specific antibacterial agents. We also outline the drugs that bind to the IDC and their modes of action.

Keywords: protein structure, tubulin, bacterial cell division, small molecule inhibitor, antibacterial, ftsZ

INTRODUCTION

The battle against infectious diseases has been a persistent challenge for humans. The development and use of antibiotics helped to prevent and control bacterial infections, but at the same time its misuse led to the development of antibacterial resistance (Ma and Ma, 2012). An increase in antibacterial resistance is now of significant concern worldwide, resulting in higher infection and mortality rates. As more bacteria become resistant to currently available antibiotics, discovery of new antibiotics and identification of new targets is more urgent than ever.

Although division of bacterial cells is key for their colonization and pathogenesis, the cell division machinery has not been fully explored for the development of antibacterial agents despite many breakthroughs in the mechanisms and regulation of this fundamental process. Cell division is initiated by the formation of a discontinuous and dynamic circumferential assembly at the

site of division called the Z ring, which is located at the cell midpoint in bacteria that divide by binary fission.

Several proteins are involved in determining the proper assembly and correct placement of the Z-ring (Hale and de Boer, 1997; Pichoff and Lutkenhaus, 2002; Bramkamp et al., 2008; Rowlett and Margolin, 2015). However, the key organizing protein is FtsZ (Filamenting temperature sensitive mutant Z), which assembles into treadmilling polymers to form a dynamic skeleton for the Z-ring, ultimately recruiting other cell division proteins to the Z-ring in a sequential manner (Bi and Lutkenhaus, 1991; Wang et al., 2020). FtsZ is present in nearly all bacteria, plant plastids, and many archaea, and is a homolog of eukaryotic tubulin (Mukherjee and Lutkenhaus, 1994; Erickson, 1995; de Pereda et al., 1996; Nogales et al., 1998a,b; Kaur et al., 2010). In search for new antibiotic targets, FtsZ has become the leading candidate, as it is essential for cell division in most bacteria and is absent in eukaryotes (Beall and Lutkenhaus, 1991; Dai and Lutkenhaus, 1991; Pinho and Errington, 2003; Li and Ma, 2015). Although FtsZ is homologous to eukaryotic tubulin, it shares little sequence identity (10–18%) with tubulin, reducing the likelihood that drugs targeting FtsZ will be toxic to eukaryotic cells (de Pereda et al., 1996).

Over the past few decades, researchers have characterized several natural as well as synthetic FtsZ inhibitors. However, the interaction sites/ binding pockets in FtsZ for many inhibitors are not yet fully characterized. To define the functional groups in a small molecule that can efficiently affect the functions of a target, it is critical to understand its binding site in the target. A detailed molecular understanding of the binding site will help to design and develop specific drugs against the target, which will further help to identify more specific and potent FtsZ inhibitors.

FtsZ contains two prominent drug binding sites, the GTP binding site, which we will refer to as the nucleotide binding domain (NBD), and the inter-domain cleft (IDC) (Casiraghi et al., 2020). The NBD is similar to that of tubulin and shares the glycine-rich signature motif GGGTG(T/S)G of tubulin (de Pereda et al., 1996; Löwe, 1998). Consequently, there is a higher chance that drugs that target the FtsZ GTP binding site may also interact with tubulin and cause toxicity in the mammalian cells. In contrast, the IDC of FtsZ exhibits less similarity to tubulin, reducing the odds of toxicity to mammalian cells (Casiraghi et al., 2020). Fortunately, most of the reported FtsZ inhibitors interact with the IDC. This review highlights different drugs that target the IDC, summarizes the residues within the IDC that are important for drug binding, and outlines what is known about the mechanism of action. We also describe why the FtsZ IDC has attracted more attention as a drug target for the development of novel antibacterial compounds.

FTSZ AND THE Z-RING

Bacterial cell division is a complex process that involves replication and segregation of its genetic material, elongation of the lateral cell wall, and formation of a division septum at midcell followed by separation of the two daughter cells. Using immune electron microscopy on *Escherichia coli* cells undergoing binary fission, Bi and Lutkenhaus provided initial proof 30 years ago that FtsZ localizes at the center of the cell and forms a ring like structure (Bi and Lutkenhaus, 1991). The correct localization of the Z-ring at midcell in many rod-shaped bacteria is controlled by diverse spatial regulatory systems. In *E. coli*, the nucleoid occlusion system prevents potentially DNA-damaging formation of the Z-ring over the unsegregated nucleoid, while the Min system oscillates between both cell poles and inhibits the formation of Z-rings at the poles (Rowlett and Margolin, 2015; Taviti and Beuria, 2017). The invagination of the cell envelope behind the Z-ring at midcell is initiated by forces generated by the Z-ring. Several independent studies showed that a ∼8 – 80 pN force generated during the constriction of the Z-ring may be sufficient to initiate this invagination (Lan et al., 2007; Hsin et al., 2012; Yao et al., 2017; Nguyen et al., 2019; Ramirez-Diaz et al., 2021).

Assembly of the Z-ring is regulated by a number of endogenous activator and inhibitor proteins, maintaining a balance between instability and stability (Hale and de Boer, 1997; Trusca et al., 1998; Pichoff and Lutkenhaus, 2002; Haeusser et al., 2004). Overproduction of FtsZ inhibitors such as SulA or MinCD, or inactivation of FtsZ stabilizing proteins such as FtsA, ZipA, or Zap proteins in *E. coli* lead to long, filamentous cells without Z-rings or with multiple stalled Z-rings (Addinall et al., 1996), ultimately preventing viability. Similarly, small molecules that inhibit Z ring formation or hyperstabilize the Z-ring also lead to a block in cell division. As FtsZ is the most important component of the Z-ring, development of FtsZ inhibitors requires a molecular understanding of FtsZ structure, drug-binding sites on FtsZ and the inhibitory effects of drugs on FtsZ functions.

OVERALL FTSZ STRUCTURE AND FUNCTION

Domains of FtsZ

FtsZ consists of a conserved globular core (residues 10–316) comprising an N-terminal domain (H1–H6, S1–S6), a core helix (H7), a spacer loop (T7 loop) and a C-terminal domain (H8–H10, S7–S10), which in turn is connected to a conserved peptide at the extreme C terminus (residues 369–383) by a flexible unstructured linker (317–368) (de Boer et al., 1992; Löwe and Amos, 1998; Nogales et al., 1998b) (**Figure 1**). In some species, such as the archaeon *Methanocaldococcus jannaschii,* FtsZ contains an additional helix (H0) in its N-terminal subdomain (Löwe, 1998).

In *E. coli* FtsZ, the N-terminal domain spans residues 1–177. It contains an unstructured and poorly conserved extreme N terminus and a highly conserved NBD (Löwe and Amos, 1998; Vaughan et al., 2004; Gardner et al., 2013). Although the N-terminal domain contains the NDB, it is not sufficient for hydrolyzing GTP (Jindal and Panda, 2013). In *E. coli,* H7 extends from residues 178 to 201, connects the N-terminal and C-terminal domains of the core, and acts like a sliding door for the opening and closing of the IDC. Some residues of H7 are crucial for FtsZ assembly. For example, a single mutation in *Bacillus subtilis* FtsZ (BsFtsZ) R191 can impede FtsZ assembly (Dhaked et al., 2016).
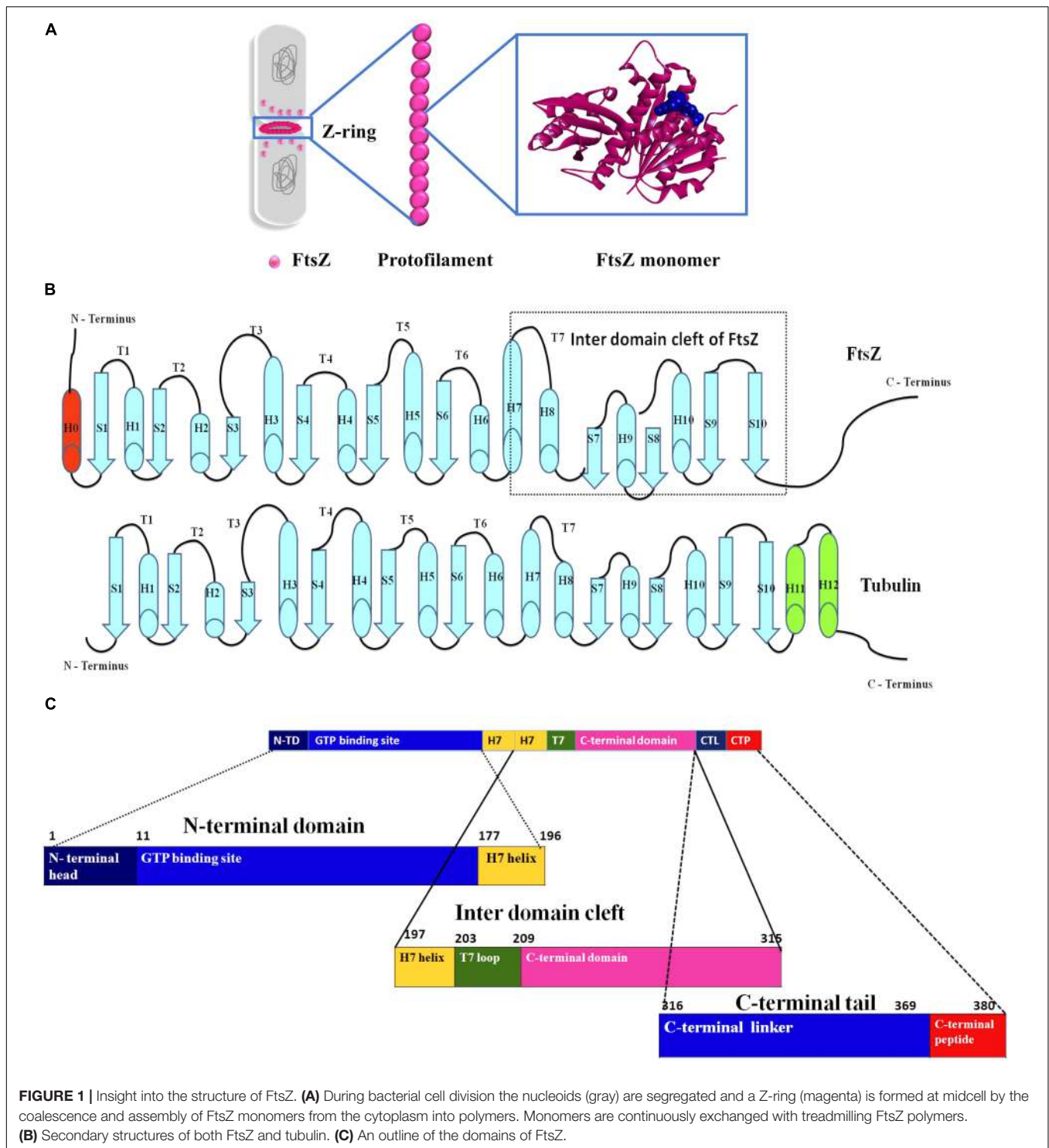
FIGURE 1 | Insight into the structure of FtsZ. **(A)** During bacterial cell division the nucleoids (gray) are segregated and a Z-ring (magenta) is formed at midcell by the coalescence and assembly of FtsZ monomers from the cytoplasm into polymers. Monomers are continuously exchanged with treadmilling FtsZ polymers. **(B)** Secondary structures of both FtsZ and tubulin. **(C)** An outline of the domains of FtsZ.

The highly conserved T7 loop in *E. coli* FtsZ (residues 202 – 209) connects H7 to H8 of the C-terminal subdomain and contains a conserved GXXNXD sequence that is important for GTP hydrolysis. Upon FtsZ assembly, the T7 loop of one FtsZ monomer inserts into the GTP binding pocket of the adjacent FtsZ monomer and initiates GTP hydrolysis

(Löwe and Amos, 1999; Scheffers et al., 2002). Drug molecules that bind to this site affect GTPase activity of FtsZ.

The C-terminal domain of the globular core of FtsZ (residues 210 to 316) is highly conserved both in sequence and structure. It consists of helices H8–H10 and beta sheets S7–S10. H10 is notably rich in acidic residues and interacts with Min proteins
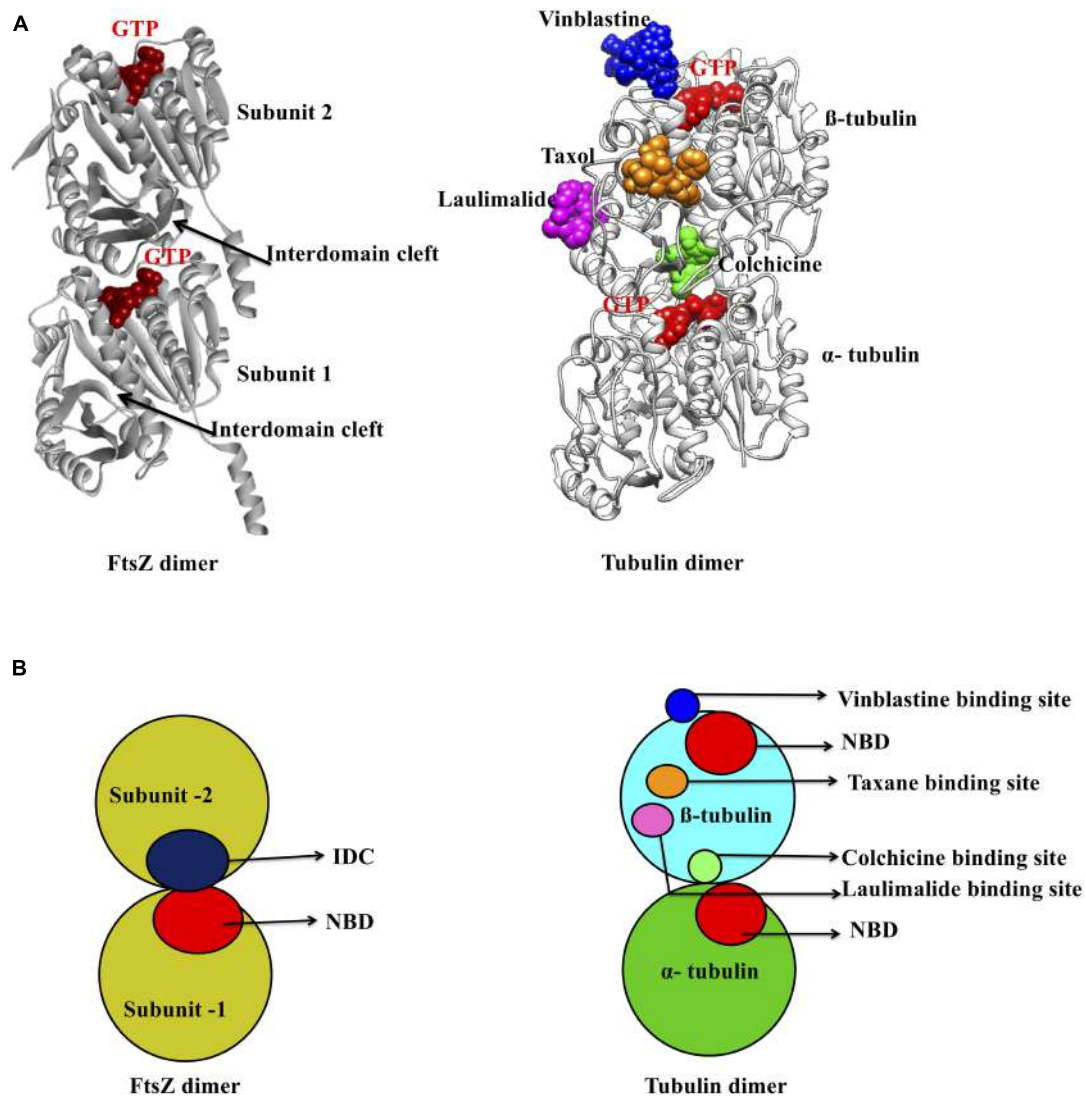
FIGURE 2 | Major inhibitor binding sites in FtsZ and tubulin: **(A)** Structure of FtsZ and tubulin dimers with major drug binding sites. **(B)** Shown is a cartoon representation of the same.
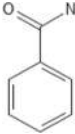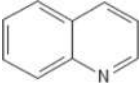
(Taviti and Beuria, 2017). This domain is followed by an unstructured C-terminal linker (CTL) that is highly variable both in composition and length (Taviti and Beuria, 2017). In *E. coli*, the CTL is ∼ 52 residues (317 – 369). In most FtsZs, the CTL connects the globular core domain of FtsZ with a highly conserved 10–20 residue peptide at the extreme end of the C-terminus called the C-terminal peptide (CTP) (Cohan et al., 2020). Although this peptide (residues 369–379 in *E. coli)* is not required for FtsZ assembly, it is crucial for interactions with other membrane-associated cell division proteins like ZipA and FtsA (Ma and Margolin, 1999; Ortiz et al., 2016). Residues D373, I374, F377 and L378 of *E. coli* FtsZ are specifically involved in these protein-protein interactions (Buske and Levin, 2012). As a result, deletion of the CTP blocks FtsZ functions and bacterial division (Din et al., 1998).

FtsZ Assembly and GTPase Activity

FtsZ, in the presence of GTP, polymerizes into head-to-tail protofilaments (Bramhill and Thompson, 1994; Mukherjee and Lutkenhaus, 1994), which then coalesce to form the Z-ring (Haeusser and Margolin, 2016). The Z–ring is anchored to the membrane with the help of other essential cell division proteins, such as FtsA and ZipA of *E. coli* (Pichoff and Lutkenhaus, 2002). In Gram positive bacteria as well as FtsZ-containing archaea, SepF is the key membrane anchor for FtsZ (Duman et al., 2013; Nussbaum et al., 2021; White and Eswara, 2021).
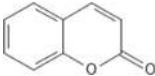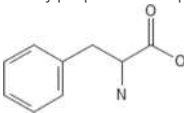
In vitro studies suggest that FtsZ assembles into short protofilaments made up of ∼30 subunits that combine laterally to form the Z-ring (Erickson et al., 2010). These lateral interactions between FtsZ protofilaments help to drive division septum formation (Krupka and Margolin, 2018; Squyres et al., 2021;

TABLE 1 | Reported FtsZ inhibitors, binding sites, and mechanisms of action.

Sl No. of core struct-ure[1]	Sl No. of drugs	Core structure	Drug	Binding site on FtsZ	Effects on assembly or GTPase activity[2]	IC_{50} in μM (tubulin/ microtubule/ eukaryotic cells)/HC_{50}	MIC in μM	IC_{50} MIC ratio	References
A.	1.	Benzamide ring	3-MBA and PC190723	IDC	E	> 180	2.81	> 64	Haydon et al., 2008
A.	2.		TXA707,TXA709 and TXA6101	IDC	E	> 233.25	3.9	> 60	Kaul et al., 2015; Fujita et al., 2017; Carro, 2019
A.	3.		3-substituted 2,6-difluorobenzamide derivatives (I1)	IDC	-	-	0.88–28.04	-	Bi et al., 2017
A.	4.		Isoxazole benzamide derivatives (I2)	IDC	E	> 331	0.04–10.4	> 32	Bi et al., 2018
A.	5.		1, 3, 4-oxadiazol-2-one-benzamide derivatives (I3)	IDC	E	> 150	0.29–2.35	> 64	Bi et al., 2019
A.	6.		3-aminobenzamide derivatives (I4)	IDC	I	> 100	3.1	> 32	Lui et al., 2019
A.	7.		BOFP	IDC		-	1.32	-	Ferrer-Gonzalez et al., 2019
B.	8.	Quinoline and quinazoline ring	Berberine	NBD	I, G	18	95–380	0.047	Yu et al., 2005; Domadia et al., 2008; Raghav et al., 2017

(Continued)

TABLE 1 | Continued

Sl No. of core struct-ure[1]	Sl No. of drugs	Core structure	Drug	Binding site on FtsZ	Effects on assembly or GTPase activity[2]	IC$_{50}$ in μ M (tubulin/ microtubule/ eukaryotic cells)/HC$_{50}$	MIC in μ M	IC$_{50}$ MIC ratio	References
A.	9.		Benzofuroquinolinium Derivatives (I5)	NBD	I, G	95.5	0.48–15.3	6.2	Zheng et al., 2018
A.	10.		9-phenoxy Berberine derivatives	IDC	I, G	-	4–65	-	Sun et al., 2014
A.	11.		Thiazole Orange Derivatives (I6)	IDC	E, G	96.5	1.36–5.45	17.7	Sun et al., 2017b
A.	12.		Indolyl-quinolinium derivatives (I7)	IDC	E	-	2.02–32	-	Cai et al., 2019; Carro, 2019
A.	13.		3-methylbenzo[d]thiazol-methylquinolinium (I8)	IDC	E, G	78.25	1.81–5.43	14.4	Sun et al., 2018
A.	14.		N-Methylbenzofuro[3,2-b] quinoline and Methylbenzoindole[3,2-b] quinoline derivatives, (I9)	IDC	I, G	-	4.16–12.5	-	Sun et al., 2017a
A.	15.		Thiazole-quinolinium derivatives (I10)	IDC	E	28.4	2.25	12.6	Li et al., 2015
C.	16.	Benzopyrone ring	Coumarin and its derivatives	IDC	I, G	> 500	3420	> 0.14	Finn et al., 2001; de Souza et al., 2005; Duggirala et al., 2014
A.	17.		Polyketides compounds (I11)	IDC	G	-	5–40	-	Matsui et al., 2017
A.	18.		Quercetin dehydrate	IDC	I	> 100	378.5	> 0.26	Mathew et al., 2016
D.	19.	Phenylpropanoid	p-coumaric acid	IDC	I, G	215	122	1.7	Hemaiswarya et al., 2011; Lou et al., 2012; Chang and Shen, 2014

(Continued)

TABLE 1 | Continued

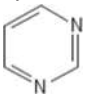| SI No. of core struct-ure[1]	SI No. of drugs	Core structure	Drug	Binding site on FtsZ	Effects on assembly or GTPase activity[2]	IC$_{50}$ in μ M (tubulin/ microtubule/ eukaryotic cells)/HC$_{50}$	MIC in μ M	IC$_{50}$ MIC ratio	References
A.	20.		Cinnamic acid	IDC		2400	9000	0.27	Rastogi et al., 2008; Hemaiswarya et al., 2011; Niero and Machado-Santelli, 2013
A.	21.		Cinnamaldehyde	IDC		9.76	7560	0.0013	Domadia et al., 2007; Ng and Wu, 2011
A.	22.		Caffeic acid	IDC		> 100	1800	> 0.055	Rastogi et al., 2008; Hemaiswarya et al., 2011; Sanderson et al., 2013
A.	23.		Ferulic acid	IDC		500	> 515	< 1	Borges et al., 2013; Eroglu et al., 2015
E.	24.	Pyrimidine ring	pyrimidine-quinuclidine derivatives	NBD	I	> 500	49.2	> 10	Chan et al., 2013; Haranahalli et al., 2016
A.	25.		2,4-disubstituted-6-thiophenyl-pyrimidine derivatives **(I12)**	NBD	I, G	> 128	4	>32	Fang et al., 2019

(Continued)

TABLE 1 | Continued

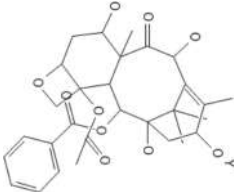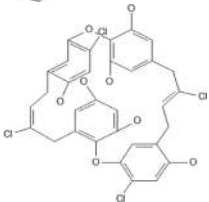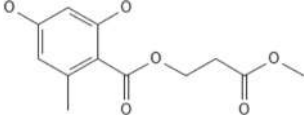| SI No. of core struct-ure[1]	SI No. of drugs	Core structure	Drug	Binding site on FtsZ	Effects on assembly or GTPase activity[2]	IC_{50} in μ M (tubulin/ microtubule/ eukaryotic cells)/HC_{50}	MIC in μ M	IC_{50} MIC ratio	References
F.	26.	Complex ring structure	SB-RA-2001	IDC	E, G	45	5	9	Huang et al., 2006; Singh et al., 2014
	27.		Doxorubicin	IDC	I, G	8.3	40	0.20	Panda et al., 2015; Oncul and Ercan, 2017
	28.		Colchicine	IDC		6.5	160	0.04	Mathew et al., 2016
	29.		CCR11	IDC		18	3	6	Singh et al., 2012
	30.		Sulindac analog (I13)	IDC		> 100	19.5	> 5.1	Mathew et al., 2016
	31.		Bt-benzo-29	IDC		17	8	2.12	Ray et al., 2015
	32.		Tiplaxtinin	IDC	E	2.7	4.5	0.6	Elokdah et al., 2004; Sun et al., 2017c
	33.		Chrysophaentin A	NBD	I,G	> 150	4.6–9.26	> 32	Plaza et al., 2010; Keffer et al., 2013
	34.		UCM44	NBD	E	44	37.1	1.18	Ruiz-Avila et al., 2013
	35.		Biphenyl derivative (I14)	NBD	I	> 100	7	>14.28	Artola et al., 2015

(Continued)

TABLE 1 | Continued

SI No. of core struct-ure[1]	SI No. of drugs	Core structure	Drug	Binding site on FtsZ	Effects on assembly or GTPase activity[2]	IC_{50} in µ M (tubulin/ microtubule/ eukaryotic cells)/HC_{50}	MIC in µ M	IC_{50} MIC ratio	References
G.	36.	Simple ring structure	Curcumin	NBD	I	18	100	0.18	Rai et al., 2008; Chakraborti et al., 2011
	37.		Plumbagin	IDC	I,G	14.6	29	0.5	Acharya et al., 2008; Bhattacharya et al., 2013
	38.		*P. cataractum* SYPF 7131 bioactive compound (I15)	IDC	G	-	192.5–293	-	Wu et al., 2018
H.	39.	Peptide inhibitor	CRAMP	IDC	I	300	20	15	Ray et al., 2014
	40.		MciZ	Near IDC	I	-	-	-	Bisson-Filho et al., 2015

[1] Non-peptide FtsZ inhibitors are classified into 7 groups based on their core ring structure (A–G).

[2] E, enhances assembly; I, inhibits assembly; G, inhibits GTPase activity; blank if unknown.

I1: 3-((2-ethylhexyl)oxy)-2,6-difluorobenzamide, **I2**: 3-((5-(4-(Tert-butyl)phenyl)isoxazol-3-yl)methoxy)-2,6-difluorobenzami, **I3**: 2,6-Difluoro-3-((4-(4-bromophenyl)-5-oxo-1,3,4-oxadiazol-2- yl)methoxy)benzamide, **I4**: 2,6-Difluoro-3-(nonylamino)benzamide, **I5**: 5-Methyl-11-((3-(3-dipropylamine)-propylbenzo[d]thiazol-2(3H)-ylidene)methyl)benzofuro[3,2-b]quinolin-5-ium iodide, **I6**: 2-((E)-4- Hydroxystyryl)-1-methyl-4-((Z)-(3-methylbenzo[d]thiazol-2(3H)-ylidene)methyl)quinolin-1-ium iodide, **I7**: (E)-2-(2-(1H-indol-2-yl)vinyl)-1-methyl-4-(piperidin-1-yl)quinolin1-ium iodide, **I8**: 2-((E)-4-fluorostyryl)-1-methyl-4-((E)-(3-methylbenzo[d]thiazol-2(3H)-ylidene)methyl) quinolin-1-ium iodide, **I9**: 5-Methyl-11-(4-methoxyphenylamino)benzoindolo[3,2-b] quinolin-5-ium iodide, **I10**: Z)-1,2-Dimethyl-4-((3-(3-(4-methylpiperidin-1-yl)propyl)benzo[d]thiazol-2(3H)-ylidene)methyl)quinolin-1-ium iodide, **I11**: Gancaonin, **I12**: [1-(4-isopropylbenzyl)-4-(2-(2-(pyridin-4-yl)-6-(thiophen-2-yl)pyrimidin-4-yl)ethyl)-1,4-diazepane (Bb2)], **I13**: (Z)-N-(2-(dimethylamino)ethyl)-2-(5-fluoro-2-methyl-1-(4-(methylthio)benzylidene)-1H-inden-3-yl)acetamide, **I14**: [Biphenyl-3,5-diyl bis(3-hydroxybenzoate)], **I15**: Penicimenolidyu B.

Whitley et al., 2021). A single FtsZ protofilament is ∼5 nm thick with slightly curved morphology, which becomes highly curved upon GTP hydrolysis (Lu et al., 2000; Romberg et al., 2001). One model proposed that GTP hydrolysis provides the required force for Z-ring constriction and septation (Allard and Cytrynbaum, 2009). As GTP hydrolysis is induced upon FtsZ assembly into polymers, FtsZ subunits within the Z ring are highly dynamic, with a half time of FtsZ subunit turnover as low as 8–9 s in *E. coli* and *B. subtilis* (Anderson et al., 2004). This turnover results from treadmilling, which allows FtsZ polymers to travel circumferentially around the site of septum formation by loss of subunits at one polymer end and gain of subunits at the other (Bisson-Filho et al., 2017; Yang et al., 2017). Surprisingly, only about ∼30% of the FtsZ in *E. coli* cells is actually in the Z-ring at any one time, while the remaining FtsZ circulates in a cytoplasmic pool that is continuously exchanged with treadmilling FtsZ polymers that comprise the Z ring (Stricker et al., 2002). Despite the rapid turnover observed in cells, purified FtsZ in solution hydrolyzes its bound GTP at a rate of only ∼2 GTP per FtsZ molecule per minute (Lu et al., 1998), suggesting that cellular factors may enhance FtsZ GTPase activity. Molecular dynamics simulations of FtsZ dimers predict the forces generated by GTP hydrolysis to be ∼30 pN per FtsZ monomer, which is within the range of force required (8 – 80 pN) to drive cytokinesis as mentioned above (Lan et al., 2007; Hsin et al., 2012). Nonetheless, inward growth of the cell division septum likely contributes significantly to the constriction of the Z ring.

SIMILARITIES AND DIFFERENCES BETWEEN TUBULIN AND FTSZ

Although FtsZ has minimal sequence similarity with tubulin, there are several regions that are highly similar in both proteins. Tubulin and FtsZ share only ∼10–18% sequence identity, yet both exhibit structural homology (de Pereda et al., 1996; Kusuma et al., 2019), suggesting convergent evolution (van den Ent et al., 2001; Battaje and Panda, 2017). Sequence alignment of FtsZ, α-tubulin and β-tubulin demonstrated that the T1 loop (common glycine), T4 loop (with the tubulin signature motif), T5 loop (common prolines), T6 loop (common asparagine), and T7 loop (common asparagine and aspartate) show high sequence identity. No significant sequence similarity was observed between tubulin and FtsZ after the T7 loop (Löwe, 1998; Löwe and Amos, 1998; Nogales et al., 1998a).

The secondary structure of both proteins contains a similar sequence of helices – strands – loops and follows similar nomenclature. FtsZ contains ten helices and ten strands. Although the secondary structures of both tubulin and FtsZ are quite similar, the two extra helices at the C-terminus and the C-terminal tail of tubulin are not long like those in FtsZ (**Figure 1B**) (Nogales et al., 1998a). In terms of tertiary structure, a structural prediction study by Pereda et al. involving 200 tubulin sequences and 12 FtsZ sequences from various organisms showed that FtsZ and tubulin have a nearly identical percentage of folds, helices and sheets (de Pereda et al., 1996).

FIGURE 3 | Structural alignment of GTP binding site and IDC in FtsZ. **(A)** IDC and NBD in FtsZ are denoted by mesh structures. **(B)** A structural level comparison of GTP binding sites and the IDC among FtsZs from *E. coli* (red), *B. subtilis* (yellow), *S. aureus* (green), *A. aeolicus* (blue), *P. aeruginosa* (violet), *M. jannaschii* (cyan), and *M. tuberculosis* (light gray). **(C)** Major residues around the GTP binding site and the IDC and their conservation in Gram positive species only (yellow), Gram negative species only (green) or in both Gram positive and Gram negative bacteria (red); non conserved residues are in blue.

However, an *in silico* study that superimposed structures of different FtsZ proteins with tubulin showed that structural differences between FtsZ and tubulin are quite high, with an RMSD value of 8–10 Å (Kusuma et al., 2019). The NBDs of both proteins exhibit a Rossman fold topology (Löwe and Amos, 1998). Both FtsZ and tubulin belong to a distinct GTPase family, which bind to GTP and self-activate GTPase concomitant with polymerization (Nogales et al., 1998a). As suggested by the lack of sequence similarities, there is no structural homology in the C-terminal domains of both proteins. Superimposition of the structures confirmed that the IDC of FtsZ is also absent in tubulin (Battaje and Panda, 2017; Kusuma et al., 2019).

Despite sharing some structural similarities, FtsZ and tubulin diverge in how they form polymers. FtsZ protofilaments are formed by FtsZ monomers, whereas tubulin protofilaments consist of both α and β- tubulin monomers and require a gamma tubulin for nucleation and initiation of tubulin assembly. Another difference is that even if α and β- tubulins show similar degree of similarities with FtsZ, only the β- tubulin can

TABLE 2 | Roles of different IDC residues in binding ligands.

	IDC residues										
*Ec*FtsZ	G191	G195	E198	L199	M206	N207	V208	N263	S297	R307	T309
*Sa*FtsZ	Q192	G196	D199	L200	V207	N208	L209	N263	V297	V307	T309
*Bs*FtsZ	Q192	G196	D199	L200	I207	N208	L209	N263	V297	V307	T309
Thiazole ring	+	+	+	+	+	+	+	+	−	−	+
Quinoline ring	−	−	+	+	−	−	−	−	+	+	+
Benzopyrone	−	−	−	−	−	+	+	−	−	−	−
Phenylpropanoid	−	−	−	−	−	+	+	+	−	−	−
Naphthalene	+	+	+	−	−	−	−	+	−	+	+
Complex ring	+	−	+	+	−	−	+	−	+	−	−
Simple ring	−	−	−	+	−	−	+	+	−	−	+
Peptide	−	−	−	−	−	+	+	−	−	−	−

(+) indicates bonding interaction; (−) indicates non-bonding residues (no interaction).

exchange its GTP, whereas all FtsZ monomers can exchange their GTP and undergo GTP-dependent assembly. Furthermore, the C terminus of FtsZ ends with a β-sheet, whereas a helix is present at the C terminus of tubulin that is responsible for interaction with motor proteins (**Figure 1B**) (Erickson, 1998; Battaje and Panda, 2017). But the key structural difference between FtsZ and tubulin at the monomer level is the presence of the IDC only in FtsZ. This has been a boon for the discovery of compounds unique to FtsZ with minimal cytotoxicity toward eukaryotic cells.

THE TWO DISTINCT DRUG BINDING POCKETS OF FTSZ

The NBD

As mentioned above, there are two main binding pockets for drug binding to FtsZ, the NBD and IDC (**Figure 2**). The NBD, at the interface between FtsZ monomers, includes helices H1–H6, sheets S1–S6 and the T1–T6 loop. It also includes the N-terminal part of H7 (Löwe, 1998; Panda et al., 2016). Seven distinct regions in FtsZ interact with GTP. The T1 loop interacts with the phosphate and the guanine base, whereas the T2 & T3 loops interact with the β- and γ-phosphates (Nogales et al., 1998a; Panda et al., 2016). The T4 loop contains the tubulin signature motif, which interacts with the α and β- phosphates (Mukherjee et al., 1993; de Pereda et al., 1996). The T5-loop interacts with the ribose sugar. The T6 loop possesses an asparagine residue (N165 in *E. coli*), which interacts with the guanine base via a hydrogen bond and is conserved in both FtsZ and tubulin (Panda et al., 2016). The guanine base is mainly recognized by amino acid residues present within the H7 helix. There are several small molecules that are known to interact with the FtsZ NBD (**Table 1**). Most of these could either interact with microtubules or were screened from a library of microtubule-interacting molecules. As the NBD is highly conserved in both FtsZ and tubulin, any molecules that bind to it may be toxic to mammalian cells. Indeed, curcumin, which binds the NBD of both FtsZ and tubulin, has an MIC of 100 μM in *B. subtilis* and an

IC$_{50}$ of 18 μM for HeLa cells (Rai et al., 2008; Chakraborti et al., 2011). Some other examples of this cross-toxicity are summarized in **Table 1** (IC$_{50}$/MIC).

The IDC

The second major binding site in FtsZ that interacts with small molecules is the IDC, formed by the C-terminal half of the H7 helix, the T7 loop and the beta sheets in the C-terminal domain (**Figure 1C**) (Sun et al., 2014). The size of the cleft, the number of amino acid residues, their conservation and types vary among different bacterial species (**Figure 3** and **Table 2**). For example, the IDC is less conserved in Gram negative bacteria (fewer than nine conserved residues) than Gram positive bacteria (more than nine conserved residues). The size of the IDC also varies among bacterial species, depending on the curvature of the H7 helix. For example, in the GTP bound state of *Staphylococcus aureus* FtsZ the curvature of the H7 helix decreases, which in turn increases the size of the cleft opening. The T7 loop of FtsZ also influences the cleft opening size. In bacteria such as *S. aureus* and *B. subtilis*, the T7 loop in the GTP bound state shifts downward, resulting in a larger cleft opening compared to the GDP bound state (Kusuma et al., 2019). As the T7 loop of one FtsZ subunit is inserted into the nucleotide-binding pocket of the adjacent FtsZ subunit to trigger GTPase activity (Panda et al., 2016), this loop is crucial for modulating FtsZ treadmilling dynamics.

In most bacterial species, many archaea, some chloroplasts and a few primitive mitochondria, the globular domains of FtsZ share 40–50% structural and functional similarity (Erickson, 1998; Tripathy and Sahu, 2019). Compared to the NBD, which exhibits 48–67% sequence identity among FtsZs from *E. coli*, *Pseudomonas aeruginosa*, *B. subtilis*, *S. aureus*, *Mycobacterium tuberculosis*, *Aquifex aeolicus*, and the archaeon *M. jannaschii*, the IDC shows less sequence conservation (34–59% identity) (Casiraghi et al., 2020). The three-dimensional structure of the NBD is quite similar among FtsZs from different bacterial species, whereas it is slightly different among various IDCs

TABLE 3 | Comparison of drug binding sites between FtsZ and tubulin.

Protein	Binding site	Secondary structures involved	References
FtsZ	NBD	H1–H7 helix, S1–S6 strands, and T1–T6 loops	Löwe, 1998
	IDC	H7 helix, S7–S10 strands, and T7 loop	Sun et al., 2014
Tubulin	NBD	H1–H7 helix, S1–S6 strands, and T1–T6 loops	Nogales et al., 1998a
	Colchicine	H7,H8 helix, S8,S9 strands, T7-loop : ß- tubulinT5-loop : α- tubulin	Ravelli et al., 2004; Steinmetz and Prota, 2018
	Taxane	H7 helix, S7 strand, H6–H7 loop, S7–H9 (M-loop) and S9–S10 loop : ß- tubulin	Kellogg et al., 2017
	Laulimalide	H9–H10 helix, H9–H9' and H10–S9 loop : ß- tubulin	Prota et al., 2014
	Vinblastine	H6 helix, T5-loop and H6–H7 loop : ß- tubulinH10 helix, S9 strand, and T7-loop : α- tubulin	Steinmetz and Prota, 2018

TABLE 4 | EcFtsZ residues within the IDC and the corresponding BsFtsZ and SaFtsZ residues.

EcFtsZ	D187	V188	K190	G191	A192	Q194	G195	I196	E198	L199	R202	P203	G204	L205	M206
BsFtsZ	N188	V189	R191	Q192	G193	Q195	G196	I197	D199	L200	T203	P204	G205	L206	I207
SaFtsZ	N188	V189	R191	Q192	G193	Q195	G196	I197	D199	L200	V203	S204	G205	E206	V207

EcFtsZ	N207	V208	V213	M225	G226	S227	V229	L261	V262	N263	T265	A266	L270	R271	L272
BsFtsZ	N208	L209	V214	M226	G227	I228	I230	L261	M262	N263	T265	G266	L270	S271	L272
SaFtsZ	N208	L209	V214	M226	G227	I228	V230	L261	M262	N263	T265	G266	L270	S271	L272

EcFtsZ	F275	G295	T296	S297	L298	D299	P300	D301	M302	N303	E305	R307	T309	V310	V311
BsFtsZ	V275	G295	S296	V297	I298	N299	E300	N301	L302	K303	E305	V307	T309	V310	I311
SaFtsZ	A275	G295	T296	V297	I298	N299	P300	E301	L302	Q303	E305	V307	T309	V310	I311

because of how the C-terminal beta sheets are organized (Kusuma et al., 2019).

The sequence level as well as structural level variability of IDCs among different FtsZs should facilitate the design of species-specific antibiotics (Casiraghi et al., 2020). For example, PC190723, an IDC inhibitor that will be described in greater detail below, is most effective against organisms that have a valine at the equivalent position of 307 in E. coli FtsZ, such as S. aureus and B. subtilis. In contrast, PC190723 is ineffective toward E. coli (Haydon et al., 2008), although inactivating the AcrAB efflux pump of E. coli significantly enhances susceptibility to the PC190723 prodrug TXY436, suggesting that resistance of Gram negative species to this compound is in part due its rapid clearance from the cytoplasm (Kaul et al., 2014).

Although the sequence and structure of the IDC as a whole is not highly conserved, components of the IDC, like the T7 loop, are highly conserved (de Pereda et al., 1996). Kusuma et al. compared the tertiary structure of staphylococcal and non-staphylococcal FtsZ proteins and showed that their structures differ mainly because of variations in the curvature of the H7-helix and organization of the C-terminal β-sheet (Kusuma et al., 2019). Superimposition of staphylococcal and non-staphylococcal FtsZs revealed that staphylococcal FtsZs were similar to each other, with an RMSD value of 0.3 Å, and non-staphylococcal FtsZs were more structurally variable among themselves (RMSD ∼1.3 Å). Conversely, S. aureus FtsZ (hereafter referred to as SaFtsZ) showed much higher variation (RMSD ∼3 Å) when superimposed

onto non-staphylococcal FtsZ. This difference was mainly due to the diversity in the arrangement of C-terminal β-sheets. Similarly, when compared the drug binding sites, both staphylococcal and non-staphylococcal FtsZ showed no significant structural differences in their GTP binding sites and T7 loops, whereas their IDCs were quite divergent. As the cleft opening size of the IDC and the curvature of helix H7 vary significantly between staphylococcal and non-staphylococcal FtsZs, compounds that bind to a staphylococcal FtsZ may not bind to non-staphylococcal FtsZ with similar affinity. Likewise, a compound targeting a non-staphylococcal FtsZ may not bind to other non-staphylococcal FtsZs with the same affinity (Kusuma et al., 2019).

Comparing the IDCs of FtsZ With Tubulin

Microtubules, formed by polymerization of α-β- tubulin, are eukaryotic cytoskeletal proteins that play important roles in several cellular processes such as cell division, cell motility, intracellular transport and maintaining cell shape. Along with the GTP binding pocket, microtubules contain at least four major drug binding sites, including those for vinblastine, colchicine, laulimalide, and taxane (Figure 2A) (Lu et al., 2012). Vinblastine binds at the interface of the α-β- tubulin heterodimer (Figure 2B), which comprises the T7- loop, H10 and S9 strand of α tubulin and H6, the T5 loop and H6–H7 loop of β- tubulin (Steinmetz and Prota, 2018). The colchicine binding site includes the T7-loop, helices H7 and H8, and strands S8 and S9 of β-tubulin plus the T5 loop of α tubulin (Ravelli et al., 2004). The laulimalide binding site comprises helices H9 and H10 and the
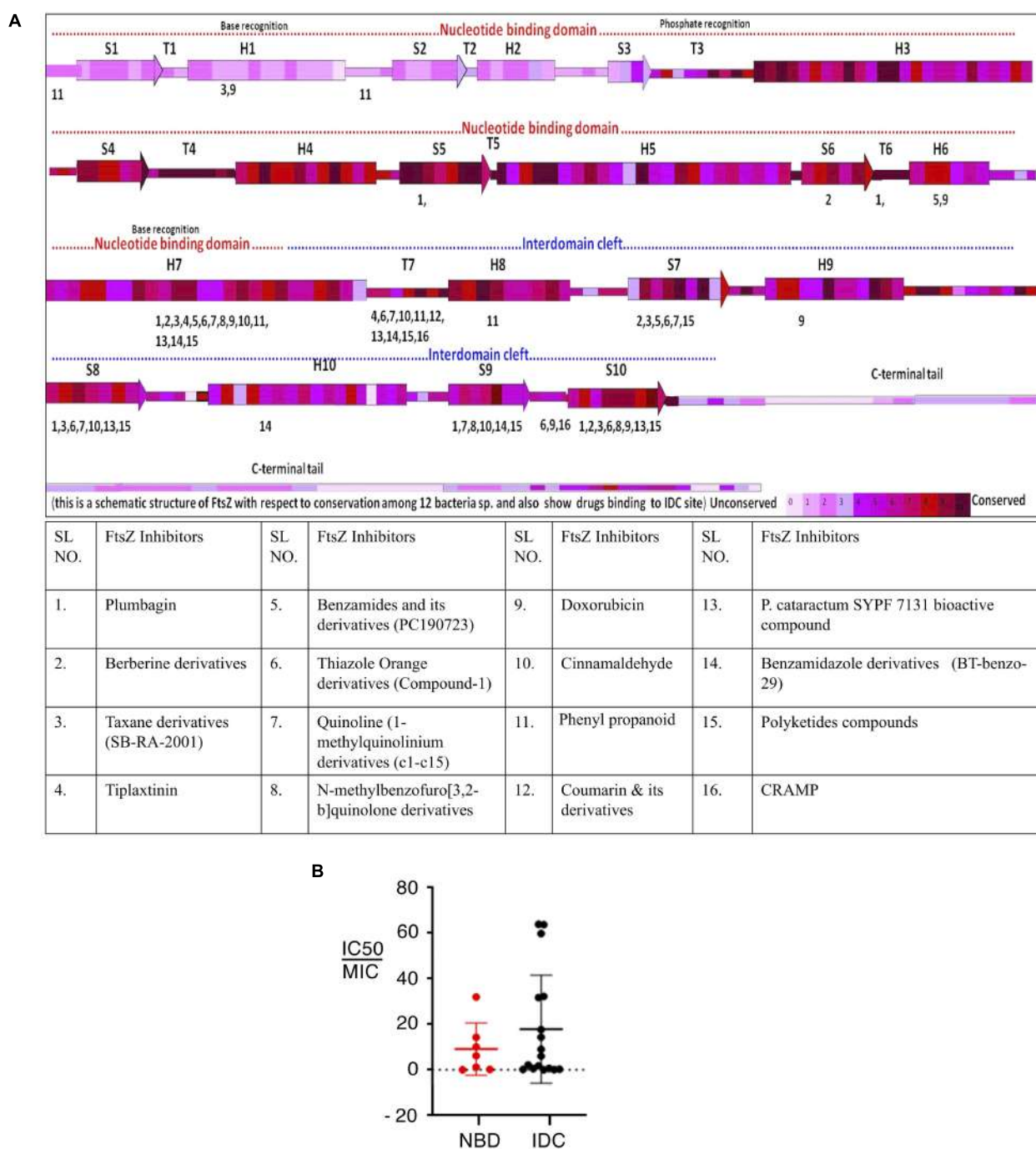
FIGURE 4 | Interaction site for IDC inhibitors and their toxicity. **(A)** Schematic representation of FtsZ with respect to its conservation among 12 bacterial species and the interaction site of IDC inhibitors. **(B)** Comparison of IC$_{50}$/MIC of both NBD and IDC inhibitors.

H10-S9 loop of β- tubulin, whereas taxol, one of three taxane derivatives commonly used as an anticancer drug, binds to the β-tubulin H7, S7, H6–H7 loop, S7–H9 (M-loop) and S9–S10 loop (Prota et al., 2014; Kellogg et al., 2017).

In contrast to this diversity of binding sites in microtubules, only the NBD and IDC of FtsZ have been identified as drug

binding targets. The IDC of FtsZ consists mainly of the H7 helix, S7–S10 strands and T7 loop that structurally map to the taxol and colchicine binding sites in tubulin (**Table 3** and **Figure 2**). Because the IDC has a lower level of sequence and structural similarity with tubulin compared with the NBD, colchicine and taxane can interact with FtsZ, but the interacting residues as well

as binding affinity do not match with tubulin (White et al., 2002; Haydon et al., 2008). For example, although colchicine can bind to the IDC in FtsZ, the colchicine binding pocket of tubulin has no sequence similarity with the colchicine binding site in FtsZ from *M. tuberculosis* (White et al., 2002; Mathew et al., 2016). In another example, PC190723 (an IDC-specific inhibitor) binds to the taxol site on tubulin, but was >64-times more inhibitory to FtsZ than to tubulin (Haydon et al., 2008). Similarly, SB-RA-2001, a taxane derivative, binds to the IDC of *Bs*FtsZ, but when the binding site was superimposed onto the taxol site of tubulin, no identical residues were found; it also binds only very weakly to tubulin (Singh et al., 2014). Consequently, the drugs that bind to the IDC in FtsZ do not interact with tubulin with similar affinity and thus are less likely to be toxic to mammalian cells.

Molecular Insights Into the IDC

The N-terminal domains of FtsZ share high sequence identity in both Gram-positive bacteria (56–89%) and Gram-negative bacteria (43–84%), whereas lower sequence identities (30–70%) are shared within the C-terminal domains and IDCs. Inter-domain clefts of diverse FtsZs are composed of mostly hydrophobic residues along with a few polar and charged amino acids. Available crystallographic structures for protein-ligand interactions indicate that most small molecules prefer to bind to the hydrophobic pockets of their protein targets (Guo et al., 2015). Thus, the hydrophobic residues in the FtsZ IDC likely enhance the binding of organic molecules in aqueous environments, making the IDC a better target for small molecule inhibitors.

Some residues within the IDC are widely conserved in all bacterial species, some are conserved only among the Gram positive bacteria or in Gram negative bacteria, whereas other residues are specific to a particular species. For example, residues V189, Q192, G193, Q195, G196, I197, D199, L200, I201, V203, S204, G205, E206, V207, N208, L209, D210, M226, G227, I228, L261, M262, N263, T265, G295, T296, V297, T309, V310, and I311 are located within 6 Å of the IDC of *Sa*FtsZ. The corresponding residues in *Ec*FtsZ are shown in **Table 4**. Of these, N208, D210, G227, and G295 are conserved throughout bacteria that have FtsZ; G193, Q195, I197, L200, I201, M226, T309, and V310 are conserved mostly in Gram-positive species, and the remaining residues are not conserved (**Figure 3C**). These residues are involved in formation of different bonds with the small molecules–hydrogen bonds, hydrophobic, van der Waals, amide bonds or other types of interactions–and depend upon the chemical nature of the inhibitors and the interacting residues. For example, V207 and N263 are mainly involved in hydrogen bonding with PC190723, while L200 and I311 form hydrophobic interactions (Matsui et al., 2012). The size of the IDC, the number of amino acid residues and their types vary among different bacterial species. For example, a multiple sequence alignment of IDCs from 12 bacteria showed that 6–12 residues are conserved between Gram-positive and Gram-negative species, whereas more than 12 residues are conserved when aligned among only Gram positive bacteria.

Although the IDC mostly consists of hydrophobic residues, it also contains several conserved hydrophilic residues that are important for interaction with small molecule inhibitors. Similarly, many residues are important for interaction with multiple inhibitors. For example, residues in *Ec*FtsZ such as G191, G195, L199, M206, N207, V208, N263, S297, R307 and T309 and their equivalent residues in both *B. subtilis* and *S. aureus* (Q192, G196, L200, V207, N208, L209, N263, V297, V307, and T309 in the latter species) mostly interact with more than one FtsZ inhibitor (**Figure 4A** and **Table 2**). Our analysis of the published literature suggests that most FtsZ inhibitors that target the IDC have higher IC_{50}/MIC ratios than inhibitors that target the NBD (**Figure 4B**). Although IDCs from different bacteria are highly hydrophobic, their lower sequence conservation and variable cleft openings should potentially facilitate development of species-specific antibacterial agents.

IDC Size and Conformational Flexibility

Structural organization of the IDC indicates that the cleft has a specific size and a specific cleft opening. The cleft opening changes for different conformers of FtsZ such as GDP/GTP bound forms, and monomeric/polymeric FtsZ. Further, the size of the cleft opening differs in different bacterial species. Recent analysis of crystal structures of diverse FtsZs by Kusuma et al. indicated that IDC size depends upon the curvature of H7: if its curvature increases, the size of the IDC opening decreases, and vice-versa (**Figure 5**) (Kusuma et al., 2019). Using *in silico* analysis, they further measured the cleft opening size and the curvature of the H7 helix in *Staphylococcus* and non-*Staphylococcus* FtsZs, providing clues to the molecular accessibility of IDCs from different bacterial species (Kusuma et al., 2019). Their analysis shows that the curvature of H7 in *Sa*FtsZ is 140.3° (PDB ID: 3WGN) and the cleft opening size is 15.9 Å, whereas, in *Bs*FtsZ it is 164.5° (PDB ID: 2RHO) and 7.5 Å, respectively. The same study showed that the drug-binding pocket is also subject to species-level variations: *S. aureus* has the widest cleft opening (~15 Å), whereas in *B. subtilis, M. tuberculosis, A. aeolicus,* and *P. aeruginosa* the cleft opening size is 9–10 Å. The IDC binder PC190723 has a size of 14.1 Å, with higher affinity for *Sa*FtsZ than *Bs*FtsZ. This wider cleft opening of *Sa*FtsZ vs. *Bs*FtsZ probably facilitates PC190723 entry and binding, and may be the major reason why it inhibits *S. aureus* cell division more effectively than that of *B. subtilis*.

Similarly, molecular dynamic simulations indicate that in the GTP bound state, the H7 helix is twisted backward and the T7 loop shifts downward, opening the cleft, whereas in GDP bound FtsZ the H7-helix is relaxed and the T7 loop shifts upward, closing the cleft's opening. The size of the cleft opening in GDP and GTP bound *Sa*FtsZ varies between 15 and 20 Å (Kusuma et al., 2019). This model is supported by fluorescence anisotropy experiments showing that a fluorescent analog of PC190723, a nitrobenzoxadiazole probe, specifically binds to the polymeric form of FtsZ (Artola et al., 2017). Molecular dynamics simulations suggest that in monomeric FtsZ the cleft is in a closed or relaxed conformation, preventing the probe from interacting with FtsZ, whereas in polymeric FtsZ the cleft is in the open or tense conformation (Wagstaff et al., 2017; Schumacher et al., 2020), allowing interaction with FtsZ and resulting in fluorescence. *In silico* analysis of the

PC190723 binding pocket in the IDC in different bacterial species showed that the microenvironment of the binding pocket affects the drug's affinity toward FtsZ (Miguel et al., 2015). Analysis of FtsZ crystal structures and molecular dynamics trajectories showed that the conformation of the PC190723 binding pocket depends upon multiple factors such as bacterial species, genetic alterations, allosteric binding and polymerization state (Miguel et al., 2015). In particular, FtsZ polymerization and allosteric binding of the guanosine nucleotide may play a crucial role in stabilizing the PC190723 pocket. For example, for PC190723, the GDP-bound SaFtsZ has a pocket score of -10.75 (PDB ID: 3VO8), whereas FtsZ without nucleotide has a pocket score of -4.29 (PDB ID 3VO9). Similarly, amino acid substitutions G193D, G196C, and N263K in SaFtsZ change the microenvironment of the binding pocket, significantly affecting the binding of PC190723 and leading to drug resistance (Haydon et al., 2008; Miguel et al., 2015).
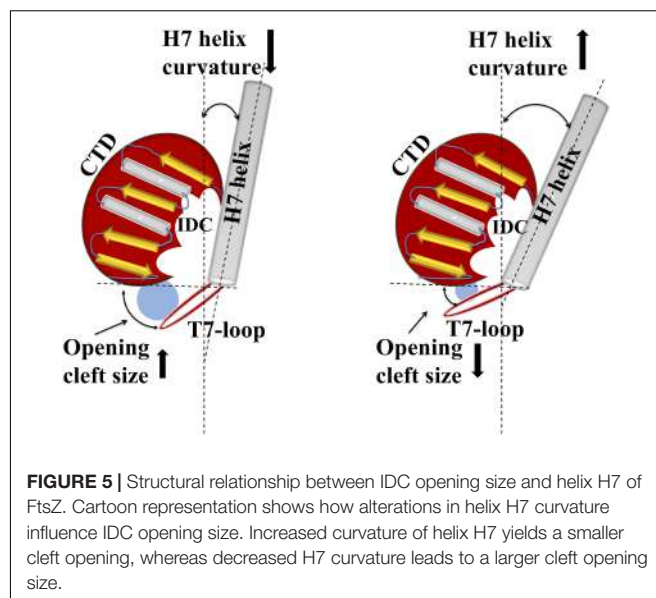
IDC INHIBITORS

Inhibitors that are known to interact with the IDC have been identified by molecular docking, simulation studies, mutational analysis, NMR and crystallographic studies. In addition, FtsZ inhibitors such as Ruthenium red, totarol, sanguinarine, OTBA, *Dichamanetin* and viriditoxin inhibit or promote FtsZ bundling, but the exact binding sites of these drugs on FtsZ are still not known (Santra et al., 2004; Beuria et al., 2005; Urgaonkar et al., 2005; Jaiswal et al., 2007; Beuria et al., 2009). Depending on their structure, we have characterized the IDC inhibitors in seven major groups, which are described below (**Table 1**).

BENZAMIDES

3-MBA, PC190723, and Derivatives

Ohashi et al. originally showed that a benzamide derivative, 3-MBA (3-Methoxybenzamide), inhibits the proliferation of bacteria by targeting FtsZ (Ohashi et al., 1999). Although 3-MBA has low antibacterial activity (MIC = 2048 μg/mL), it provided a strong starting point for FtsZ-targeted fragment-based drug discovery. Screening more than 500 benzamide analogs led to the discovery of the aforementioned PC190723, which contains a thiazolopyridine moiety fused to the benzamide by an ether linkage that makes it ∼2000 times more potent than the parent 3-MBA (MIC = 0.5–1 μg/ml). Molecular docking and X-ray crystallography demonstrated that PC190723 binds to the IDC, interacting specifically with R191, Q192, N263, V307, and T309 in BsFtsZ (Haydon et al., 2008). Similarly, crystallography showed that PC190723 binding site in SaFtsZ comprises Q192, G193,G196, I197, D199, L200, V203, G205, V207, N208, L209, M226, G227, I228, N263, G295, T296, T309, V310, and I311 (**Table 4**) (Matsui et al., 2012). PC190723 binding to the IDC disrupts the normal assembly of the Z ring by causing multiple FtsZ aggregates to distribute throughout the cell that are not able to form a coherent Z ring (Haydon et al., 2008).

FIGURE 5 | Structural relationship between IDC opening size and helix H7 of FtsZ. Cartoon representation shows how alterations in helix H7 curvature influence IDC opening size. Increased curvature of helix H7 yields a smaller cleft opening, whereas decreased H7 curvature leads to a larger cleft opening size.

Not surprisingly, *S. aureus* developed resistance to PC190723 by altering SaFtsZ residues R191 G193, G196, V214, N263, or G266. G196 mainly interacts with the thiazolopyridine moiety and changes at this residue are commonly found in PC190723-resistant *S. aureus*. Interestingly, however, some PC190723-resistant mutants such as R191P and G196A in SaFtsZ and G196S in BsFtsZ remain sensitive to 3-MBA, suggesting that the less specific 3-MBA can still bind to an IDC pocket that occludes PC190723 binding (Adams et al., 2016). Moreover, some substitutions in FtsZ that render cells non-susceptible to PC190723, such as R191P, G193D, and G266S, at the same time confer benzamide dependence for normal cell division (Adams et al., 2016), although the mechanism for this drug dependent function of FtsZ is not clear. Interestingly, a 3-MBA-resistant mutant (A47) remains susceptible to PC190723 (Haydon et al., 2008).

A notable advance in optimizing benzamide action against FtsZ was the replacement of the chlorine atom on the pyridyl ring of PC190723 with a CF3 group, exemplified by a derivative called TXA707, which increases the drug's metabolic stability and anti-staphylococcal activity (MIC: 0.25–2 μg/ml). Nonetheless, TXA707 is less effective on FtsZs with residue changes at G196 and others that mediate resistance, probably for the reason discussed above. A modification made in TXA707, in which a five membered oxazole and six membered phenyl ring (i.e., TXA6101) are flexibly linked, not only improved the binding affinity but also increased its activity against both wild-type methicillin resistant *S. aureus* (MRSA) and mutants carrying residue changes at FtsZ G196 (MIC = 0.125 μg/mL and 1 μg/mL, respectively) (Fujita et al., 2017). Crystallography and biochemical studies showed that both TXA707 and TXA6101 interact with the IDC. TXA6101 induces a conformational rearrangement of I197, M226, and I311 that leads to the formation of an inner hydrophobic pocket, with M226 acting as a gate that opens access to the pocket (Fujita et al., 2017).

Further advances have been made using improved benzamide prodrugs. TXY541 is a prodrug of PC190723 that is 143-times more soluble in an aqueous acid vehicle than PC190723 (Kaul et al., 2013). A prodrug of TXA707, TXA709, is structurally similar to TXY541 except that TXA709 contains a CF3 group instead of Cl group on the pyridyl ring, which increases the metabolic stability of the compound. Currently, TXA709 is in phase-I clinical trials. Recent reports showed that clinically isolated MRSA display resistance toward TXA709 at a frequency of 1 x 10^{-8}, which is similar to that for PC190723. TXA709-resistant isolates carried mutations in FtsZ at G196S, N263K, G193D, G196C, and G196A, similar to residues that confer *S. aureus* resistance to PC190723 (Kaul et al., 2015).

In another study of benzamides, Bi et al. designed and synthesized a series of 3-substituted 2,6-difluorobenzamide derivatives, of which a chloroalkoxy derivative (**7**), a 3-bromoalkoxy derivative (**12**) and a 3-alkyloxy derivative (**17**) exhibited good antibacterial activity against *B. subtilis* and susceptible/resistant *S. aureus* (Bi et al., 2017). Using structure-based drug design to target the IDC, they designed and synthesized a series of isoxazole (isoxazol-3-yl- and isoxazol-5-yl) containing benzamide derivatives. Some of these isoxazol-5-yl benzamide derivatives (B14) were ∼32 fold more potent against *B. subtilis* than PC190723 (Bi et al., 2018). In another study, Bi et al synthesized a series of 1, 3, 4-oxadiazol-2-one containing benzamide derivatives. Out of many derivatives, compound A14 showed the highest antibacterial activity against Gram positive bacteria (MIC 0.125-1 μg/mL) and less cytotoxicity against HeLa cells (IC$_{50}$ > 64 μg/mL). *In silico* docking revealed that compound A14 binds to the IDC (Bi et al., 2019). A recent study of benzodioxane-benzamides identified a derivative (compound 8) with very high potency against MRSA and *B. subtilis*, with MICs at or below 0.1 μg/ml, good solubility, and very low toxicity to human cells. Like the original PC190723 (Haydon et al., 2008), compound 8 caused the delocalization of Z rings in *B. subtilis* into subcellular foci that were unable to function in cell division (Straniero et al., 2021) (**Figure 6**).

3-Aminobenzamide Derivatives

Using cell-based screening, Lui et al screened 47 derivatives of 3-aminobenzamide and showed that their compound 28 interacts with the FtsZ IDC. This compound exhibits high antibacterial activity (MIC 0.5–1 μg/mL against *S. aureus*) and less cytotoxicity (IC$_{50}$ ≥ 100 μM, mouse L929 cell line) and worked in synergy with β-lactam antibiotics. Molecular docking studies showed that the C3 amino group of compound 28 interacts with the hydroxyl group of T309 in *Sa*FtsZ. The other *Sa*FtsZ residues in its proximity are G193, G196, M262, and N263 (**Table 4**). They also found that the M262I residue change is resistant to this molecule (Lui et al., 2019).

Fluorescent Benzamide Derivatives That Bind to the IDC

Recently, Ferrer-González et al. developed a structure-guided fluorescent benzamide derivative by conjugating BODIPY to
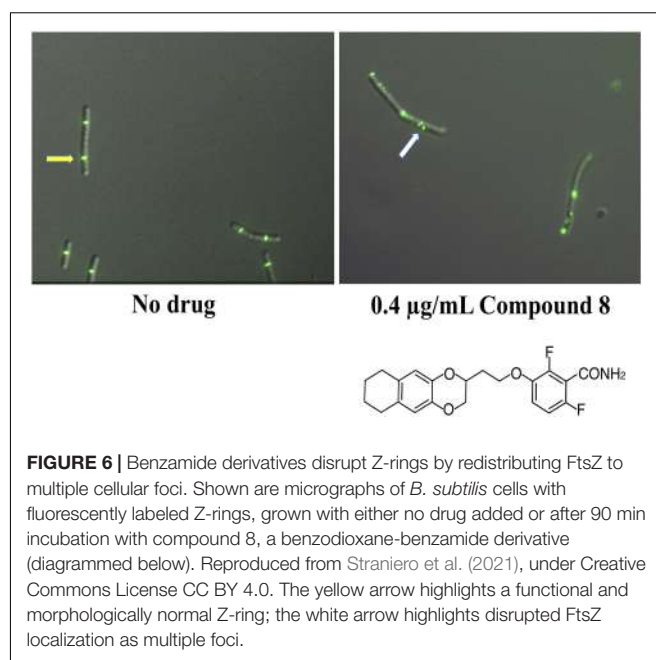

No drug   0.4 μg/mL Compound 8

FIGURE 6 | Benzamide derivatives disrupt Z-rings by redistributing FtsZ to multiple cellular foci. Shown are micrographs of *B. subtilis* cells with fluorescently labeled Z-rings, grown with either no drug added or after 90 min incubation with compound 8, a benzodioxane-benzamide derivative (diagrammed below). Reproduced from Straniero et al. (2021), under Creative Commons License CC BY 4.0. The yellow arrow highlights a functional and morphologically normal Z-ring; the white arrow highlights disrupted FtsZ localization as multiple foci.

an oxazole benzamide FtsZ inhibitor (BOFP). BOFP binds to FtsZ from both Gram positive and Gram negative bacteria with K$_d$s of 0.6–4.6 and 0.2–0.8 μM, respectively (Ferrer-Gonzalez et al., 2019). BOFP binds to the IDC, where the BODIPY moiety interacts with residues I228 and V307 of *Bs*FtsZ (**Table 4**). As it can label FtsZs within diverse bacteria, BOFP holds great promise for the screening of non-fluorescent FtsZ inhibitors and determining whether they perturb Z ring assembly in cells. In a recent study, Huecas et al. developed a competitive binding assay using specific high-affinity fluorescent probes to screen allosteric compounds that can interact with the IDC and inhibit FtsZ assembly. The probes displayed higher anisotropy in the presence of FtsZ polymer, where the IDC is open, compared with FtsZ monomers, where the IDC is closed. The specificity of this probe was assessed using a competitive assay with PC190723. The study demonstrated that the anisotropy of the probe decreased considerably upon binding of the IDC specific inhibitor PC190723, whereas it did not change upon binding of non-specific inhibitors. Thus, this probe can be used to identify inhibitors that specifically bind to the IDC (Artola et al., 2017; Huecas et al., 2021).

QUINOLINE RING COMPOUNDS

Quinolinium derivatives have been widely used as therapeutics due to their antibacterial potency. Here, we describe recent developments in quinolinium molecules that target FtsZ. Berberine, a quinolinium derivative, was first described by Domadia et al. (2008) as an FtsZ interacting molecule and FtsZ inhibitor (Domadia et al., 2008). Since then, several other quinolinium derivatives were identified or synthesized that interact with the IDC and inhibit FtsZ function.

Berberine and Its Derivatives

Berberine is a benzylisoquinoline alkaloid that has been used as an antimicrobial therapeutic for centuries. After identification of its interaction with FtsZ, Wong et al. used *in silico* structure-based design to synthesize a number of 9-phenoxyalkyl berberine derivatives that bind to the IDC of *Sa*FtsZ (Sun et al., 2014). A positively charged amine on these derivatives interacts with *Sa*FtsZ residue D199 and a C-9 methoxy binds to several hydrophobic residues (I228, V230 and V307) in the IDC. Modifications of these two moieties make the derivatives more potent than berberine (MIC = 100–400 µg/mL) and enable them to inhibit growth of MRSA and vancomycin-resistant Enterococci (VRE), with MICs of 2–8 µg/mL and 4–16 µg/mL, respectively. These compounds also exhibit moderate antimicrobial activity against Gram negative strains such as *E. coli* (MIC 32–128 µg/mL). Similarly, 9-phenoxy berberine derivatives inhibit FtsZ GTPase activity (IC_{50} 37.8 – 63.7 µM) more potently than the parent berberine molecule (IC_{50} = 272 µM) and showed similar effects on FtsZ polymerization. This confirms that the substitution of the 9-phenoxy group in berberine increases its affinity toward FtsZ and its antibacterial activity.

Thiazole Orange Derivatives

Quinolines fused with a thiazole orange derivative confer broad spectrum antibacterial activities. Among them, 2-((E)-4- Hydroxystyryl)-1-methyl-4-((Z)-(3-methylbenzo[d]thiazol-2 (3H)-ylidene) methyl) quinolin-1-ium iodide (1) (compound-1) exhibits high antibacterial activity against *S. aureus* (MIC ~ 1.5–3 µg/mL), other *staphylococci* (MIC ~ 0.75–3.0 µg/mL) and *E. coli* (MIC ~ 1.5 µg/mL). This compound enhances FtsZ bundling at lower concentrations (10 nm – 90 nm), inhibits GTPase activity (IC_{50} = 5 µg/mL) and is significantly less toxic to mammalian cells (IC_{50} = 98.15 µM). Molecular docking studies showed that it binds to the IDC of *Sa*FtsZ through both hydrophobic interactions at residues L200, M226, I228, L261, V297, L302, V307, and I311 and hydrogen bonding to V203 and L209 (**Table 4**) (Sun et al., 2017b).

Quinolinium and Quinolone Derivatives

High throughput phenotypic screening by the NIH screened 215,110 molecules against the *M. tuberculosis* (Mtb) H37Rv strain and the data are freely available. Using the results from this screen, Mathew and coworkers found that quinoline and quinazoline can inhibit *Mtb*FtsZ functions (Mathew et al., 2013). Subsequently, Cai et al. synthesized a series of 1-methylquinolinium derivatives (c1-c15) by combining an indole fragment at the 2-position with different amino groups at the 4-position (Cai et al., 2019). These compounds strongly inhibited FtsZ activity and growth of MRSA and VRE, with MIC values between 1 and 4 µg/mL. C2 and c9 derivatives enhanced bactericidal activity with an MIC of 1 µg/mL in *S. aureus* (ATCC 29213). Both compounds possess a common piperidine group at the 4-position of the 1-methylquinolinium core that might increase its antibacterial properties compared with other indole-quinolinium derivatives. Molecular docking studies predicted that these derivatives bind to the IDC of *Sa*FtsZ mostly through

hydrophobic interactions with residues Q192, G196, L200, V203, L209, M226, G227, I228, and V297 and electrostatic interaction with D199 (**Table 4**).

Several quinolone and quinoline derivatives exhibited antibacterial activity against Gram positive and Gram negative bacteria (Piddock and Walters, 1992; Aldred et al., 2014; Zhang et al., 2018). Sun et al. synthesized a series of quinoline derivatives containing the unique quaternary pyridinium core, many of which demonstrated antibacterial activities (Sun et al., 2017a). These compounds interacted hydrophobically with FtsZ residues D199, L200, V297, and V307, and the imino group of these derivatives could hydrogen-bond with FtsZ T309. These compounds showed ~50-fold better antibacterial activity against *B. subtilis* (MIC ~2–8 µg/mL) compared with berberine (MIC = 128 µg/mL). In their next study, Sun et al. synthesized sixteen 3-methylbenzo[d]thaizol-methylquinolinium derivatives with different groups added to the ortho-position of the 1-methylquinolinium core (Sun et al., 2018). One of the derivatives, A2, showed strong antibacterial activity (MIC = 1.5 µg/mL) by inhibiting FtsZ functions, and like the others, exhibited low toxicity toward mammalian cells (IC50 = 78.25 µM) (Sun et al., 2018). A docking study showed that A2 interacts with residues D199, L200, M226, I228, V297, T309, and I311 of *Sa*FtsZ (Sun et al., 2018).

From previous studies, it was clear that thiazole and quinolinium groups are important for antibacterial activity. Li et al. synthesized various thiazole-quinolinium derivatives and evaluated their antibacterial activities against Gram positive and Gram negative species (Li et al., 2015). All compounds showed good antibacterial activity (MIC 1–32 µg/mL) against *S. aureus*. A methyl group substitution at the quinolinium ring resulted in better antibacterial potency than the bulky indolyl group. These derivatives were effective against antibiotic resistant strains, did not induce antibiotic resistance, and showed less cytotoxicity toward mammalian cells (16HBE, HK-2 L929 with IC50 12–26 µg/mL). Molecular docking studies determined that thiazole-quinolinium derivatives interact with the IDC through numerous hydrophobic bonds with residues D199, L200, M226, I228, V297 and van der Waals interactions with Q195, V310, G205, and I311 of *Sa*FtsZ (**Table 4**).

BENZOPYRONE RING COMPOUNDS (COUMARIN AND ITS DERIVATIVES)

Compounds harboring a benzopyrone ring are known to inhibit assembly and GTPase activity of FtsZ. Coumarin (1, 2- benzopyrone) is a natural polyphenolic compound with a benzopyrone ring (Detsi et al., 2017). Duggirala et al. screened several natural compounds including benzopyrone derivatives and showed that coumarins, specifically scopoletin and daphnetin, inhibit FtsZ polymerization and GTPase activity. Molecular docking studies showed that coumarin binds to the IDC via its interaction with highly conserved amino acids such as N207, D209, and D212 in the T7 loop of *Ec*FtsZ (Duggirala et al., 2014). In the case of scopoletin,

the hydroxyl group of coumarin interacts with *Ec*FtsZ residue G204 and the keto group interacts with N207 via hydrogen bonding, whereas daphnetin interacts with G104. In other coumarin derivatives such as umbelliferone and 7-diethylamino-4-methyl coumarin, an oxygen group interacts with N207 and F210 of *Ec*FtsZ. The anti-tubercular activity of coumarin derivatives is reviewed elsewhere (Keri et al., 2015). Apart from the IDC, coumarin derivatives might also interact with the NBD of FtsZ in different organisms. Molecular docking studies revealed that most coumarin derivatives interact with the NBD of *Mycobacterium smegmatis* FtsZ via hydrogen bonding with residues N41, G103 and R140 (Sridevi et al., 2017).

PHENYLPROPANOIDS (CINNAMALDEHYDE AND ITS DERIVATIVES)

Plant-derived natural products are attractive for antibiotic development because they often are less toxic to mammalian cells. Phenylpropanoids are a group of natural organic compounds that are synthesized by plants using phenylalanine and tyrosine. Most phenylpropanoid derivatives possess antibacterial activity, and include cinnamic acid, p-coumaric acid, caffeic acid, chlorogenic acid, eugenol, and ferulic acid (Puupponen-Pimia et al., 2001; Hemaiswarya and Doble, 2009, 2010). These compounds inhibit GTPase activity of FtsZ and are able to disassemble preformed FtsZ polymers with varying effectiveness. For example, the IC_{50} values of FtsZ assembly for eugenol, ferulic acids and 3, 4-dimethoxycinnamic acids are more than 250 µM, whereas cholinergic acid, cinnamic acid, p-coumaric acid and caffeic acid have IC_{50} values of 70 µM, 238 µM, 190 µM, and 106 µM, respectively.

Molecular docking studies indicate that all the phenylpropanoids interact with the T7-loop of IDC. For example, chlorogenic acid, 3, 4-dimethoxycinnamic acid, 2, 4, 5-trimethoxycinnamic acid and ferulic acid interact with residues A11, G36, N207, V208, D209, and F210 of *Ec*FtsZ via hydrogen bonds and P203, N207 *via* hydrophobic bonds (Hemaiswarya et al., 2011). Other phenylpropanoids such as cinnamic acid, p-coumaric acid and caffeic acid bind to M206 and T296 of *Ec*FtsZ through hydrogen bonding. Among phenylpropanoid derivatives, chlorogenic and caffeic acid possesses two hydroxyl groups on their benzene ring, making them more hydrophilic than the other compounds containing methoxy substituents, resulting in higher affinity toward FtsZ (Hemaiswarya et al., 2011). Thus, the presence of hydroxyl groups in phenylpropanoids favor hydrogen bonding with the side chains of FtsZ active site residues that makes the compounds more effective.

Cinnamaldehyde, a phenylpropanoid, exhibits broad spectrum antibacterial activity against diverse species such as *E. coli* (MIC ∼ 1000 µg/mL), *B. subtilis* (MIC ∼ 500 µg/mL) and MRSA (MIC ∼ 250 µg/mL) (Domadia et al., 2007).

It contains an aromatic benzene ring with an α, β-unsaturated carbonyl moiety and inhibits FtsZ assembly and GTPase activity in a dose dependent manner (Li and Ma, 2015). *In silico* docking and STD NMR spectroscopy showed that H2 and H3 of cinamaldehyde interact with residues G295 and V208 of FtsZ. The aromatic ring of cinnamaldehyde is in close proximity to the aliphatic side chains of residues F203, M206, N207, and V208, whereas its carbonyl group is in close proximity to the side chain of N203, the guanidium group of R202 and the hydroxyl group of S297 (Domadia et al., 2007). These studies suggest that cinnamaldehyde preferably interacts with the IDC of FtsZ. Furthermore, multiple sequence alignment shows that the cinnamaldehyde-interacting residues such as G295, V208, R202, N263, and S297 are conserved among FtsZs from different bacterial species.

TAXANE RING COMPOUNDS

The structural kinship between FtsZ and tubulin suggest that some microtubule targeting drugs might also target FtsZ, and taxanes are attractive candidates. Indeed, a screen of 120 taxane derivatives identified several taxanes that bind to FtsZ and exhibit effective anti-tubercular activity (Huang et al., 2006). Among those, SB-RA-2001, a derivative of a non-cytotoxic taxane, contains a 3-naphtha-2yl acryloyl group at the C13 position and showed promising anti-tubercular activity against both drug sensitive and resistant *M. tuberculosis* strains. *In silico* docking studies revealed that this compound binds to the IDC of FtsZ at the PC190723 interaction site (Singh et al., 2014). The SB-RA-2001 binding pocket in *Bs*FtsZ includes residues R29, E32, N33, N188, R191, Q192, Q195, G196, D199, I230, N263, T265, N299, N301, L302, K303, E305, V307, T309 (**Table 4**) of which many are present in the IDC. Its major interaction with *Bs*FtsZ is via hydrogen bonding with residues E305, R191, Q192, N188, and N33. Structural alignment of the taxane binding site on FtsZ and the paclitaxel binding site on tubulin indicated that no identical residues exist between these two sites.

OTHER SMALL MOLECULES WITH SIMPLE AND COMPLEX RING GROUPS

Apart from molecules discussed above, there are several other small molecules with different size and ring structures that are reported to interact with the IDC.

Plumbagin

Plumbagin (5-hydroxy-2-methyl-4, 4-naphthoquinone) is a naturally occurring naphthoquinone originally isolated from the plumbago plant (de Paiva et al., 2003; Aziz et al., 2008). It inhibits proliferation of diverse species such as *S. aureus, P. aeruginosa*, *B. subtilis* (MIC∼29 µM)*, Proteus vulgaris* and *M. smegmatis* (MIC ∼ 31 µM) (de Paiva et al., 2003; Mathew et al., 2010). Plumbagin binds to *Bs*FtsZ and inhibits its assembly and GTPase activity (Bhattacharya et al., 2013). *In vitro* and

in silico assessment studies demonstrated that the plumbagin binding site is distinct from the NBD in *Bs*FtsZ (Bhattacharya et al., 2013). The residues of *Bs*FtsZ that constitute the plumbagin binding site include the H7 helix and other residues in the IDC such as R191, Q192, Q195, G196, D199, N263, T265, N299, V307, and T309 (**Table 4**). Of these, R191, Q195, D199, and N299 of *Bs*FtsZ are involved in hydrogen bonding with plumbagin (Bhattacharya et al., 2013). Mutational studies confirmed that D199 and V307 of *Bs*FtsZ play an important role in plumbagin binding. *In silico* studies showed that the plumbagin binding site in *Ec*FtsZ includes residues G21, M104, T132, P134, E138, R142, N165, F182, A185, and L189 (Bhattacharya et al., 2013). Notably, these residues are in a completely different part of FtsZ than the plumbagin binding pocket of *Bs*FtsZ, suggesting that FtsZs of different bacteria may have different ligand binding properties.

Fungal Compounds

Since the discovery of penicillin, it is well known that bioactive molecules of fungi show strong antimicrobial properties. While screening 58 fungal compounds from 24 different genera, Wu et al. found that *Penicillium cataractum* SYPF 7131 has strong antibacterial activity against *S. aureus* (Wu et al., 2018). Out of the 8 known and unknown isolates from its fermentation broth, 3 compounds showed effective antibacterial activity (MIC 10–65 µg/mL) and strong interaction with FtsZ. An *in silico* study suggested that these compounds interact with the IDC of *Sa*FtsZ by hydrogen bonding with residues G205, N263, T309, L209, G196, G227, and G193, and hydrophobic interaction with L200, L209, I311 L261, V307, V203, I228, I311 V297, and V203 (**Table 4**).

Doxorubicin

Doxorubicin is an anthracycline antibiotic which inhibits bacterial proliferation with moderate inhibition against *E. coli* (MIC 40 µM) and strong inhibition against *S. aureus* (MBC 5 µM). In the presence of doxorubicin, *E. coli* becomes highly filamentous without affecting chromosome segregation, indicating a cell division defect. Panda et al. showed that doxorubicin binds to a site in FtsZ distinct from the NBD. The amino sugar region of doxorubicin sits in a polar cavity and involves hydrogen-bond interactions with E32, R33, and D187 of *Ec*FtsZ, whereas the ethyloxy side chain involves hydrogen-bond interaction with E305 (Panda et al., 2015). The hydrophobic part of the molecule (the aromatic rings) sits in a cavity lined by hydrophobic residues of FtsZ, *e.g.,* V171, V188, M225, V229, and L248. The binding site contains many highly conserved residues, including E32, R33, V171, D187, V188, M225, G226, P247, L248, M302, N303, E305, and R307.

CCR-11

Rhodanine derivatives can perturb the assembly of FtsZ polymers and inhibit bacterial proliferation. Singh et al. screened a library of 151 rhodanine derivatives, of which 8 compounds showed good antibacterial activity (MIC ∼2 µM) and 3 specifically inhibited division of *B. subtilis* cells (Singh et al., 2012). One of these molecules, CCR-11, interacts with FtsZ with a Kd of 1.5 ± 0.3 µM and inhibits FtsZ assembly and GTPase activity.

Docking studies revealed that CCR-11 binds to the IDC. The fluorine atoms of the CCR-11 trifluoromethylphenyl side chain interact with *Bs*FtsZ T203 and CCR-11 also interacts with *Bs*FtsZ G205, I207, L272, V275, and I298 through hydrophobic interactions. The thiazolidine ring of CCR-11 interacts with T203 and D199 of *Bs*FtsZ. CCR-11 inhibited HeLa cell proliferation with an IC_{50} value of 18.1 ± 0.2 µM, which is 6 times higher than the MIC (3 µM) of CCR11 on *B. subtilis* (Singh et al., 2012).

Bt-Benzo-29

Ray et al. screened 100 benzamidazole compounds for them) ability to elongate *B. subtilis* cells, out of which one compound, N-(4-sec-butylphenyl)-2- (thiophen-2-yl)-1H-benzo[d]imidazole-4-carboxamide (BT-benzo-29), causes cell filamentation. BT-benzo-29 inhibits FtsZ functions by interacting with FtsZ (Kd = 24 ± 3 µM) and inhibits proliferation of *B. subtilis* with an MIC of 17 µM (Ray et al., 2015). A molecular docking study proposed that BT-benzo-29 binds to the *Bs*FtsZ C-terminal portion of the globular domain, near the T7 loop. The interaction involves hydrogen bonding with L206 and S296 and hydrophobic interactions with D199, T203, P204, G205, L206, N208, L270, S271, L272, V275, S296, V297, I298, and E300 residues (Ray et al., 2015). Mutational studies showed that L272A and V275A mutants had weaker inhibitory effects on the assembly and GTPase activity. Unfortunately, BT-benzo-29 inhibits HeLa cell proliferation with an IC_{50} 17 ± 2 µM, only ∼4 times higher than the IC_{50} for *B. subtilis*.

Tiplaxtinin

Tiplaxtinin is an indole oxoacetic acid derivative (Elokdah et al., 2004). Using a cell based screen of 250 compounds, Sun et al. identified Tiplaxtinin as a bacterial cell division inhibitor (Sun et al., 2017c). Tiplaxtinin has strong antibacterial activity against Gram-positive pathogens, with MICs of 4.55–9.10 µM (2–4 µg/mL). Both *in vitro* and *in vivo* findings indicate that tiplaxtinin is capable of effectively disrupting dynamic assembly of FtsZ, GTPase function and Z-ring formation; tiplaxtinin-induced multiple FtsZ foci in *B. subtilis* cells is similar to the *in vivo* effects of benzamides. Molecular docking studies of this compound in *Sa*FtsZ revealed that tiplaxtinin binds near the T7-loop and H7 helix in the IDC region. The trifluoromethoxy group of tiplaxtinin forms hydrogen bonds with G193 and G227 and halogen bonds with V189, Q192, G193, and M226 (Sun et al., 2017c). Similarly, the carbonyl group interacts with T265 through a hydrogen bond. Tiplaxtinin also interacts with V189, Q192, G193 D199, L200, L209, M226, G227, I228, and V297 residues via hydrophobic interactions (**Table 4**).

SMALL INHIBITORY PEPTIDES THAT BIND NEAR THE IDC

Cathelin related antimicrobial peptide (CRAMP) is present in multicellular organisms and helps the innate immune system in the fight against microbes (Bergman et al., 2006). Like many antimicrobial peptides, CRAMP has an amphipathic α helical conformation. The active part of CRAMP consists of 18 amino

acid residues from 16 to 33 (GEKLKKIGQKIKNFFQKL), which inhibits bacterial proliferation (MIC 20–50 µM) and GTPase activity of FtsZ in concentration dependent manner (IC50 ∼ 70 ± 14 µM) (Ray et al., 2014). Molecular docking studies suggest that both hydrophobic and hydrophilic amino acid residues of CRAMP can bind to the T7 loop (L206, I207, N208, and D210) and C-terminal residues adjacent to T7 loop. CRAMP binding to FtsZ is stabilized through salt bridges, hydrogen bonding, hydrophilic and hydrophobic interactions. K25 of CRAMP binds to D210 of T7 loop through a salt bridge and the G16, K27, K32 of CRAMP form hydrogen bonds with both R286 and D287 residues of FtsZ.

Another small FtsZ-inhibitory peptide is MciZ, a 40-aa peptide produced during sporulation of *B. subtilis*. MciZ interacts directly with FtsZ, inhibiting FtsZ polymerization and Z ring assembly *in vivo* (Handler et al., 2008; Ray et al., 2013). Using crystallography and computational techniques, Bisson-Filho et al. demonstrated that MciZ interacts with the C-terminal domain of FtsZ and thus does not bind to the NBD (Bisson-Filho et al., 2015). However, MciZ does not bind to the IDC either, and instead interacts with H10 and beta strand 9 of FtsZ. This results in occlusion of subunit-subunit contacts that causes capping of the growing FtsZ protofilament end (Araujo-Bazan et al., 2019). Other peptide inhibitors of FtsZ, including Kil from bacteriophage lambda and GP0.4 from bacteriophage T7, disrupt assembly of *Ec*FtsZ protofilaments, but their binding sites on FtsZ are not yet known (Kiro et al., 2013; Haeusser et al., 2014; Hernandez-Rocamora et al., 2015).

CONCLUSION AND FUTURE PERSPECTIVES

We have described many small molecules that can interact with the IDC of FtsZ. Despite structurally mapping to the taxol and colchicine binding sites in tubulin, the IDC shares a low level of sequence and structural similarities with tubulin, reducing the likelihood that small molecules targeting the IDC will be toxic to mammalian cells. Molecules targeting the FtsZ NBD, on the other hand, are likely to have adverse effects on tubulin, and thus mammalian cells.

In most species, the IDC in FtsZ extends from residues 186 to 320 in *Ec*FtsZ. However, there are only a handful of residues that are specifically involved in interacting with small molecules (**Table 2**). Many of these residues are hydrophobic and favor interaction with small molecules, making the IDC a good druggable site. Fortunately, a few of these residues are conserved in both Gram positive and Gram negative bacteria and are essential for FtsZ functions. For example, G191 of *Ec*FtsZ is important for FtsZ assembly and G193 and G196 of *Sa*FtsZ are essential for interaction with anti-FtsZ drugs. Not surprisingly, alterations to any of these residues either inhibit FtsZ assembly

or result in drug resistance. The G196A substitution in *Sa*FtsZ remains sensitive to 3-MBA despite conferring resistance to PC190723, suggesting that acquiring drug resistance comes with a fitness cost. It is notable that the V307 residue in FtsZ is important for FtsZ interaction with several drug classes including benzamides, plumbagin, quinolines, taxanes (SB-RA-2001), and berberine derivatives. Likewise, the T7-loop residue M206 of *Ec*FtsZ interacts with phenylpropanoid derivatives, and additional residues in the T7-loop interact with other drug molecules. Although the specter of resistant mutations is a significant challenge, molecules targeting the T7 loop may be less likely to induce resistant mutations because of its requirement in GTP hydrolysis.

Apart from the differences in residues among bacterial FtsZs, the size of the IDC and the cleft opening also varies in different bacterial species, with PC190723 binding to the larger cleft opening in *Sa*FtsZ with high affinity, and to the smaller cleft opening in *Bs*FtsZ with very low affinity. As a result, compounds can be tailored for specific species by targeting their IDCs. The limited number of FtsZ crystal structures and the lack of understanding of drug binding pockets in FtsZ have so far hindered such fine tuning, and consequently anti-FtsZ drugs are not yet ready for the clinic. Most of the IDC-drug interaction studies rely on *in silico* studies, whereas only a few drug molecules such as PC190723 and some of its derivatives have been subject to experimental genetic and structural studies. Nonetheless, recently reported derivatives of PC190723 exhibit very low MICs on important Gram-positive pathogens and have low toxicity profiles. Targeting FtsZs in Gram-negative pathogens will be more challenging because of increased barriers to permeability due to the outer membrane, but the small size of many of the compounds reviewed here, along with combination therapy using adjuvants that perturb the outer membrane and/or drug efflux pumps, provide promising future avenues (Khare et al., 2019). Continued development of better small molecule inhibitors that target FtsZ, as well as discovery of small molecules that can inhibit the activity of other conserved bacterial cell division proteins, will require continued collaboration between medicinal chemists, structural biologists and microbiologists.

AUTHOR CONTRIBUTIONS

All authors listed have made a substantial, direct and intellectual contribution to the work, and approved it for publication.

FUNDING

REFERENCES

Acharya, B. R., Bhattacharyya, B., and Chakrabarti, G. (2008). The natural naphthoquinone plumbagin exhibits antiproliferative activity and disrupts the microtubule network through tubulin binding. *Biochemistry* 47, 7838–7845. doi: 10.1021/bi800730q

Adams, D. W., Wu, L. J., and Errington, J. (2016). A benzamide-dependent ftsZ mutant reveals residues crucial for Z-ring assembly. *Mol. Microbiol.* 99, 1028–1042. doi: 10.1111/mmi.13286

Addinall, S. G., Bi, E., and Lutkenhaus, J. (1996). FtsZ ring formation in fts mutants. *J. Bacteriol.* 178, 3877–3884. doi: 10.1128/jb.178.13.3877-3884.1996

Aldred, K. J., Kerns, R. J., and Osheroff, N. (2014). Mechanism of quinolone action and resistance. *Biochemistry* 53, 1565–1574. doi: 10.1021/bi5000564

Allard, J. F., and Cytrynbaum, E. N. (2009). Force generation by a dynamic Z-ring in *Escherichia coli* cell division. *Proc. Natl. Acad. Sci. U.S.A.* 106, 145–150. doi: 10.1073/pnas.0808657106

Anderson, D. E., Gueiros-Filho, F. J., and Erickson, H. P. (2004). Assembly dynamics of FtsZ rings in *Bacillus subtilis* and *Escherichia coli* and effects of FtsZ-regulating proteins. *J. Bacteriol.* 186, 5775–5781. doi: 10.1128/JB.186.17.5775-5781.2004

Araujo-Bazan, L., Huecas, S., Valle, J., Andreu, D., and Andreu, J. M. (2019). Synthetic developmental regulator MciZ targets FtsZ across *Bacillus* species and inhibits bacterial division. *Mol. Microbiol.* 111, 965–980. doi: 10.1111/mmi.14198

Artola, M., Ruiz-Avila, L. B., Ramirez-Aportela, E., Martinez, R. F., Araujo-Bazan, L., Vazquez-Villa, H., et al. (2017). The structural assembly switch of cell division protein FtsZ probed with fluorescent allosteric inhibitors. *Chem. Sci.* 8, 1525–1534. doi: 10.1039/c6sc03792e

Artola, M., Ruiz-Avila, L. B., Vergonos, A., Huecas, S., Araujo-Bazan, L., Martin-Fontecha, M., et al. (2015). Effective GTP-replacing FtsZ inhibitors and antibacterial mechanism of action. *ACS Chem. Biol.* 10, 834–843. doi: 10.1021/cb500974d

Aziz, M. H., Dreckschmidt, N. E., and Verma, A. K. (2008). Plumbagin, a medicinal plant-derived naphthoquinone, is a novel inhibitor of the growth and invasion of hormone-refractory prostate cancer. *Cancer Res.* 68, 9024–9032. doi: 10.1158/0008-5472.CAN-08-2494

Battaje, R. R., and Panda, D. (2017). Lessons from bacterial homolog of tubulin, FtsZ for microtubule dynamics. *Endocr. Relat. Cancer* 24, T1–T21. doi: 10.1530/ERC-17-0118

Beall, B., and Lutkenhaus, J. (1991). FtsZ in *Bacillus subtilis* is required for vegetative septation and for asymmetric septation during sporulation. *Genes Dev.* 5, 447–455. doi: 10.1101/gad.5.3.447

Bergman, P., Johansson, L., Wan, H., Jones, A., Gallo, R. L., Gudmundsson, G. H., et al. (2006). Induction of the antimicrobial peptide CRAMP in the blood-brain barrier and meninges after meningococcal infection. *Infect. Immun.* 74, 6982–6991. doi: 10.1128/IAI.01043-06

Beuria, T. K., Santra, M. K., and Panda, D. (2005). Sanguinarine blocks cytokinesis in bacteria by inhibiting FtsZ assembly and bundling. *Biochemistry* 44, 16584–16593.

Beuria, T. K., Singh, P., Surolia, A., and Panda, D. (2009). Promoting assembly and bundling of FtsZ as a strategy to inhibit bacterial cell division: a new approach for developing novel antibacterial drugs. *Biochem. J.* 423, 61–69. doi: 10.1042/BJ20090817

Bhattacharya, A., Jindal, B., Singh, P., Datta, A., and Panda, D. (2013). Plumbagin inhibits cytokinesis in *Bacillus subtilis* by inhibiting FtsZ assembly–a mechanistic study of its antibacterial activity. *FEBS J.* 280, 4585–4599. doi: 10.1111/febs.12429

Bi, E. F., and Lutkenhaus, J. (1991). FtsZ ring structure associated with division in *Escherichia coli*. *Nature* 354, 161–164. doi: 10.1038/354161a0

Bi, F., Guo, L., Wang, Y., Venter, H., Semple, S. J., Liu, F., et al. (2017). Design, synthesis and biological activity evaluation of novel 2,6-difluorobenzamide derivatives through FtsZ inhibition. *Bioorg. Med. Chem. Lett.* 27, 958–962. doi: 10.1016/j.bmcl.2016.12.081

Bi, F., Song, D., Qin, Y., Liu, X., Teng, Y., Zhang, N., et al. (2019). Discovery of 1,3,4-oxadiazol-2-one-containing benzamide derivatives targeting FtsZ as highly potent agents of killing a variety of MDR bacteria strains. *Bioorg. Med. Chem.* 27, 3179–3193. doi: 10.1016/j.bmc.2019.06.010

Bi, F., Song, D., Zhang, N., Liu, Z., Gu, X., Hu, C., et al. (2018). Design, synthesis and structure-based optimization of novel isoxazole-containing benzamide derivatives as FtsZ modulators. *Eur. J. Med. Chem.* 159, 90–103. doi: 10.1016/j.ejmech.2018.09.053

Bisson-Filho, A. W., Discola, K. F., Castellen, P., Blasios, V., Martins, A., Sforca, M. L., et al. (2015). FtsZ filament capping by MciZ, a developmental regulator of bacterial division. *Proc. Natl. Acad. Sci. U.S.A.* 112, E2130–E2138. doi: 10.1073/pnas.1414242112

Bisson-Filho, A. W., Hsu, Y. P., Squyres, G. R., Kuru, E., Wu, F., Jukes, C., et al. (2017). Treadmilling by FtsZ filaments drives peptidoglycan synthesis and bacterial cell division. *Science* 355, 739–743. doi: 10.1126/science.aak9973

Borges, A., Ferreira, C., Saavedra, M. J., and Simoes, M. (2013). Antibacterial activity and mode of action of ferulic and gallic acids against pathogenic bacteria. *Microb. Drug Resist.* 19, 256–265. doi: 10.1089/mdr.2012.0244

Bramhill, D., and Thompson, C. M. (1994). GTP-dependent polymerization of *Escherichia coli* FtsZ protein to form tubules. *Proc. Natl. Acad. Sci. U.S.A.* 91, 5813–5817. doi: 10.1073/pnas.91.13.5813

Bramkamp, M., Emmins, R., Weston, L., Donovan, C., Daniel, R. A., and Errington, J. (2008). A novel component of the division-site selection system of *Bacillus subtilis* and a new mode of action for the division inhibitor MinCD. *Mol. Microbiol.* 70, 1556–1569. doi: 10.1111/j.1365-2958.2008.06501.x

Buske, P. J., and Levin, P. A. (2012). Extreme *C* terminus of bacterial cytoskeletal protein FtsZ plays fundamental role in assembly independent of modulatory proteins. *J. Biol. Chem.* 287, 10945–10957. doi: 10.1074/jbc.M111.330324

Cai, S., Yuan, W., Li, Y., Huang, X., Guo, Q., Tang, Z., et al. (2019). Antibacterial activity of indolyl-quinolinium derivatives and study their mode of action. *Bioorg. Med. Chem.* 27, 1274–1282. doi: 10.1016/j.bmc.2019.02.024

Carro, L. (2019). Recent progress in the development of small-molecule FtsZ inhibitors as chemical tools for the development of novel antibiotics. *Antibiotics (Basel)* 8:217. doi: 10.3390/antibiotics8040217

Casiraghi, A., Suigo, L., Valoti, E., and Straniero, V. (2020). Targeting bacterial cell division: a binding site-centered approach to the most promising inhibitors of the essential protein FtsZ. *Antibiotics (Basel)* 9:69. doi: 10.3390/antibiotics9020069

Chakraborti, S., Das, L., Kapoor, N., Das, A., Dwivedi, V., Poddar, A., et al. (2011). Curcumin recognizes a unique binding site of tubulin. *J. Med. Chem.* 54, 6183–6196. doi: 10.1021/jm2004046

Chan, F. Y., Sun, N., Neves, M. A., Lam, P. C., Chung, W. H., Wong, L. K., et al. (2013). Identification of a new class of FtsZ inhibitors by structure-based design and in vitro screening. *J. Chem. Inf. Model.* 53, 2131–2140. doi: 10.1021/ci400203f

Chang, M. Y., and Shen, Y. L. (2014). Linalool exhibits cytotoxic effects by activating antitumor immunity. *Molecules* 19, 6694–6706. doi: 10.3390/molecules19056694

Cohan, M. C., Eddelbuettel, A. M. P., Levin, P. A., and Pappu, R. V. (2020). Dissecting the functional contributions of the intrinsically disordered C-terminal tail of *Bacillus subtilis* FtsZ. *J. Mol. Biol.* 432, 3205–3221. doi: 10.1016/j.jmb.2020.03.008

Dai, K., and Lutkenhaus, J. (1991). ftsZ is an essential cell division gene in *Escherichia coli*. *J. Bacteriol.* 173, 3500–3506. doi: 10.1128/jb.173.11.3500-3506.1991

de Boer, P., Crossley, R., and Rothfield, L. (1992). The essential bacterial cell-division protein FtsZ is a GTPase. *Nature* 359, 254–256. doi: 10.1038/359254a0

de Paiva, S. R., Figueiredo, M. R., Aragao, T. V., and Kaplan, M. A. (2003). Antimicrobial activity in vitro of plumbagin isolated from *Plumbago* species. *Mem. Inst. Oswaldo. Cruz.* 98, 959–961. doi: 10.1590/s0074-02762003000700017

de Pereda, J. M., Leynadier, D., Evangelio, J. A., Chacon, P., and Andreu, J. M. (1996). Tubulin secondary structure analysis, limited proteolysis sites, and homology to FtsZ. *Biochemistry* 35, 14203–14215. doi: 10.1021/bi961357b

de Souza, S. M., Delle Monache, F., and Smania, A. Jr. (2005). Antibacterial activity of coumarins. *Z. Naturforsch. C. J. Biosci.* 60, 693–700. doi: 10.1515/znc-2005-9-1006

Detsi, A., Kontogiorgis, C., and Hadjipavlou-Litina, D. (2017). Coumarin derivatives: an updated patent review (2015-2016). *Expert Opin. Ther. Pat.* 27, 1201–1226. doi: 10.1080/13543776.2017.1360284

Dhaked, H. P., Bhattacharya, A., Yadav, S., Dantu, S. C., Kumar, A., and Panda, D. (2016). Mutation of Arg191 in FtsZ impairs cytokinetic abscission of *Bacillus subtilis* cells. *Biochemistry* 55, 5754–5763. doi: 10.1021/acs.biochem.6b00493

Din, N., Quardokus, E. M., Sackett, M. J., and Brun, Y. V. (1998). Dominant C-terminal deletions of FtsZ that affect its ability to localize in *Caulobacter* and its interaction with FtsA. *Mol. Microbiol.* 27, 1051–1063. doi: 10.1046/j.1365-2958.1998.00752.x

Domadia, P., Swarup, S., Bhunia, A., Sivaraman, J., and Dasgupta, D. (2007). Inhibition of bacterial cell division protein FtsZ by cinnamaldehyde. *Biochem. Pharmacol.* 74, 831–840. doi: 10.1016/j.bcp.2007.06.029

Domadia, P. N., Bhunia, A., Sivaraman, J., Swarup, S., and Dasgupta, D. (2008). Berberine targets assembly of *Escherichia coli* cell division protein FtsZ. *Biochemistry* 47, 3225–3234. doi: 10.1021/bi7018546

Duggirala, S., Nankar, R. P., Rajendran, S., and Doble, M. (2014). Phytochemicals as inhibitors of bacterial cell division protein FtsZ: coumarins are promising candidates. *Appl. Biochem. Biotechnol.* 174, 283–296. doi: 10.1007/s12010-014-1056-2

Duman, R., Ishikawa, S., Celik, I., Strahl, H., Ogasawara, N., Troc, P., et al. (2013). Structural and genetic analyses reveal the protein SepF as a new membrane anchor for the Z ring. *Proc. Natl. Acad. Sci. U.S.A.* 110, E4601–E4610. doi: 10.1073/pnas.1313978110

Elokdah, H., Abou-Gharbia, M., Hennan, J. K., McFarlane, G., Mugford, C. P., Krishnamurthy, G., et al. (2004). Tiplaxtinin, a novel, orally efficacious inhibitor of plasminogen activator inhibitor-1: design, synthesis, and preclinical characterization. *J. Med. Chem.* 47, 3491–3494. doi: 10.1021/jm049766q

Erickson, H. P. (1995). FtsZ, a prokaryotic homolog of tubulin? *Cell* 80, 367–370. doi: 10.1016/0092-8674(95)90486-7

Erickson, H. P. (1998). Atomic structures of tubulin and FtsZ. *Trends Cell Biol.* 8, 133–137. doi: 10.1016/s0962-8924(98)01237-9

Erickson, H. P., Anderson, D. E., and Osawa, M. (2010). FtsZ in bacterial cytokinesis: cytoskeleton and force generator all in one. *Microbiol. Mol. Biol. Rev.* 74, 504–528. doi: 10.1128/MMBR.00021-10

Eroglu, C., Secme, M., Bagci, G., and Dodurga, Y. (2015). Assessment of the anticancer mechanism of ferulic acid via cell cycle and apoptotic pathways in human prostate cancer cell lines. *Tumour. Biol.* 36, 9437–9446. doi: 10.1007/s13277-015-3689-3

Fang, Z., Zheng, S., Chan, K. F., Yuan, W., Guo, Q., Wu, W., et al. (2019). Design, synthesis and antibacterial evaluation of 2,4-disubstituted-6-thiophenyl-pyrimidines. *Eur. J. Med. Chem.* 161, 141–153. doi: 10.1016/j.ejmech.2018.10.039

Ferrer-Gonzalez, E., Fujita, J., Yoshizawa, T., Nelson, J. M., Pilch, A. J., Hillman, E., et al. (2019). Structure-guided design of a fluorescent probe for the visualization of FtsZ in clinically important gram-positive and gram-negative bacterial pathogens. *Sci. Rep.* 9:20092. doi: 10.1038/s41598-019-56557-x

Finn, G. J., Creaven, B., and Egan, D. A. (2001). Study of the in vitro cytotoxic potential of natural and synthetic coumarin derivatives using human normal and neoplastic skin cell lines. *Melanoma Res.* 11, 461–467. doi: 10.1097/00008390-200110000-00004

Fujita, J., Maeda, Y., Mizohata, E., Inoue, T., Kaul, M., Parhi, A. K., et al. (2017). Structural flexibility of an inhibitor overcomes drug resistance mutations in *Staphylococcus aureus* FtsZ. *ACS Chem. Biol.* 12, 1947–1955. doi: 10.1021/acschembio.7b00323

Gardner, K. A., Moore, D. A., and Erickson, H. P. (2013). The C-terminal linker of *Escherichia coli* FtsZ functions as an intrinsically disordered peptide. *Mol. Microbiol.* 89, 264–275. doi: 10.1111/mmi.12279

Guo, Z., Li, B., Cheng, L. T., Zhou, S., McCammon, J. A., and Che, J. (2015). Identification of protein-ligand binding sites by the level-set variational implicit-solvent approach. *J. Chem. Theory Comput.* 11, 753–765. doi: 10.1021/ct500867u

Haeusser, D. P., Hoashi, M., Weaver, A., Brown, N., Pan, J., Sawitzke, J. A., et al. (2014). The Kil peptide of bacteriophage lambda blocks *Escherichia coli* cytokinesis via ZipA-dependent inhibition of FtsZ assembly. *PLoS Genet.* 10:e1004217. doi: 10.1371/journal.pgen.1004217

Haeusser, D. P., and Margolin, W. (2016). Splitsville: structural and functional insights into the dynamic bacterial Z ring. *Nat. Rev. Microbiol.* 14, 305–319.

Haeusser, D. P., Schwartz, R. L., Smith, A. M., Oates, M. E., and Levin, P. A. (2004). EzrA prevents aberrant cell division by modulating assembly of the cytoskeletal protein FtsZ. *Mol. Microbiol.* 52, 801–814. doi: 10.1111/j.1365-2958.2004.04016.x

Hale, C. A., and de Boer, P. A. (1997). Direct binding of FtsZ to ZipA, an essential component of the septal ring structure that mediates cell division in *E. coli*. *Cell* 88, 175–185. doi: 10.1016/s0092-8674(00)81838-3

Handler, A. A., Lim, J. E., and Losick, R. (2008). Peptide inhibitor of cytokinesis during sporulation in *Bacillus subtilis*. *Mol. Microbiol.* 68, 588–599. doi: 10.1111/j.1365-2958.2008.06173.x

Haranahalli, K., Tong, S., and Ojima, I. (2016). Recent advances in the discovery and development of antibacterial agents targeting the cell-division protein FtsZ. *Bioorg. Med. Chem.* 24, 6354–6369. doi: 10.1016/j.bmc.2016.05.003

Haydon, D. J., Stokes, N. R., Ure, R., Galbraith, G., Bennett, J. M., Brown, D. R., et al. (2008). An inhibitor of FtsZ with potent and selective anti-staphylococcal activity. *Science* 321, 1673–1675. doi: 10.1126/science.1159961

Hemaiswarya, S., and Doble, M. (2009). Synergistic interaction of eugenol with antibiotics against Gram negative bacteria. *Phytomedicine* 16, 997–1005. doi: 10.1016/j.phymed.2009.04.006

Hemaiswarya, S., and Doble, M. (2010). Synergistic interaction of phenylpropanoids with antibiotics against bacteria. *J. Med. Microbiol.* 59(Pt 12), 1469–1476. doi: 10.1099/jmm.0.022426-0

Hemaiswarya, S., Soudaminikkutty, R., Narasumani, M. L., and Doble, M. (2011). Phenylpropanoids inhibit protofilament formation of *Escherichia coli* cell division protein FtsZ. *J. Med. Microbiol.* 60(Pt 9), 1317–1325. doi: 10.1099/jmm.0.030536-0

Hernandez-Rocamora, V. M., Alfonso, C., Margolin, W., Zorrilla, S., and Rivas, G. (2015). Evidence that bacteriophage lambda kil peptide inhibits bacterial cell division by disrupting FtsZ protofilaments and sequestering protein subunits. *J. Biol. Chem.* 290, 20325–20335. doi: 10.1074/jbc.M115.653329

Hsin, J., Gopinathan, A., and Huang, K. C. (2012). Nucleotide-dependent conformations of FtsZ dimers and force generation observed through molecular dynamics simulations. *Proc. Natl. Acad. Sci. U.S.A.* 109, 9432–9437. doi: 10.1073/pnas.1120761109

Huang, Q., Kirikae, F., Kirikae, T., Pepe, A., Amin, A., Respicio, L., et al. (2006). Targeting FtsZ for antituberculosis drug discovery: noncytotoxic taxanes as novel antituberculosis agents. *J. Med. Chem.* 49, 463–466. doi: 10.1021/jm050920y

Huecas, S., Araujo-Bazan, L., Ruiz, F. M., Ruiz-Avila, L. B., Martinez, R. F., Escobar-Pena, A., et al. (2021). Targeting the FtsZ allosteric binding site with a novel fluorescence polarization screen, cytological and structural approaches for antibacterial discovery. *J. Med. Chem.* 64, 5730–5745. doi: 10.1021/acs.jmedchem.0c02207

Jaiswal, R., Beuria, T. K., Mohan, R., Mahajan, S. K., and Panda, D. (2007). Totarol inhibits bacterial cytokinesis by perturbing the assembly dynamics of FtsZ. *Biochemistry* 46, 4211–4220. doi: 10.1021/bi602573e

Jindal, B., and Panda, D. (2013). Understanding FtsZ assembly: cues from the behavior of its N- and C-terminal domains. *Biochemistry* 52, 7071–7081. doi: 10.1021/bi400129j

Kaul, M., Mark, L., Zhang, Y., Parhi, A. K., LaVoie, E. J., and Pilch, D. S. (2013). Pharmacokinetics and in vivo antistaphylococcal efficacy of TXY541, a 1-methylpiperidine-4-carboxamide prodrug of PC190723. *Biochem. Pharmacol.* 86, 1699–1707. doi: 10.1016/j.bcp.2013.10.010

Kaul, M., Mark, L., Zhang, Y., Parhi, A. K., Lyu, Y. L., Pawlak, J., et al. (2015). TXA709, an FtsZ-targeting benzamide prodrug with improved pharmacokinetics and enhanced in vivo efficacy against methicillin-resistant *Staphylococcus aureus*. *Antimicrob. Agents Chemother.* 59, 4845–4855. doi: 10.1128/AAC.00708-15

Kaul, M., Zhang, Y., Parhi, A. K., Lavoie, E. J., and Pilch, D. S. (2014). Inhibition of RND-type efflux pumps confers the FtsZ-directed prodrug TXY436 with activity against Gram-negative bacteria. *Biochem. Pharmacol.* 89, 321–328. doi: 10.1016/j.bcp.2014.03.002

Kaur, S., Modi, N. H., Panda, D., and Roy, N. (2010). Probing the binding site of curcumin in *Escherichia coli* and *Bacillus subtilis* FtsZ–a structural insight to unveil antibacterial activity of curcumin. *Eur. J. Med. Chem.* 45, 4209–4214. doi: 10.1016/j.ejmech.2010.06.015

Keffer, J. L., Huecas, S., Hammill, J. T., Wipf, P., Andreu, J. M., and Bewley, C. A. (2013). Chrysophaentins are competitive inhibitors of FtsZ and inhibit Z-ring formation in live bacteria. *Bioorg. Med. Chem.* 21, 5673–5678. doi: 10.1016/j.bmc.2013.07.033

Kellogg, E. H., Hejab, N. M. A., Howes, S., Northcote, P., Miller, J. H., Diaz, J. F., et al. (2017). Insights into the distinct mechanisms of action of taxane and non-taxane microtubule stabilizers from cryo-EM structures. *J. Mol. Biol.* 429, 633–646. doi: 10.1016/j.jmb.2017.01.001

Keri, R. S., Sasidhar, B. S., Nagaraja, B. M., and Santos, M. A. (2015). Recent progress in the drug development of coumarin derivatives as potent antituberculosis agents. *Eur. J. Med. Chem.* 100, 257–269. doi: 10.1016/j.ejmech.2015.06.017

Khare, S., Hsin, J., Sorto, N. A., Nepomuceno, G. M., Shaw, J. T., Shi, H., et al. (2019). FtsZ-Independent mechanism of division inhibition by the small molecule PC190723 in *Escherichia coli*. *Adv. Biosyst.* 3:e1900021. doi: 10.1002/adbi.201900021

Kiro, R., Molshanski-Mor, S., Yosef, I., Milam, S. L., Erickson, H. P., and Qimron, U. (2013). Gene product 0.4 increases bacteriophage T7 competitiveness by inhibiting host cell division. *Proc. Natl. Acad. Sci. U.S.A.* 110, 19549–19554. doi: 10.1073/pnas.1314096110

Krupka, M., and Margolin, W. (2018). Unite to divide: oligomerization of tubulin and actin homologs regulates initiation of bacterial cell division. *F1000Res.* 7:235.

Kusuma, K. D., Griffith, R., Harry, E. J., Bottomley, A. L., and Ung, A. T. (2019). In silico analysis of FtsZ crystal structures towards a new target for antibiotics. *Aust. J. Chem.* 72, 184–193. doi: 10.1071/CH18347

Lan, G., Wolgemuth, C. W., and Sun, S. X. (2007). Z-ring force and cell shape during division in rod-like bacteria. *Proc. Natl. Acad. Sci. U.S.A.* 104, 16110–16115. doi: 10.1073/pnas.0702925104

Li, X., and Ma, S. (2015). Advances in the discovery of novel antimicrobials targeting the assembly of bacterial cell division protein FtsZ. *Eur. J. Med. Chem.* 95, 1–15. doi: 10.1016/j.ejmech.2015.03.026

Li, Y., Sun, N., Ser, H.-L., Long, W., Li, Y., Chen, C., et al. (2015). Antibacterial activity evaluation and mode of action study of novel thiazole-quinolinium derivatives. *RSC Adv.* 10, 15000–15014. doi: 10.1039/D0RA00691B

Lou, Z., Wang, H., Rao, S., Sun, J., Chaoyang, m, and Li, J. (2012). P-Coumaric acid kills bacteria through dual damage mechanisms. *Food Control* 25, 550–554. doi: 10.1016/j.foodcont.2011.12.022

Löwe, J. (1998). Crystal structure determination of FtsZ from *Methanococcus jannaschii*. *J. Struct. Biol.* 124, 235–243. doi: 10.1006/jsbi.1998.4041

Löwe, J., and Amos, L. A. (1998). Crystal structure of the bacterial cell-division protein FtsZ. *Nature* 391, 203–206. doi: 10.1038/34472

Löwe, J., and Amos, L. A. (1999). Tubulin-like protofilaments in Ca2+-induced FtsZ sheets. *EMBO J.* 18, 2364–2371. doi: 10.1093/emboj/18.9.2364

Lu, C., Reedy, M., and Erickson, H. P. (2000). Straight and curved conformations of FtsZ are regulated by GTP hydrolysis. *J. Bacteriol.* 182, 164–170. doi: 10.1128/JB.182.1.164-170.2000

Lu, C., Stricker, J., and Erickson, H. P. (1998). FtsZ from *Escherichia coli*, *Azotobacter vinelandii*, and *Thermotoga maritima*–quantitation, GTP hydrolysis, and assembly. *Cell Motil. Cytoskeleton* 40, 71–86. doi: 10.1002/(SICI)1097-0169199840:1<71::AID-CM7>3.0.CO;2-I

Lu, Y., Chen, J., Xiao, M., Li, W., and Miller, D. D. (2012). An overview of tubulin inhibitors that interact with the colchicine binding site. *Pharm. Res.* 29, 2943–2971. doi: 10.1007/s11095-012-0828-z

Lui, H. K., Gao, W., Cheung, K. C., Jin, W. B., Sun, N., Kan, J. W. Y., et al. (2019). Boosting the efficacy of anti-MRSA beta-lactam antibiotics via an easily accessible, non-cytotoxic and orally bioavailable FtsZ inhibitor. *Eur. J. Med. Chem.* 163, 95–115. doi: 10.1016/j.ejmech.2018.11.052

Ma, S., and Ma, S. (2012). The development of FtsZ inhibitors as potential antibacterial agents. *ChemMedChem* 7, 1161–1172. doi: 10.1002/cmdc.201200156

Ma, X., and Margolin, W. (1999). Genetic and functional analyses of the conserved C-terminal core domain of *Escherichia coli* FtsZ. *J. Bacteriol.* 181, 7531–7544.

Mathew, B., Hobrath, J. V., Ross, L., Connelly, M. C., Lofton, H., Rajagopalan, M., et al. (2016). Screening and development of new inhibitors of FtsZ from *M. Tuberculosis*. *PLoS One* 11:e0164100. doi: 10.1371/journal.pone.0164100

Mathew, B., Ross, L., and Reynolds, R. C. (2013). A novel quinoline derivative that inhibits mycobacterial FtsZ. *Tuberculosis (Edinb.)* 93, 398–400. doi: 10.1016/j.tube.2013.04.002

Mathew, R., Kruthiventi, A. K., Prasad, J. V., Kumar, S. P., Srinu, G., and Chatterji, D. (2010). Inhibition of mycobacterial growth by plumbagin derivatives. *Chem. Biol. Drug Des.* 76, 34–42. doi: 10.1111/j.1747-0285.2010.00987.x

Matsui, T., Lallo, S., Nisa, K., and Morita, H. (2017). Filamenting temperature-sensitive mutant Z inhibitors from *Glycyrrhiza glabra* and their inhibitory mode of action. *Bioorg. Med. Chem. Lett.* 27, 1420–1424. doi: 10.1016/j.bmcl.2017.01.095

Matsui, T., Yamane, J., Mogi, N., Yamaguchi, H., Takemoto, H., Yao, M., et al. (2012). Structural reorganization of the bacterial cell-division protein FtsZ from *Staphylococcus aureus*. *Acta Crystallogr. D Biol. Crystallogr.* 68(Pt 9), 1175–1188. doi: 10.1107/S0907444912022640

Miguel, A., Hsin, J., Liu, T., Tang, G., Altman, R. B., and Huang, K. C. (2015). Variations in the binding pocket of an inhibitor of the bacterial division protein FtsZ across genotypes and species. *PLoS Comput. Biol.* 11:e1004117. doi: 10.1371/journal.pcbi.1004117

Mukherjee, A., Dai, K., and Lutkenhaus, J. (1993). *Escherichia coli* cell division protein FtsZ is a guanine nucleotide binding protein. *Proc. Natl. Acad. Sci. U.S.A.* 90, 1053–1057. doi: 10.1073/pnas.90.3.1053

Mukherjee, A., and Lutkenhaus, J. (1994). Guanine nucleotide-dependent assembly of FtsZ into filaments. *J. Bacteriol.* 176, 2754–2758. doi: 10.1128/jb.176.9.2754-2758.1994

Ng, L. T., and Wu, S. J. (2011). Antiproliferative activity of *Cinnamomum cassia* constituents and effects of pifithrin-alpha on their apoptotic signaling pathways in Hep G2 Cells. *Evid. Based Complement Alternat. Med.* 2011:492148. doi: 10.1093/ecam/nep220

Nguyen, L. T., Oikonomou, C. M., Ding, H. J., Kaplan, M., Yao, Q., Chang, Y. W., et al. (2019). Simulations suggest a constrictive force is required for Gram-negative bacterial cell division. *Nat. Commun.* 10:1259. doi: 10.1038/s41467-019-09264-0

Niero, E. L., and Machado-Santelli, G. M. (2013). Cinnamic acid induces apoptotic cell death and cytoskeleton disruption in human melanoma cells. *J. Exp. Clin. Cancer Res.* 32:31. doi: 10.1186/1756-9966-32-31

Nogales, E., Downing, K. H., Amos, L. A., and Löwe, J. (1998a). Tubulin and FtsZ form a distinct family of GTPases. *Nat. Struct. Biol.* 5, 451–458. doi: 10.1038/nsb0698-451

Nogales, E., Wolf, S. G., and Downing, K. H. (1998b). Structure of the alpha beta tubulin dimer by electron crystallography. *Nature* 391, 199–203. doi: 10.1038/34465

Nussbaum, P., Gerstner, M., Dingethal, M., Erb, C., and Albers, S. V. (2021). The archaeal protein SepF is essential for cell division in *Haloferax volcanii*. *Nat. Commun.* 12:3469. doi: 10.1038/s41467-021-23686-9

Ohashi, Y., Chijiiwa, Y., Suzuki, K., Takahashi, K., Nanamiya, H., Sato, T., et al. (1999). The lethal effect of a benzamide derivative, 3-methoxybenzamide, can be suppressed by mutations within a cell division gene, ftsZ, in *Bacillus subtilis*. *J. Bacteriol.* 181, 1348–1351. doi: 10.1128/JB.181.4.1348-1351.1999

Oncul, S., and Ercan, A. (2017). Discrimination of the effects of doxorubicin on two different breast cancer cell lines on account of multidrug resistance and apoptosis. *Indian J. Pharm. Sci.* 79, 599–607. doi: 10.4172/pharmaceutical-sciences.1000268

Ortiz, C., Natale, P., Cueto, L., and Vicente, M. (2016). The keepers of the ring: regulators of FtsZ assembly. *FEMS Microbiol. Rev.* 40, 57–67.

Panda, D., Bhattacharya, D., Gao, Q. H., Oza, P. M., Lin, H. Y., Hawkins, B., et al. (2016). Identification of agents targeting FtsZ assembly. *Future Med. Chem.* 8, 1111–1132. doi: 10.4155/fmc-2016-0041

Panda, P., Taviti, A. C., Satpati, S., Kar, M. M., Dixit, A., and Beuria, T. K. (2015). Doxorubicin inhibits *E. coli* division by interacting at a novel site in FtsZ. *Biochem. J.* 471, 335–346. doi: 10.1042/BJ20150467

Pichoff, S., and Lutkenhaus, J. (2002). Unique and overlapping roles for ZipA and FtsA in septal ring assembly in *Escherichia coli*. *EMBO J.* 21, 685–693. doi: 10.1093/emboj/21.4.685

Piddock, L. J., and Walters, R. N. (1992). Bactericidal activities of five quinolones for *Escherichia coli* strains with mutations in genes encoding the SOS response or cell division. *Antimicrob. Agents Chemother.* 36, 819–825. doi: 10.1128/aac.36.4.819

Pinho, M. G., and Errington, J. (2003). Dispersed mode of *Staphylococcus aureus* cell wall synthesis in the absence of the division machinery. *Mol. Microbiol.* 50, 871–881. doi: 10.1046/j.1365-2958.2003.03719.x

Plaza, A., Keffer, J. L., Bifulco, G., Lloyd, J. R., and Bewley, C. A. (2010). Chrysophaentins A-H, antibacterial bisdiarylbutene macrocycles that inhibit the bacterial cell division protein FtsZ. *J. Am. Chem. Soc.* 132, 9069–9077. doi: 10.1021/ja102100h

Prota, A. E., Bargsten, K., Northcote, P. T., Marsh, M., Altmann, K. H., Miller, J. H., et al. (2014). Structural basis of microtubule stabilization by laulimalide and peloruside A. *Angew Chem. Int. Ed. Engl.* 53, 1621–1625. doi: 10.1002/anie.201307749

Puupponen-Pimia, R., Nohynek, L., Meier, C., Kahkonen, M., Heinonen, M., Hopia, A., et al. (2001). Antimicrobial properties of phenolic compounds from berries. *J. Appl. Microbiol.* 90, 494–507. doi: 10.1046/j.1365-2672.2001.01271.x

Raghav, D., Ashraf, S. M., Mohan, L., and Rathinasamy, K. (2017). Berberine induces toxicity in HeLa cells through perturbation of microtubule polymerization by binding to tubulin at a unique site. *Biochemistry* 56, 2594–2611. doi: 10.1021/acs.biochem.7b00101

Rai, D., Singh, J. K., Roy, N., and Panda, D. (2008). Curcumin inhibits FtsZ assembly: an attractive mechanism for its antibacterial activity. *Biochem. J.* 410, 147–155. doi: 10.1042/BJ20070891

Ramirez-Diaz, D. A., Merino-Salomon, A., Meyer, F., Heymann, M., Rivas, G., Bramkamp, M., et al. (2021). FtsZ induces membrane deformations via torsional stress upon GTP hydrolysis. *Nat. Commun.* 12:3310. doi: 10.1038/s41467-021-23387-3

Rastogi, N., Domadia, P., Shetty, S., and Dasgupta, D. (2008). Screening of natural phenolic compounds for potential to inhibit bacterial cell division protein FtsZ. *Indian J. Exp. Biol.* 46, 783–787.

Ravelli, R. B., Gigant, B., Curmi, P. A., Jourdain, I., Lachkar, S., Sobel, A., et al. (2004). Insight into tubulin regulation from a complex with colchicine and a stathmin-like domain. *Nature* 428, 198–202. doi: 10.1038/nature02393

Ray, S., Dhaked, H. P., and Panda, D. (2014). Antimicrobial peptide CRAMP (16-33) stalls bacterial cytokinesis by inhibiting FtsZ assembly. *Biochemistry* 53, 6426–6429. doi: 10.1021/bi501115p

Ray, S., Jindal, B., Kunal, K., Surolia, A., and Panda, D. (2015). BT-benzo-29 inhibits bacterial cell proliferation by perturbing FtsZ assembly. *FEBS J.* 282, 4015–4033. doi: 10.1111/febs.13403

Ray, S., Kumar, A., and Panda, D. (2013). GTP regulates the interaction between MciZ and FtsZ: a possible role of MciZ in bacterial cell division. *Biochemistry* 52, 392–401. doi: 10.1021/bi301237m

Romberg, L., Simon, M., and Erickson, H. P. (2001). Polymerization of Ftsz, a bacterial homolog of tubulin. is assembly cooperative? *J. Biol. Chem.* 276, 11743–11753. doi: 10.1074/jbc.M009033200

Rowlett, V. W., and Margolin, W. (2015). The Min system and other nucleoid-independent regulators of Z ring positioning. *Front. Microbiol.* 6:478. doi: 10.3389/fmicb.2015.00478

Ruiz-Avila, L. B., Huecas, S., Artola, M., Vergonos, A., Ramirez-Aportela, E., Cercenado, E., et al. (2013). Synthetic inhibitors of bacterial cell division targeting the GTP-binding site of FtsZ. *ACS Chem. Biol.* 8, 2072–2083. doi: 10.1021/cb400208z

Sanderson, J. T., Clabault, H., Patton, C., Lassalle-Claux, G., Jean-Francois, J., Pare, A. F., et al. (2013). Antiproliferative, antiandrogenic and cytotoxic effects of novel caffeic acid derivatives in LNCaP human androgen-dependent prostate cancer cells. *Bioorg. Med. Chem.* 21, 7182–7193. doi: 10.1016/j.bmc.2013.08.057

Santra, M. K., Beuria, T. K., Banerjee, A., and Panda, D. (2004). Ruthenium red-induced bundling of bacterial cell division protein, FtsZ. *J. Biol. Chem.* 279, 25959–25965. doi: 10.1074/jbc.M312473200

Scheffers, D. J., de Wit, J. G., den Blaauwen, T., and Driessen, A. J. (2002). GTP hydrolysis of cell division protein FtsZ: evidence that the active site is formed by the association of monomers. *Biochemistry* 41, 521–529. doi: 10.1021/bi011370i

Schumacher, M. A., Ohashi, T., Corbin, L., and Erickson, H. P. (2020). High-resolution crystal structures of *Escherichia coli* FtsZ bound to GDP and GTP. *Acta Crystallogr. F Struct. Biol. Commun.* 76(Pt 2), 94–102. doi: 10.1107/S2053230X20001132

Singh, D., Bhattacharya, A., Rai, A., Dhaked, H. P., Awasthi, D., Ojima, I., et al. (2014). SB-RA-2001 inhibits bacterial proliferation by targeting FtsZ assembly. *Biochemistry* 53, 2979–2992. doi: 10.1021/bi401356y

Singh, P., Jindal, B., Surolia, A., and Panda, D. (2012). A rhodanine derivative CCR-11 inhibits bacterial proliferation by inhibiting the assembly and GTPase activity of FtsZ. *Biochemistry* 51, 5434–5442. doi: 10.1021/bi201813u

Squyres, G. R., Holmes, M. J., Barger, S. R., Pennycook, B. R., Ryan, J., Yan, V. T., et al. (2021). Single-molecule imaging reveals that Z-ring condensation is essential for cell division in *Bacillus subtilis*. *Nat. Microbiol.* 6, 553–562.

Sridevi, D., Sudhakar, K. U., Ananthathatmula, R., Nankar, R. P., and Doble, M. (2017). Mutation at G103 of MtbFtsZ altered their sensitivity to coumarins. *Front. Microbiol.* 8:578. doi: 10.3389/fmicb.2017.00578

Steinmetz, M. O., and Prota, A. E. (2018). Microtubule-targeting agents: strategies to hijack the cytoskeleton. *Trends Cell Biol.* 28, 776–792. doi: 10.1016/j.tcb.2018.05.001

Straniero, V., Sebastian-Perez, V., Suigo, L., Margolin, W., Casiraghi, A., Hrast, M., et al. (2021). Computational design and development of benzodioxane-benzamides as potent inhibitors of FtsZ by exploring the hydrophobic subpocket. *Antibiotics (Basel)* 10:442. doi: 10.3390/antibiotics10040442

Stricker, J., Maddox, P., Salmon, E. D., and Erickson, H. P. (2002). Rapid assembly dynamics of the *Escherichia coli* FtsZ-ring demonstrated by fluorescence recovery after photobleaching. *Proc. Natl. Acad. Sci. U.S.A.* 99, 3171–3175. doi: 10.1073/pnas.052595099

Sun, N., Chan, F. Y., Lu, Y. J., Neves, M. A., Lui, H. K., Wang, Y., et al. (2014). Rational design of berberine-based FtsZ inhibitors with broad-spectrum antibacterial activity. *PLoS One* 9:e97514. doi: 10.1371/journal.pone.0097514

Sun, N., Du, R. L., Zheng, Y. Y., Guo, Q., Cai, S. Y., Liu, Z. H., et al. (2018). Antibacterial activity of 3-methylbenzo[d]thiazol-methylquinolinium derivatives and study of their action mechanism. *J. Enzyme Inhib. Med. Chem.* 33, 879–889. doi: 10.1080/14756366.2018.1465055

Sun, N., Du, R. L., Zheng, Y. Y., Huang, B. H., Guo, Q., Zhang, R. F., et al. (2017a). Antibacterial activity of N-methylbenzofuro[3,2-b]quinoline and N-methylbenzoindolo[3,2-b]-quinoline derivatives and study of their mode of action. *Eur. J. Med. Chem.* 135, 1–11. doi: 10.1016/j.ejmech.2017.04.018

Sun, N., Lu, Y. J., Chan, F. Y., Du, R. L., Zheng, Y. Y., Zhang, K., et al. (2017b). A thiazole orange derivative targeting the bacterial protein FtsZ shows potent antibacterial activity. *Front. Microbiol.* 8:855. doi: 10.3389/fmicb.2017.00855

Sun, N., Zheng, Y. Y., Du, R. L., Cai, S. Y., Zhang, K., So, L. Y., et al. (2017c). New application of tiplaxtinin as an effective FtsZ-targeting chemotype for an antimicrobial study. *Medchemcomm* 8, 1909–1913. doi: 10.1039/c7md00387k

Taviti, A. C., and Beuria, T. K. (2017). MinD directly interacting with FtsZ at the H10 helix suggests a model for robust activation of MinC to destabilize FtsZ polymers. *Biochem. J.* 474, 3189–3205. doi: 10.1042/BCJ20170357

Tripathy, S., and Sahu, S. K. (2019). FtsZ inhibitors as a new genera of antibacterial agents. *Bioorg. Chem.* 91:103169. doi: 10.1016/j.bioorg.2019.103169

Trusca, D., Scott, S., Thompson, C., and Bramhill, D. (1998). Bacterial SOS checkpoint protein SulA inhibits polymerization of purified FtsZ cell division protein. *J. Bacteriol.* 180, 3946–3953. doi: 10.1128/JB.180.15.3946-3953.1998

Urgaonkar, S., La Pierre, H. S., Meir, I., Lund, H., RayChaudhuri, D., and Shaw, J. T. (2005). Synthesis of antimicrobial natural products targeting FtsZ: (+/−)-dichamanetin and (+/−)-2′′-hydroxy-5′′-benzylisouvarinol-B. *Org. Lett.* 7, 5609–5612. doi: 10.1021/ol052269z

van den Ent, F., Amos, L., and Löwe, J. (2001). Bacterial ancestry of actin and tubulin. *Curr. Opin. Microbiol.* 4, 634–638. doi: 10.1016/s1369-5274(01)00262-4

Vaughan, S., Wickstead, B., Gull, K., and Addinall, S. G. (2004). Molecular evolution of FtsZ protein sequences encoded within the genomes of archaea, bacteria, and eukaryota. *J. Mol. Evol.* 58, 19–29. doi: 10.1007/s00239-003-2523-5

Wagstaff, J. M., Tsim, M., Oliva, M. A., Garcia-Sanchez, A., Kureisaite-Ciziene, D., Andreu, J. M., et al. (2017). A polymerization-associated structural switch in FtsZ that enables treadmilling of model filaments. *mBio* 8:e00254-17. doi: 10.1128/mBio.00254-17

Wang, M., Fang, C., Ma, B., Luo, X., and Hou, Z. (2020). Regulation of cytokinesis: FtsZ and its accessory proteins. *Curr. Genet.* 66, 43–49. doi: 10.1007/s00294-019-01005-6

White, E. L., Suling, W. J., Ross, L. J., Seitz, L. E., and Reynolds, R. C. (2002). 2-Alkoxycarbonylaminopyridines: inhibitors of *Mycobacterium tuberculosis* FtsZ. *J. Antimicrob. Chemother.* 50, 111–114. doi: 10.1093/jac/dkf075

White, M. L., and Eswara, P. J. (2021). ylm has more than a (Z Anchor) ring to It! *J. Bacteriol.* 203:e00460-20. doi: 10.1128/JB.00460-20

Whitley, K. D., Jukes, C., Tregidgo, N., Karinou, E., Almada, P., Cesbron, Y., et al. (2021). FtsZ treadmilling is essential for Z-ring condensation and septal constriction initiation in *Bacillus subtilis. Nat. Commun.* 12:2448.

Wu, Y. Y., Zhang, T. Y., Zhang, M. Y., Cheng, J., and Zhang, Y. X. (2018). An endophytic Fungi of *Ginkgo biloba* L. produces antimicrobial metabolites as potential inhibitors of FtsZ of *Staphylococcus aureus. Fitoterapia* 128, 265–271. doi: 10.1016/j.fitote.2018.05.033

Yang, X., Lyu, Z., Miguel, A., McQuillen, R., Huang, K. C., and Xiao, J. (2017). GTPase activity-coupled treadmilling of the bacterial tubulin FtsZ organizes septal cell wall synthesis. *Science* 355, 744–747. doi: 10.1126/science.aak9995

Yao, Q., Jewett, A. I., Chang, Y. W., Oikonomou, C. M., Beeby, M., Iancu, C. V., et al. (2017). Short FtsZ filaments can drive asymmetric cell envelope constriction at the onset of bacterial cytokinesis. *EMBO J.* 36, 1577–1589. doi: 10.15252/embj.201696235

Yu, H. H., Kim, K. J., Cha, J. D., Kim, H. K., Lee, Y. E., Choi, N. Y., et al. (2005). Antimicrobial activity of berberine alone and in combination with ampicillin or oxacillin against methicillin-resistant *Staphylococcus aureus. J. Med. Food* 8, 454–461. doi: 10.1089/jmf.2005.8.454

Zhang, G. F., Zhang, S., Pan, B., Liu, X., and Feng, L. S. (2018). 4-Quinolone derivatives and their activities against Gram positive pathogens. *Eur. J. Med. Chem.* 143, 710–723. doi: 10.1016/j.ejmech.2017.11.082

Zheng, Y. Y., Du, R. L., Cai, S. Y., Liu, Z. H., Fang, Z. Y., Liu, T., et al. (2018). Study of benzofuroquinolinium derivatives as a new class of potent antibacterial agent and the mode of inhibition targeting FtsZ. *Front. Microbiol.* 9:1937. doi: 10.3389/fmicb.2018.01937